

10-9-2009

Optical Sensing with CdSe Quantum Dots in Condensed Phase Media

Melissa Fisher
Florida State University

Follow this and additional works at: <http://diginole.lib.fsu.edu/etd>

Recommended Citation

Fisher, Melissa, "Optical Sensing with CdSe Quantum Dots in Condensed Phase Media" (2009). *Electronic Theses, Treatises and Dissertations*. Paper 4449.

This Dissertation - Open Access is brought to you for free and open access by the The Graduate School at DigiNole Commons. It has been accepted for inclusion in Electronic Theses, Treatises and Dissertations by an authorized administrator of DigiNole Commons. For more information, please contact lib-ir@fsu.edu.

THE FLORIDA STATE UNIVERSITY

COLLEGE OF ARTS AND SCIENCES

OPTICAL SENSING WITH CDSE QUANTUM DOTS IN CONDENSED PHASE MEDIA

By

MELISSA FISHER

A Dissertation submitted to the
Department of Chemistry and Biochemistry
in partial fulfillment of the
requirements for the degree of
Doctor of Philosophy

Degree Awarded:
Fall Semester, 2009

The members of the committee approve the dissertation of Melissa L. Fisher defended on October 9, 2009.

Geoffrey F. Strouse
Professor Directing Dissertation

Samuel C. Grant
University Representative

Albert E. Stiegman
Committee Member

Naresh Dalal
Committee Member

Approved:

Joe Schlenoff, Chair, Department of Chemistry and Biochemistry

Professor Joseph Travis, Dean, College of Arts and Sciences

The Graduate School has verified and approved the above-named committee members.

ACKNOWLEDGEMENTS

I would like to thank Professor Geoffrey F. Strouse for his insight and patience over the years. I would also like to thank the members of the Strouse group, both past and present, for all the helpful conversations and support. To Professor Stiegman and his research group, thank you for patiently answering all the crazy questions I had about sol-gels. I would like to thank my husband Artjay and my family for their unflagging belief in me.

— Melissa

TABLE OF CONTENTS

List of Figures	vii
Abstract	xii
1. INTRODUCTION TO OPTICAL TRANSITIONS IN NANOMATERIALS .	1
1.1 The Scope of this Introduction	1
1.2 Nanomaterials	1
1.3 Quantum Effects	5
1.4 The Exciton	7
1.5 Optical Transitions in CdSe Quantum Dots	11
1.6 Chemically Prepared CdSe Quantum Dots	14
1.7 Overview of Chapters	17
2. OPTICALLY PROBED MOLECULAR ADSORPTION ON NANOSCALE CDSE SURFACES	19
2.1 Introduction	19
2.2 Experimental	25
2.3 Results and Discussion	26
2.4 Overview	35
2.5 Chapter Summary	38
3. PHOTOLUMINESCENCE OF QUANTUM DOT EMBEDDED XEROGELS	40
3.1 Motivation	40
3.2 Introduction	41
3.3 Experimental Method	43
3.4 Results	45
3.5 Chapter Summary	53
4. IMPROVED STABILITY OF QUANTUM-DOT EMBEDDED XEROGELS .	54
4.1 Motivation	54
4.2 Introduction	54
4.3 Experimental	58
4.4 Curing: Heat, Vacuum, Humidity	60
4.5 Super Dry Xerogels	63
4.6 Solvent Effects	67

4.7 Different Quantum Dot Guests	67
4.8 Chapter Summary	74
5. CDSE QUANTUM DOTS EMBEDDED INTO POROUS GLASS	75
5.1 Motivation	75
5.2 Introduction	76
5.3 Experimental Methods	77
5.4 Results and Discussion	78
5.5 Chapter Summary	86
6. NANOCRYSTALLINE SENSORS: VAPOR SENSING IN GLASS, FILM, PLASTIC AND LIQUID	87
6.1 Motivation	87
6.2 Introduction	88
6.3 Experimental	92
6.4 CdSe Quantum Dots Dissolved in Toluene	94
6.5 Thin Evaporated Films of CdSe Quantum Dots	96
6.6 CdSe Quantum Dots Embedded in Polystyrene	98
6.7 CdSe Quantum Dots Embedded in VYCOR [®]	102
6.8 Chapter Summary	106
7. EXCITED STATE THERMALIZATION OF CDSE QUANTUM DOTS WITH THE DETAILED BALANCE METHOD	108
7.1 Motivation	108
7.2 Overview of Excited State Processes	108
7.3 Thermal Relaxation in Quantum Dots	113
7.4 Experimental	115
7.5 Overview of the Detailed Balance Method	115
7.6 Typical Molecular Fluorophores	117
7.7 CdSe Carrier Temperatures	117
7.8 The Photoluminescence Lineshape	122
7.9 Integrated Photoluminescence	124
7.10 Explaining Thermal Relaxation	124
7.11 Chapter Summary	126
APPENDICES	128
A. DERIVATION OF THE STERN VOLMER EQUATION	128
A.1 Equation	128
APPENDICES	130
B. STERN VOLMER DILUTION CORRECTIONS	130
B.1 Experimental Description	130
B.2 Volume Correction for Quencher Concentration	131

B.3 Intensity Correction for Dilution of Sensitizer	131
B.4 An MSEExcel Algorithm	132
C. MATHEMATICA® ALGORITHM: SAMPLE STERN VOLMER CALCULATIONS	134
APPENDICES	145
D. DERIVATION: THE BOLTON-ARCHER EQUATION USING A DETAILED BALANCE APPROACH	145
D.1 Thermal Equilibrium	145
D.2 The Absorption Rate	145
D.3 The Emission Rate	146
D.4 The Boltzmann distribution	146
D.5 Graphical Analysis	146
E. MATHEMATICA® ALGORITHM: SAMPLE HOT BAND CALCULATIONS	147
REFERENCES	152
BIOGRAPHICAL SKETCH	156

LIST OF FIGURES

1.1	This diagram shows how the nano-scale relates to commonly conceived entities. These scales (measured in the units of meters) are marked logarithmically	3
1.2	This diagram dimensions confinement reducing a bulk structure as well as the generally accepted names for such structures. The left-hand column is a cartoon depicting a typical solid based on the number of dimensions of confinement (middle column)	4
1.3	Plot of surface-to-volume ratio of a perfect sphere as a function of sphere diameter. The x-axis is shown in nanometers to correlate with typical quantum dot sizes. Shaded area represents the region of interest in CdSe quantum dot sizes.	8
1.4	Photoluminescence and absorbance spectra of 3.5nm CdSe quantum dots coated with hexadecylamine, dissolved in toluene	12
1.5	Chemical Structure of some common ligands that are used to passivate the CdSe quantum dot surface. This is done either during preparation or as a second step following it. Ligand A is hexadecylamine (HDA), Ligand B is dodecylamine (DDA), Ligand C is tri-octylphosphine oxide (TOPO), and Ligand D is aminopropylethoxysilane (APeS)	16
2.1	Emission spectrum ($\lambda_{ex} = 360$) of anthracene ($1 \times 10^{-5} M$) in toluene at room temperature with 3.5nm DDA capped CdSe quantum dots. Arrows indicate the loss of anthracene emission and the increase in CdSe emission with increasing CdSe concentration. Inset: Stern-Volmer Plot of the steady state quenching data. Data is fit to Eq. 3 as shown by the solid line	27
2.2	Time resolved quenching study of anthracene emission in toluene at room temperature with increasing 4nm DDA-CdSe concentration. Closed circles indicate the change in the lifetime fit to a first order decay. Open circles indicate the change in the total emission intensity as a function of CdSe concentration.	29

2.3	The static association constant, as found in Eq 3 was plotted against the surface area, using a spherical model of CdSe, with different sizes and capping ligand of CdSe. Circles represent the dots capped with DDA, squares are capped with HDA, and triangles are the TOP/TOPO capped dots. Lines shown are guides to the eye.	32
2.4	The static association constant for anthracene and 3.5nm HDA-CdSe, as found in Eq 3 was plotted against the mole fraction of toluene with different co-solvents hexane (closed circle), chloroform (open circle), acetonitrile (inverted triangle). Lines shown are guides to the eye.	36
2.5	Proposed kinetic model for dye interaction with quantum dots. Photoexcitation of pre-associated dye results in instantaneous quenching. There is an equilibrium between the complexed and non-complexed dye that is described by the static association constant, K_s . However, the non-complexed dye still in solution becomes excited and then diffuses to the dot, becoming quenched at a maximum rate of k_d , limited by the solvent type. Proposed quenching mechanism is likely to be resonant energy transfer.	37
3.1	Diagram of CdSe Sol. The top diagram shows the CdSe nanocrystals embedded in the sol-gel matrix while the bottom figure is an expanded view to show how the nanocrystals are connected to the sol matrix. The primary amine in APeS binds to the nanocrystal surface while its silicate end has cross-polymerized with TMOS.	44
3.2	Photograph of a representative monolith at room temperature taken with a commercially available digital camera. CdSe nanocrystals (3.5nm diameter) capped with APES (Amino-propyl ethoxysilane) are embedded in a silica based sol-gel. (A) The sol-gel is in the test tube mold that was used to cast the gel in. (B) The sample is illuminated by a UV handlamp at approximately 365 nanometers under room light. (C) The sample is illuminated by a UV handlamp at approximately 365 nanometers with no other light source. The photograph was not digitally enhanced.	46
3.3	Photoluminescence spectra of a CdSe nanocrystal (3.5nm), dissolved in solution (solid line) and incorporated into the sol-gel matrix (dashed line)	48
3.4	Plot of the photoluminescence CdSe nanocrystal (3.5nm) as a function of the concentration of water used in the initial reaction. The traces represent different TMOS:water:methanol ratios: (A) 3:2:6, (B) 3:1:6, (C) 3:0.5:6, (D) 3:0.25:6, (E) 3:0:6	50

3.5	Photoluminescence intensity of CdSe nanocrystals embedded in a sol-gel matrix tracked over time for different concentrations of water. The traces represent different TMOS:water:methanol ratios: (A) 3:2:6, (B) 3:1:6, (C) 3:0.5:6, (D)3:0.25:6	52
4.1	Photograph of a standard gel drying apparatus. Shown in the picture are a desiccator, a sol-gel within the test tube reactor, and a hydrometer. The humidity in the desiccator was monitored by the hydrometer.	61
4.2	The photoluminescence intensity of a 3.5nm CdSe embedded sol-gel sealed in a desiccator was monitored during its curing phase and beyond. The sol-gel remained in the dry dessicator environment over the course of the entire experiment. The line connecting the points is a guide to the eye.	64
4.3	The emission intensity of a gel that had been carefully dried for 2 weeks in a humidity controlled environment was monitored when it was exposed to ambient conditions. This data is plotted as a percent change, with the max intensity at time zero being 100. At the same time, corresponding measurements of the samples mass were recorded.	66
4.4	Two 3.5nmCdSe embedded sol-gels were created under identical synthetic conditions, with the only variation being the solvent used. The initial emission from the gel synthesized with aceto is almost double the emission intensity of the gel created using methanol as a co-solvent.	68
4.5	The photoluminescence intensity of xerogels containing either: CdS, CdSe or CdTe quantum dots. monitored over the course of gel curing. Time zero corresponds to the addition of the reaction mixture. Curing took place under ambient conditions.	69
4.6	Photoluminescence spectra of ZnS-coated CdSe quantum dots embedded in a silica xerogel, with different starting water concentrations (A,B,C). All quantum dots showed identical emission spectra at the moment of reaction (represented by the curve called Initial). Two months after curing, the emission spectra changed depending on water concentration: 2 parts water (A), 1 part water (B) and 0.5 parts water (C).	72
4.7	Digital photograph of three ZnS-coated CdSe quantum-dot embedded xerogels inside their reaction test tubes, illuminated with a UV light after two months curing in ambient conditions. The labels (A), (B) and (C) correspond to their respective spectra in Figure 4.6	73
5.1	Photograph of disks of VYCOR [®] embedded with CdSe-HDA, under UV illumination. The fractured disk (both halves are labeled A) is embedded with 3.5nm CdSe-HDA. The disk labeled B is embedded with 5nm CdSe-HDA. The VYCOR [®] disks emit brightly and are translucent to the eye. . . .	79

5.2	Photoluminescence spectra of a VYCOR® disk soaked in a solution 5nm CdSe-HDA/toluene is shown at differnt time intervals. There is a steady increase in emission intensity over a 48 hour period of immersion.	81
5.3	Photoluminescence spectra of a 5.0nm CdSe embedded VYCOR® disc before and after (8 hours) immersion in pure toluene	83
5.4	The maximum photoluminescence intensity of a sample of VYCOR® embedded with 5nm CdSe quantum dots was monitored over time. After 48 hours the sample was removed from the quantum dot soak and allowed to dry under ambient conditions. The emission intensity remained steady over time. . . .	85
6.1	Stern-Volmer plot of 3.5nm CdSe-HDA quantum dots being quenched by TNT. Inset: Corresponding photoluminescence spectra of CdSe quantum dot photoluminescence at different concentrations of TNT. AS TNT concentration increases, photoluminescence intensity decreases (as indicated by the arrow)	95
6.2	A and B are two drop-cast films of 3.5nm CdSe-HDA quantum dots. A was used as a control while B was exposed to TNT for 24 hours. After 24 hours Film A is shown in Panel C , and Film B in D	97
6.3	Photoluminescence spectra of 3.5nm CdSe quantum dots embedded in a polystyrene film compared to its parent solution (in toluene)	100
6.4	Photoluminescence spectra of 3.5nm CdSe in a polystyrene film after TNT exposure for 24 hours	101
6.5	Digital Photographs of 3.5nm CdSe quantum dots embedded in a polystyrene film, illuminated with a UV handlamp. Image A is the (unexposed) control while Image B has been exposed to TNT for 24 hours	103
6.6	Photograph of CdSe quantum dots embedded into VYCOR® discs. Disc on the left has been exposed to TNT, disc on the right has not. Note that only the surface of the left disc was TNT exposed, thus the edge is still emitting .	104
6.7	Photoluminescence spectra, before and after exposure to TNT, from 3.5nm CdSe quantum dots in in VYCOR®	105
7.1	Excitation spectrum of anthracene in ethanol (solid line), overlayed with the excitation-energy dependent excited state temperatures as determined with the Bolton-Archer method (open circles with error bars).	118
7.2	Fit (solid line) of Eqn. 7.1 (open circles) for CdSe(3.5nm)-HDA/toluene excited at 320nm. The fitted slope of the line is -20.3 which corresponds to a temperature of 570K by solving for the temperature in Eqn. 7.1. Inset shows the absorbance spectrum and the emission spectrum of the sample at 320nm.	119

7.3	CdSe(3.5nm)-HDA dissolved in toluene at room temperature extinction spectrum, and excited state temperatures extracted at different excitation energies using the detailed balance method. Vertical dashed lines indicate expected positions of $1P_{3/2} - 1P_e$ and $1P_{1/2} - 1P_e$	121
7.4	The intensity-normalized photoluminescence lineshape obtained for CdSe(3.5nm) at different excitation energies.	123
7.5	CdSe(3.5nm)-HDA dissolved in toluene at room temperature, extinction spectrum, and spectrally integrated band-edge photoluminescence(arb.u.) at different excitation energies	125
7.6	Illustration of the effect of the efficiency of carrier-phonon-bath coupling on the photoluminescence lineshape, showing “poor coupling” (left) and “strong coupling” (right). The states shown are: bee=band-edge exciton, cgs=crystal ground state and e/h=higher-lying excited state.	127

ABSTRACT

The next generation of sensors built upon nanotechnology is rapidly coming to the forefront of scientific applications, with particular application to contemporary global concerns including counterterrorism and device miniaturization. The challenge of incorporating these materials as a stable sensor package is discussed, with special emphasis on condensed phase media, particularly sol-gels, porous glasses and organic solutions. Specifically, incredibly stable, strongly emitting CdSe quantum dots have been incorporated into several glasses and plastics, and are able to detect the presence of organic moieties, the most notorious of which is TNT, through photoluminescence quenching. The mechanism by which this operates is a through-space, long-range resonant transfer of electronic excitation energy, which is further enhanced by a strong binding affinity of the various analytes to the quantum dot surface. New sensor technology based upon quantum-confined, optically-active semiconductor nanomaterials represents an important step in realizing small-scale, highly sensitive and smart sensors.

CHAPTER 1

INTRODUCTION TO OPTICAL TRANSITIONS IN NANOMATERIALS

1.1 The Scope of this Introduction

This chapter is provided primarily for the chemist who is new to the field of nanomaterials[1]. It contains an overview of the field with a focus on the important aspects and terminology of nanomaterials in general. Additionally, it contains the unique perspective of a chemist's approach to understanding solid-state physics by showing how solid-state phenomena have their molecular counterparts. The approach is of a conceptual understanding of nanomaterials rather than a rigorous mathematical description of quantum phenomena. Specifically it contains the necessary background to understand the photoluminescence of quantum dots, which is the underpinning phenomenon that permeates this entire dissertation.

1.2 Nanomaterials

1.2.1 The Age of Nanotechnology

Advances in Lithography and Fabrication

The last 30 years have seen an explosion in the growth of humankind's ability to manipulate structures at incredibly small scales. Technologically speaking, the importance of this scale has been driven primarily by the miniaturization of electronic components. Since the birth of the transistor, the pressing need to create smaller and smaller solid-state semiconductor structures for computational purposes has spurred the development of a variety of analytical tools (TEM, SEM, etc...) and fabrication methods that allow direct observation and manipulation of objects at the nanometer scale.

Modern lithographic methods utilize etching methods on bulk silicon, metal evaporation

or beam lithography to produce these hyperfine structures. While these methods have been shown to produce complex, controlled architectures, they are limited in scale and material. The role of non-lithographic methods for creating complex architectures from a “bottom-up” perspective is currently being realized.

The Role of Chemistry

Arguably, chemistry has been doing nanomaterials for hundreds of years: large molecules are measured in tens of nanometers. However, the role of chemistry in the nanomaterials field is relatively young compared with its engineering counterparts. The big difference is the focus of the nanomaterials field on the importance of the solid-state[2], which contains important processes not found in macromolecules, the most important of which is electrical conduction. The young chemically-related fields emerging to fill this need are primarily the creation of organic solid-state devices (conjugated polymers, etc.) and the synthesis of inorganic nanostructures[3].

1.2.2 The Nanometer Scale

The realm of “nano” is defined by the measurement of $10^{-9}m$. Intuitively this can be difficult to conceptualize, as it is far beyond anything that can be seen with the bare human eye. Figure 1.1 shows some recognizable objects as they relate to a scale in which they can be measured.

Solid-state Nanomaterials

While any material, organic or inorganic, that falls into this minute size range can be classified as a nanomaterial, the focus of this work will be on nano-sized clusters of bulk materials known as nanoparticles or quantum dots. These small clusters of atoms have been known for centuries, but only recently has their potential been fully explored. With intriguing optical properties not observed in bulk materials, extremely high surface to volume ratios, and facile synthetic options, these materials have a range of potential applications from sensors, solid state lighting, catalysis, cancer and disease treatment, gene therapy, and even simply shrinking the size of existing electronic devices.

The “Nano-scale”

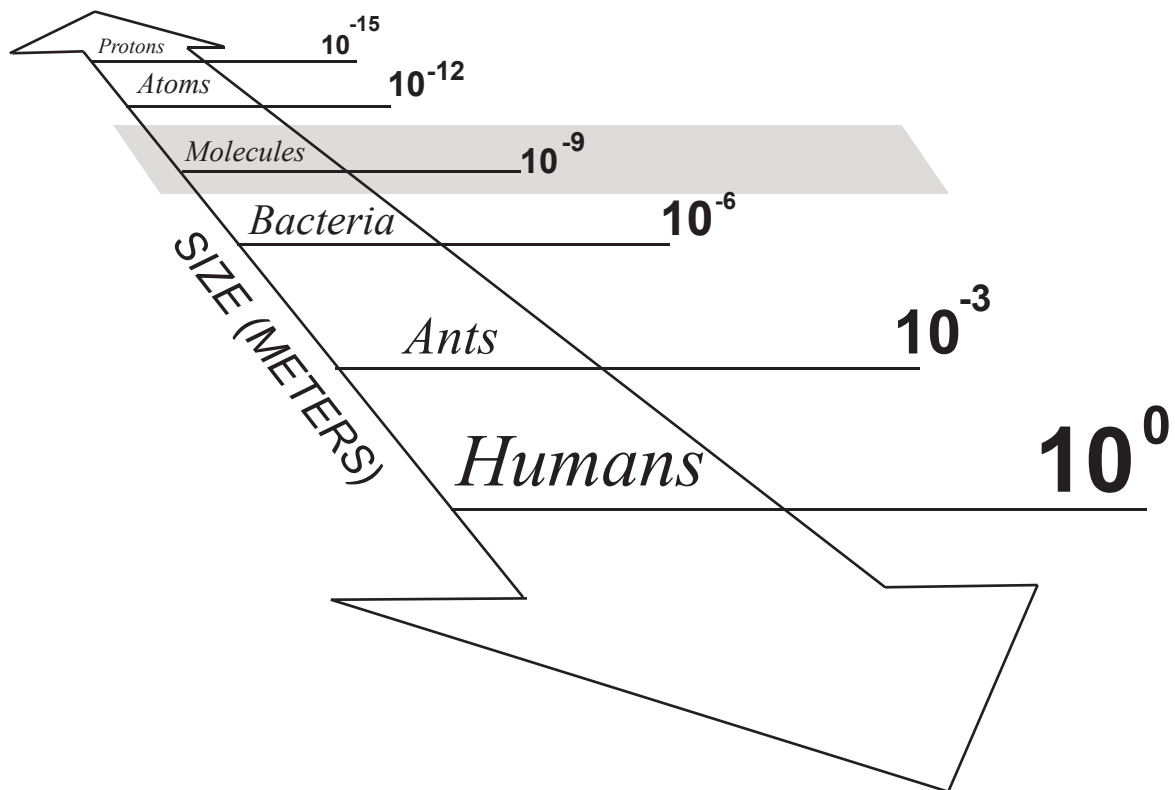


Figure 1.1: This diagram shows how the nano-scale relates to commonly conceived entities. These scales (measured in the units of meters) are marked logarithmically

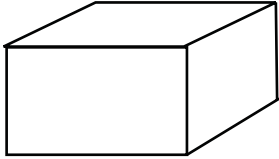
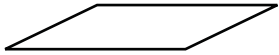


Shape	Dimensional Confinement	Name
	0	Bulk
	1	Quantum Well
	2	Quantum Wire
	3	Quantum Dot

Figure 1.2: This diagram dimensions confinement reducing a bulk structure as well as the generally accepted names for such structures. The left-hand column is a cartoon depicting a typical solid based on the number of dimensions of confinement (middle column)

1.3 Quantum Effects

1.3.1 Quantum Confinement

The quantum nature of matter is an undeniable, though not always obvious part of material study. Therefore, even though quantum interactions are the underpinning foundations of matter itself, it is not unusual to describe them with their own term. In this case, in the study of the solid-state, the idea of quantum confinement comes directly from our understanding of quantum phenomena beginning to manifest themselves as a function of decreasing material size[4].

1.3.2 Quantum Effects in the Bulk

For example, let's examine a bulk 3-dimensional solid composed of atoms. In many ways these atoms act coherently and it is commonplace to define their collective vibrations in terms of phonons, which is simply a crystal vibration. As we will see later, other particles are defined in the solid-state such as excitons and polarons[2], all of which by definition require an infinitely large crystal as their mathematical definition. This requirement comes, for example, from the symmetry of their overlapping electronic wavefunctions which can define other solid-state phenomena such as the band gap[2]. Indeed, much of the solid-state physics derives directly from these quantum phenomena which themselves require infinitely large solids for infinite accuracy.

In reality no solid is infinitely large but these bulk phenomena are still present in solid-state materials which contain hundreds of thousands of atoms. Therefore, the very foundation of solid-state physics has an intrinsic size requirement because these interesting solid-state pseudo-particles would not exist otherwise. In other words, a phonon does not exist with only two bound atoms. Importantly, this interaction is a molecular vibration and a rudimentary way of describing a phonon is simply a sum of coherent molecular vibrations from many interlinked bound pairs of atoms[5]. In essence, this is the defining feature of nanomaterials: the boundary where solid-state physics begins to emerge from molecular chemistry.

1.3.3 Quantum Wells: 1D Confinement

If we take a bulk solid and begin to chip away at its top and bottom, we slowly begin to approach the dimensions of a plane. As we continue this process and the solid shrinks more it reaches the thickness of a sheet of paper. As we continue to shrink the solid beyond this limit, we will begin to witness the appearance of quantum effects in this incredibly thin sheet. This very thin sheet of bulk solid can now be called a “quantum well.” Typically, quantum wells are formed by ion beam lithography or evaporation methods, wherein atoms are deposited on flat solid substrates to form very thin films.

1.3.4 Quantum Wires: 2D Confinement

If we take the quantum well we just formed and begin chipping away at it from the left and right, it will begin to narrow. Continuing further, its width decreases so that the material itself now resembles something like a string, then something more like a human hair, then becomes even smaller so that it can only be really visualized in an electron microscope. This new material is a “quantum wire.” Sometimes, when the aspect ratio decreases this can be called a “quantum rod” or a “nanorod,” though usually this term is reserved for preparations that are related to quantum dots (described below). Many lithography and wet chemical methods can be used to make these quantum wires.

1.3.5 Quantum Dots: 3D Confinement

If the ends of the quantum wire are chipped away slowly, it will begin to shrink. As this process is continued, the wire becomes a rod and eventually the aspect ratio is very close to unity and we are left with the “quantum dot.” This is the model of quantum confinement, being restricted in all three dimensions. This is also the ideal model for studying quantum phenomena because it lacks any bulk characteristics in which the electronic and vibrational degrees of freedom can be described by a periodic coherent oscillation over a given volume or number of atoms. For example, a quantum wire could conceivably have a phonon vibration because its atoms are lined up side by side for a very long distance, allowing the coherent oscillation of all atoms to be described as a periodic function along the 1-D line. A quantum dot, therefore, manifests only phenomena related to quantum confinement in a lattice that is smaller than the volume required (number of repeating atoms) to describe the periodic

properties of the system.. These particles can be made using beam lithography or through wet-chemical methods. Wet chemical methods happen to prepare the more versatile of these at a lower cost, and typically of better performance and with less structural defects.

1.3.6 Surface to Volume Ratio

As the particle decreases in dimension, the surface to volume ratio changes as $1/r$. This leads to another important aspect of nanomaterials, the large surface-to-volume ratio. The surface is a useful material feature since it provides the interface between the material itself and its environment. For example, the action of catalytic converters are dependent on the interaction of a gas with the metal catalyst surface. With increased surface area, this process could proceed faster. Moreover, if the surface to volume ratio could be manipulated, then surface-dependent processes could be increased without increasing the mass itself.

In Figure 1.3, the surface-to-volume ratio of a simple sphere($3/r$) is plotted as a function of size (sphere radius, r). It should be noted that a sphere is the shape with the smallest surface-to-volume ratio, which is the most conservative estimation. Solids of similar size can be formed with higher ratios. For example, actual quantum dots have faceted surfaces and aspect ratios slightly greater than unity, and consequently their surface-to-volume ratios will be slightly higher than Figure 1.3.

As can be seen, the surface-to-volume ratio increases as sphere decreases. The shaded region represents the region-of-interest for CdSe quantum dots. Sizes below the shaded region exhibit molecular characteristics and cannot really be called quantum dots, and are better referred to as clusters. Sizes above the region of interest show limited quantum effects, primarily due to the size beginning to approach the exciton Bohr radius (discussed in detail below). These larger nanomaterial sizes fall into the “weakly confined regime” and their behavior is much more related to bulk semiconductors.

1.4 The Exciton

1.4.1 Semiconductor Optical Processes

Electronic transitions in semiconductors are generally described by the promotion of an electron from the valence band to the conduction band, where the energy for the transition is the band gap. When the band gap energy is 1.55eV to 3.1eV, these transitions fall within

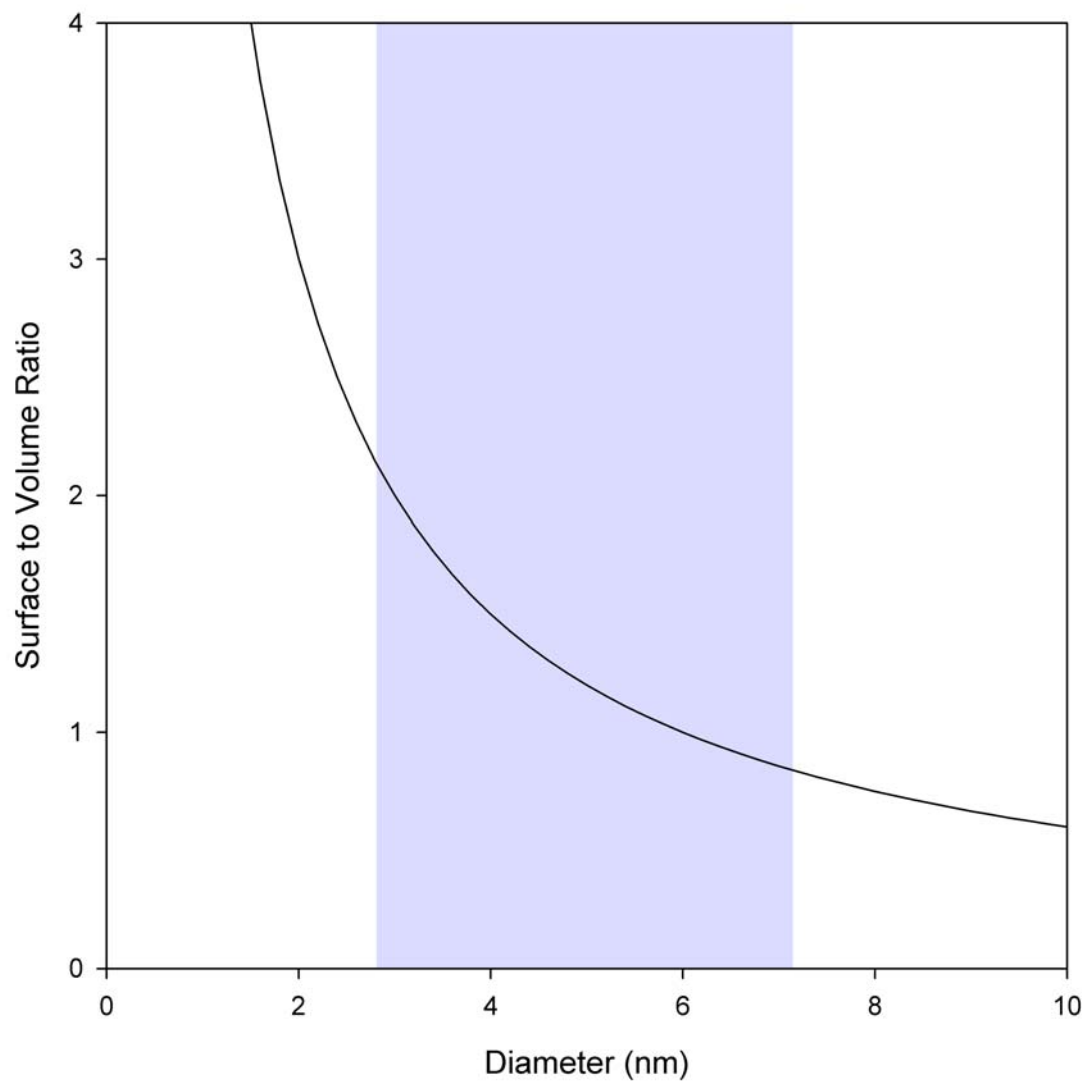


Figure 1.3: Plot of surface-to-volume ratio of a perfect sphere as a function of sphere diameter. The x-axis is shown in nanometers to correlate with typical quantum dot sizes. Shaded area represents the region of interest in CdSe quantum dot sizes.

the visible range, and are called optical transitions[2]. The absorption of a photon of light results in the promotion of an electron in the valence band to the conduction band, leaving behind a “hole” in the valence band where the electron used to be. In this excited state, both the electron and the hole are free to migrate within the crystal lattice itself, being bound only by the physical boundaries of the crystal. Since the electron and hole can have different energies, they exhibit different momentum and can behave either as individual carriers if the binding energy is small, or as a wave packet if the binding energy is large. Interesting solid-state processes can occur with these charge carriers at this point, for example, interacting with a crystal vibration (phonon) to form a “polaron,” in effect, a charged distortion of the crystal lattice.

1.4.2 The Exciton Bohr Radius

The Exciton Binding Energy

Typically however, the existence of a negative charge (electron) and a positive charge (hole) in a finite crystal will inevitably lead to a mutual Coulombic attraction and the electron and hole will be pulled toward each other. This new entity, which consists of a bound electron-hole pair is called an “exciton” [2]. Upon formation, kinetic energy is released into the crystal lattice as the exciton settles into a lower energy state. The energy lost is called the “exciton binding energy” to signify that if energy is added to the exciton of that same amount, the electron and hole will have enough energy to escape the Coulombic force that holds them. Consequently, the net energy of the exciton itself is the difference between the electronic band gap and the exciton binding energy. Importantly, because of this, the exciton is the lowest energy excited state and is very likely to form within the crystal. Generally speaking, all excited state relax toward the exciton state rapidly, and consequently, most excited state phenomenon is derived directly from the exciton.

The Bohr Radius

An important feature of the exciton is the so-called “exciton Bohr radius” which describes the average distance between the electron and hole in an exciton. The Bohr radius is based solely on the chemical composition of the crystal lattice. It is a function of only two parameters: the dielectric constant of the semiconductor and the effective mass of the exciton. The exciton effective mass is itself based on the electron and hole effective masses, which are directly

dependent on the nature of the lattice. The larger the Bohr radius, the weaker the exciton binding energy. Different semiconductors have different exciton Bohr radii. For CdSe, the Bohr radius is roughly 5.5nm. This factor is critical to understanding quantum dot behavior.

1.4.3 Quantum Confinement Regimes

Typically, two size regimes of semiconductor nanomaterials are defined based upon the Bohr radius, and therefore vary from material to material. Sizes of nanomaterials with dimensions larger than the Bohr radius are described as “weakly confined” and their quantum effects are notably diminished as compared with their smaller cousins. Nanomaterials with dimensions smaller than the exciton Bohr radius are “strongly confined” and possess strongly size-dependent behavior. Quantum effects manifest themselves dramatically in this regime and the effect of size is undeniable. Consequently, the strongly confined regime is the most studied, and the most useful.

Intuitively, we can see why the Bohr radius is important. As the size of the crystallite itself becomes smaller than the average distance between the electron and hole, they become squeezed into a tighter space, and their energy increases because of this additional stress. Their wavefunctions have been confined strongly into this very small space. When the crystallite is larger than the average distance between the electron and hole, there is no additional stress, and the exciton behaves similarly to the identical bulk material.

Strong Confinement: Particle-in-a-Box

There exists a very simple method of looking at quantum confinement and making predictions on the energy levels based on size. To do this, the particle-in-a-box method can be utilized[6]. It is important to recall here, that this model is different from other quantum chemical calculations due to the shape of the potential well, and thus the energy spacings will be different from molecular counterparts. As an example, the hydrogenic atom utilizes a central potential and the energy spacings grow smaller as they increase. Likewise, the simple harmonic oscillator’s potential is parabolic and the energy spacing remains constant with higher energy levels. For particle-in-a-box, the potential well is zero within the box, and infinite at the edges and consequently, the energy spacing increases with increasing energy. In our utilization of this model for quantum dots, it is natural to use the exciton as the particle

and the quantum dot as the box, with the exciton effective mass replacing the particle mass and the boundaries of the box defined as the boundaries of the small crystallite.

1.4.4 The Brus Equation

An intuitive approach to understanding quantum dots utilizing the particle-in-a-box approach was performed by L.E. Brus[7], and popularly called the “Brus Equation.” Several particle-in-a-box relationships can be seen in it:

$$E = E_{gap} + \frac{\hbar^2 \pi^2}{2\mu R^2} - E_{ex} \quad (1.1)$$

Here, μ is the exciton effective mass, R is the quantum dot radius, E_{gap} is the bulk electronic band gap, ϵ is the semiconductor dielectric constant. Note that the appearance of the effective mass and the dielectric constant show that the Bohr radius is implicitly contained in this equation. The term with $1/R^2$ is typically called the confinement term and is identical to the particle-in-a-box relationship. The term containing $-1/R$ is typically referred to as the Coulombic term since it represents the attraction of the electron and hole for each other. Intuitively we can see the direct effect of quantum confinement from this elegant equation. The first and third terms are the electronic band gap and exciton binding energy, which are found in all bulk semiconductors of this type. The second term contains the size-dependent quantum behavior that is the defining characteristic of all quantum dots in the strongly confined regime.

1.5 Optical Transitions in CdSe Quantum Dots

1.5.1 Absorbance

Bulk CdSe

The absorbance spectra of CdSe quantum dots shares many similarities with both bulk semiconductor spectra as well as those of molecules. Bulk semiconductors typically show a weak transition slightly below the band edge that corresponds to the exciton, followed by an increasing and smooth absorption profile toward low wavelengths. This smooth profile is a result of the nearly continuous absorption of photons by creating electrons and holes higher in their respective bands. CdSe quantum dots display this smooth continuous profile.

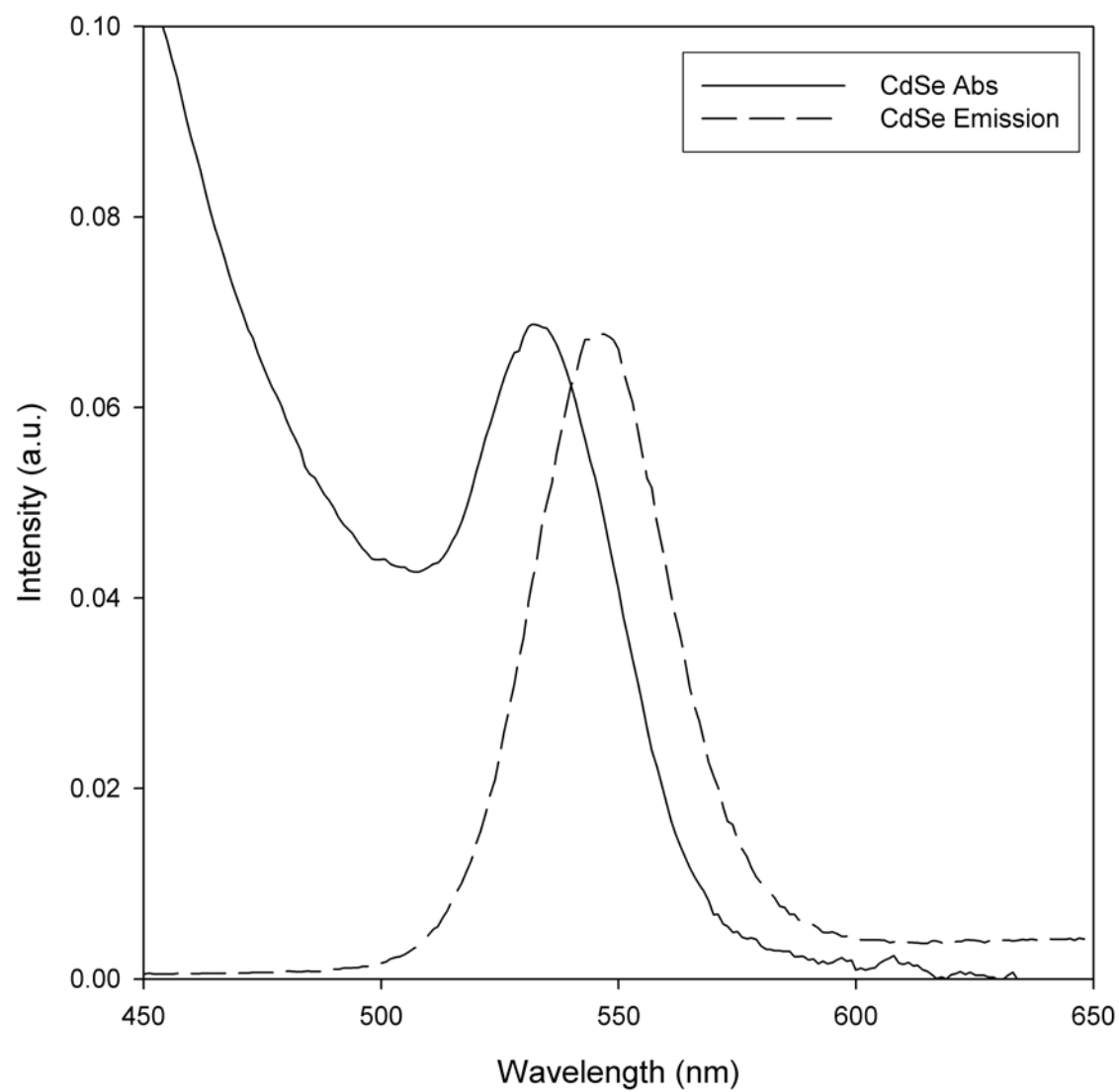


Figure 1.4: Photoluminescence and absorbance spectra of 3.5nm CdSe quantum dots coated with hexadecylamine, dissolved in toluene

Band Edge Exciton

Molecular transitions, being discrete, typically have much sharper features with some vibrational component coupling with the electronic transition. These sharp transitions correspond to specific excited states typically involving the π -molecular orbitals for UV-visible transitions. CdSe quantum dots possess these discrete transitions as well, resulting from higher energy excited states which are actually derived from the exciton and follow particle-in-a-box rules with regard to their energy dispersion versus size.

Therefore, the lowest energy exciton is called the “band edge exciton,” and similar to the bulk semiconductor, it lies just below the band edge energy. However, unlike the bulk semiconductors wherein the exciton is typically a weak feature that is often very difficult to distinguish, the band edge exciton in quantum dots is a very sharp and strong feature. This feature stands out so well from the continuous background absorption that the size of the quantum dot itself can be determined from the peak of the band edge exciton absorption. This strong transition is aided primarily by the small quantum dot sizes, which makes exciton formation much more likely since it confines the carriers, restricting them from diffusing away from each other as they likely would in a bulk semiconductor.

Term Symbols for Excitons

There exists an elaborate terminology for labeling the exciton states in CdSe quantum dots[8]. Briefly, these term symbols separate the electron and hole states and label each with their spin-band coupling number($J = 1/2, 3/2, \dots$), which is necessary due to valence band degeneracy. The conduction band is non-degenerate and therefore is always the same: the spin of the electron, $s = 1/2$, and is commonly left out, writing this quantum number only as “ e ”. The exciton states are additionally labeled with the orbital shape resulting from a single carrier trapped in a particle-in-a-box ($L = S, P, D, \dots$). Finally each energy level is labeled numerically, starting with the lowest energy (1,2,3...). Just from this description, we can tell that the band-edge exciton will result from the lowest energy states of both the electron and hole and will therefore contain two “1’s.” The term symbol for the band-edge exciton (the most important excited state) is $1S_{3/2} - 1S_e$.

1.5.2 Photoluminescence

Decay Pathways

The photoluminescence from quantum dots results exclusively from the band-edge exciton. From this starting point (which follows photo-excitation and relaxation), the band-edge exciton will spontaneously decay through several pathways. Like molecular photochemistry[5], these pathways can be separated into radiative and non-radiative. The radiative decay is only the photoluminescence (since it results in a photon of light)[9], while the non-radiative decay composes a variety of different processes. Like molecules, one of these non-radiative processes is the dissipation of that excitation energy through vibrations and translations, which results in heat being released to the environment.

However, just like molecular photo-chemistry another pathway is “photo-degradation” wherein the high energy excited state results in destruction of the particle. The most common of these is photo-oxidation wherein reaction of the high energy carriers with oxygen results in oxidation of the particle surface. This process is highly problematic for quantum dot stability and will be a major focus of this dissertation.

Like molecules, the excitation energy can be transferred to other nearby agents. Typically these agents must be nearby, unexcited and have an electronic transition that is close to the energy of the excitation energy. This process is called “electronic excitation energy transfer”[5]. The result of this transfer is that the quantum dot returns to its ground state, while the species accepting energy is promoted to its excited state. This process is highly manipulable and will be the focus of a large part of this dissertation.

1.6 Chemically Prepared CdSe Quantum Dots

1.6.1 Preparation

Organometallic

Chemical preparation produce the highest quality and largest quantity of quantum dots. The most prominent of these methods is the injection of organometallic cadmium into a hot coordinating ligand solution in inert atmosphere. The resulting solution is then purified by selective precipitation and the resulting particles are reasonably mono-disperse and capped with ligands like tri-octylphosphine oxide (TOPO) and tri-octylphosphine (TOP). The chemical structure of TOPO can be seen in Fig. 1.5.

Seed Method

A second method that also produces very high quality quantum dots uses a different approach[3]. “Seeds,” small molecular clusters containing cadmium, are introduced into a hot coordinating solvent. Unlike the organometallic method, these quantum dots are grown slowly from these “seed crystals,” increasing in size as the reaction progresses. Once purified, these solutions are also reasonably mono-disperse. Typically the ligand used for this process is a primary amine like hexadecylamine(HDA), which is shown in Fig. 1.5. The majority of the quantum dots used in this work have been prepared with this method[3].

1.6.2 Ligand Exchange

The ligands used in synthesizing quantum dots can be replaced by other ligands. This is done by simply placing the quantum dots in a concentrated solution containing these ligands (and heating if necessary). Stronger coordinating ligands tend to work better, since this process is controlled by an equilibrium between bound and unbound states of the ligand and the quantum dot. Strong coordination favors the bound state and with enough time, the majority of the quantum dot surface can be “recapped” with an appropriate ligand. Some advantages of this step include the ability to functionalize the quantum dot surface with moieties that chemistry can be performed on. This dissertation uses ligand exchange in several places, notably in the creation of sol-gels wherein aminopropylsilane (APS) and aminopropylethoxysilane (APeS) displaces hexadecylamine (HDA).

1.6.3 Inorganic Shells

Another post-synthesis step that is used to improve the performance (especially optical) of CdSe quantum dots is the addition of an inorganic shell. Typically this shell has a higher bandgap and is more resistant to oxidation. The most common of these are ZnS and ZnSe. This overcoating process has been shown to dramatically improve the photoluminescence quantum efficiency as well as long-term stability. The higher band gap discourages oxidation by further confining the carriers to within the dot. Additionally the more stable material prevents photo-oxidation by obstructing oxygen from physically interacting with the dot surface.

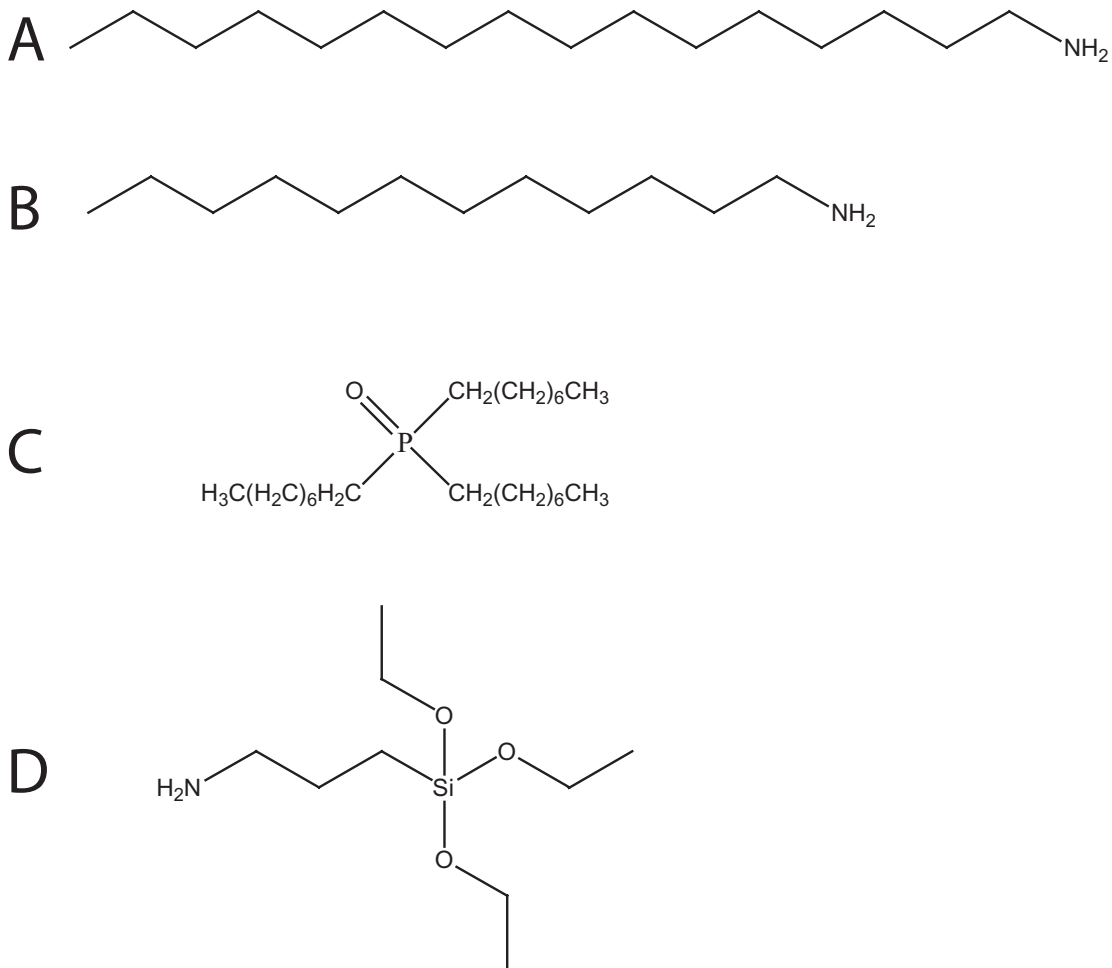


Figure 1.5: Chemical Structure of some common ligands that are used to passivate the CdSe quantum dot surface. This is done either during preparation or as a second step following it. Ligand A is hexadecylamine (HDA), Ligand B is dodecylamine (DDA), Ligand C is tri-octylphosphine oxide (TOPO), and Ligand D is aminopropylethoxysilane (APeS)

1.7 Overview of Chapters

1.7.1 Liquid Phase Studies

Stern-Volmer

In Chapter 2, solution phase interactions between CdSe and a simple organic dye, anthracene, are used to optically explore the fundamental interactions between the quantum dot and an analyte. Use of Stern-Volmer analysis show that there is a large static pre-association event that dominates over diffusion controlled quenching. The surface area of the quantum dot, choice of ligand, and solvent polarity all play a role in determining the affinity that an analyte has for the pre-association.

Carrier Temperatures

Carrier temperatures were determined for CdSe using the detailed balance method in Chapter 7. High temperature values are measured, suggesting that poor phonon-bath coupling may be occurring.

1.7.2 Solid-State Studies

Sol-gels

Chapter 3 and Chapter 4 CdSe quantum dots were embedded in a sol-gel. The quantum dots were first capped with aminopropylethoxysilane and then added to the sol-gel mixture. Water, essential for sol-gel production, was shown to also negatively effect both the intensity and long term stability of emission from CdSe. The highest quality materials were produced under conditions that minimized water in the sol-gel reaction and aged the gels in dry environments.

Porous Glasses

In Chapter 5 CdSe quantum dots were embedded in a commercially available material, porous VYCOR[®]. The VYCOR[®] was placed in a solution of CdSe. Unlike the previous sol-gel work, the resulting material was not a true hybrid; the quantum dots only appeared to be associated with the surface of the VYCOR, rather than dispersed throughout the material. However, the CdSe-VYCOR[®] produced robust materials with long term photostability.

TNT Sensing

The incorporation of CdSe quantum dots into various substrates and matrices for potential TNT sensing is explored in Chapter 6. Simple devices created using the emission of CdSe as a reporting signal quickly showed that a porous framework is important for detection. Based on experimental results, CdSe embedded porous glass VYCOR[®], provided both quantum dot stability as well as sensitivity to TNT.

CHAPTER 2

OPTICALLY PROBED MOLECULAR ADSORPTION ON NANOSCALE CDSE SURFACES

2.1 Introduction

2.1.1 Motivation

Many proposals have centered around the idea of using nanomaterials as sensors for a variety of chemical and biological agents. The high surface to volume ratio of a quantum dot, coupled with the variety of potential surface ligands and unique optical properties work together to elevate nanomaterials as prime candidates for detection media. If these ideas are to be utilized then the fundamental interaction between the agents that are to be detected and the surface of the nanomaterial need to be explored.

While by no means complete, solution-based interactions between simple organic molecules with inorganic nanomaterials offer an excellent starting point for the basic understanding of the potentially complex interactions that may arise from the nanomaterial and the organic agents. A significant number of questions remain about the fundamental nanomaterial-organic agent interaction: What is the basis for this interaction? In what range does this interaction dominate?

2.1.2 Experimental Design: The approach to the problem

Similarities to Chromatography

The driving force for molecular adsorption on surfaces of materials is an important phenomenon in a wide range of areas as diverse as chromatography, molecular sensing, surface catalysis, or biological interfaces[10, 11, 12, 13, 14]. The binding of molecules at surfaces is dictated by the nature of the microscopic electrostatic (van der Waals) and ionic (Madelung)

interactions and is quite adequately described by Langmuir isotherms.

Affinity chromatography defines these interactions in terms of a partition coefficient ($K = \frac{C_s}{C_M}$), where $C_{s(m)}$ represents the concentration of the analyte in the stationary (mobile) phases. With regard to a nanomaterial system, the molecule serves as the analyte, the ligands bound to the nanomaterial surface serve as the stationary phase and the solvent system represents the mobile phase. Effectively, an equilibrium exists between the adsorption of a molecule onto a spherical particle (stationary phase) coated with an organic molecules and the desorption of the molecule into the solvent (mobile phase)[15]. Therefore, several features of the fundamental nature of this interaction can be deduced from the kinetics.

An important aspect of developing this system for sensor design involves specificity: the ability to distinguish between two slightly different chemical agents. This property, which chromatographers call the resolution, is primarily a function of the analyte-stationary-mobile interaction, but can be adjusted by varying extrinsic aspects such as temperature and flow (viscosity). The resolution, $R_s = \frac{2N^{1/2}(K_2-K_1)}{(K_2+K_1)}$, between two molecules is determined by their respective partition coefficients, where N is the number of theoretical plates. Increasing N increases the resolution. This is achieved in affinity chromatography by controlling surface area, the organic chain length, and the solvent choice[16].

A model system: CdSe nanocrystals and organic dyes

Analogous to a small molecule interacting with a silica particle, the concept of affinity chromatography provides a platform to describe the microscopic molecular level interactions of molecules interacting with the passivant shell of a CdSe nanocrystal. For these measurements, an organic dye is utilized as the analyte, the ligand shell capping the nanocrystal is used as the stationary phase, and the surrounding solvent is used as the mobile phase. The surface of the nanoparticle closely resembles a self-assembled monolayer over short distances that is reminiscent of a silica particle in chromatography.

The tail group and chain of the passivant are the primary agents that interact with dissolved molecules and can allow for multi-particle interactions in a scenario called “slotting,” wherein the organic dye is solvated by adjacent chains[17, 18]. Short range dipole-induced dipole or London forces can account for this situation.

Detecting the contact: energy transfer

An important piece still remains in the execution of this three-part nano-chromatography system, which is particularly how to determine that an individual dye interacts with a nanomaterial surface, or if that cannot be determined, how can that be inferred statistically. Specifically, there must be a signal that reports that the dye and nanomaterial are close enough to interact. With the appropriate choice of materials, such an interaction can be engineered so that the reported event is the spontaneous emission of a photon, which can be detected. Statistically, the emitted light intensity will vary with average dye-nanomaterial distance.

The proximity of the organic dye to the semiconductor surface can influence the nature of the packing and ultimately the optical properties of the materials[19]. Because both the organic dye and the nanocrystal are optically active species, an opportunity exists for the exchange of electronic excitations in conjunction with the restriction that the electronic transitions are spectrally overlapping. This sort of situation is referred to as “resonance energy transfer” and can proceed by a variety of mechanisms.

Measuring the molecular affinity for a nanoparticle surface is achievable using optical probes such as Förster energy transfer, commonly referred to as FRET (Fluorescence Resonance Energy Transfer) in the biological literature[20, 21]. Use of resonant energy transfer for molecular adsorption has been applied in a wide-range of studies ranging from chemical to immunoassay sensing[13, 20, 22, 23]. By investigating the efficiency of energy transfer from an organic donor molecule to the CdSe nanoparticle acceptor, the affinity partition coefficient can be directly measured by the magnitude of the intensity quenching of the donor molecule. This allows the affinity for organic molecules with the surface to be measured, a potentially important technique for sensor applications.

The complexities of quenching

A simple sensor can thus be made constituting only a solvated nanomaterial. The nanocrystals are interrogated by a beam of light, whose intensity will depend on the concentration of analyte. However, this simple design lends itself to other questions, which with some careful modeling can yield surprising results: Is the electronic ground state or excited state more likely to interact with the nanomaterial surface? How can we tell that difference?

The next three sections will cover in detail how, from simple optical measurements, the kinetics of this interaction were determined and its mechanism deduced.

2.1.3 Fluorescence Quenching

Any process that causes a decline in the fluorescence intensity of an emitting molecule can be referred to as fluorescence quenching[24], with the agent causing this effect being referred to as the “quencher”. If the fluorophore and donor diffuse freely in solution, the process follows bimolecular kinetics. In a situation like this, as the concentration of quencher species in solution increases, a decrease in the fluorescence is expected since the number of quenching events will increase proportionately.

Two mechanisms that can cause fluorescence quenching are known as static and dynamic quenching, and both are very common in solution phase bimolecular quenching. With both of these processes, contact between the donor (the fluorescing molecule) and acceptor (the quenching molecule) must occur. However, with static quenching there is a pre-association complex formed before the excitation of the donor molecule occurs. With either cause, the Stern Volmer approach can be used to measure the rates of quenching.

2.1.4 Stern Volmer Approach to Bimolecular Quenching

The simplest kinetic model for solution-phase quenching was developed with regard to a sequence where excitation of the donor species preceded contact with the acceptor, which is referred to as the Stern-Volmer model. A limitation is implied in this model: the ground states of the fluorophore and quencher have little or no attraction to each other. Quenching occurs purely by the statistical meeting of fluorophore and quencher species as they diffuse toward each other in solution, an event called “collision” in the Stern-Volmer model.

However, not every collision event results in a quenching event. The quenching event itself has its own kinetic rate, which in this case is quantum-mechanically controlled. The quenching rate k_q takes into account two processes; (1) how easily two microscopic bodies encounter each other in solution and (2) how the excited states of the donor and acceptor interact with each other. Because of (2), the quenching rate will vary from different combinations of donors and acceptors, and the Stern-Volmer model imposes the following range on the quenching rate: $0 > k_q > k_d$, where k_d is the diffusion rate.

In the case of “no quenching,” which physically means that the acceptor cannot quench the donor, $k_q = 0$. Situations like these typically occur due to energy restrictions between the donor and acceptor such as very small spectral overlap, and are inherently quantum-mechanical in nature.

In the case of “total quenching,” wherein every single collision event results in a quenching event, $k_q = k_d$. This case represents an incredibly efficient quantum-mechanical interaction of the donor and acceptor, where typically strong spectral resonance is present along with relatively short acceptor excited state lifetimes.

In every case, the quenching rate can be determined from simple steady-state fluorescence measurements by varying the quencher concentration through the Stern-Volmer equation. A derivation appears in Appendix A. The most popular form of the Stern-Volmer equation is:

$$\frac{I_o}{I} = 1 + k_q\tau_o[Q] = 1 + K_{SV}[Q] \quad (2.1)$$

where I_o is the intensity of the donor with no quencher present, I the intensity with increasing aliquots of quencher added, k_q is the rate of quenching, τ_o is the lifetime of the donor without quencher present, and $[Q]$ is the concentration of the quencher in solution.

It can be seen why Eqn. 2.1, is the most useful form since the slope of a plot of $\frac{I_o}{I}$ vs concentration of quencher molecules, $[Q]$, provides a direct measure of k_q . It is important to note that in this model, the lifetime and steady state photoluminescence for the donor and molecule will decrease inversely with increasing quencher concentration[24].

An important limitation of the Stern-Volmer mechanism is that k_q cannot exceed the diffusional rate constant k_d for a given solution at a given temperature. Such a case is physically impossible because it implies that the quencher and donor diffuse toward each other faster Brownian motion. In these cases, more physically meaningful mechanisms must be explored, such as static quenching.

Static Quenching Mechanism

A static quenching mechanism is often called “pre-association,” which refers to the event of fluorophore excitation. Whereas the dynamic mechanism of Stern-Volmer quenching has the excitation event preceding the association, or collision event, the static mechanism has the excitation event follow the collision event. This simple interchange of steps in the mechanism has important consequences for the physical interpretation of the Stern-Volmer plot.

The static mechanism has an equation strikingly similar to the Stern-Volmer equation:

$$\frac{I_o}{I} = 1 + K_S[Q] \quad (2.2)$$

with the exception that the Stern-Volmer K_{SV} has been replaced with K_S , where K_S has a distinctly different definition in this mechanism:

$$K_S = \frac{[Donor - AcceptorComplex]}{[Donor][Acceptor]} \quad (2.3)$$

K_S is an equilibrium constant derived from the pre-association step in the mechanism:



Whereas the upper limit of K_{SV} was $K_{SV} \leq 1$, the upper limit of K_S is not bounded. A large K_S value implies strong association of the donors and acceptors such that the equilibrium lies toward the donor-acceptor complex. A very small value of K_S implies very little donor-acceptor association. As this value diminishes, it reaches the upper Stern-Volmer dynamic boundary of little or no interaction, where quenching occurs only from random collisional events.

In static quenching, the measured rate of quenching can exceed the diffusional rate and is described purely by the Förster rate theory. Aside from the steady-state fluorescence measurement, static quenching can be inferred from the time-resolved lifetimes. In this model, the lifetime of the donor will be independent of the quencher concentration, while the intensity will scale linearly since the donor is instantaneously quenched upon excitation. The reason for this observation is that any molecules that are near the quencher are instantaneously quenched and do not contribute to the photoluminescence signal at all. The only contributors are molecules away from the so-called “quenching sphere of action,” which decay with their natural lifetime. Therefore, the observed fluorescence decay will be totally independent of quencher concentration since only unquenched fluorophores contribute to the decay. However, the trend of the donor intensity arises from a statistical population of quenchers caught within that quenching sphere.

Both the static and dynamic mechanisms represent empirical situations wherein the Stern-Volmer plot is linear and differ only in the interpretation of the obtained slope.

However these are simply two limiting cases, and one can envision that as the donor-acceptor affinity increases, the low dynamic slope must transition toward the steep static slope. However if both static and dynamic pathways are present, they appear together and can produce a super-linear Stern-Volmer plot.

Combined Mechanism

A competitive process between static and diffusional quenching can occur. In this situation, the contribution from each depends on the solvent and in the case of nanomaterials, surface passivant and the nanoparticle size. In this case, rather than the simple Stern-Volmer equation, a second order equation must be applied to account for a pre-association equilibrium process.

The hallmark of this situation is the Stern-Volmer plot is nonlinear. Specifically, the Stern-Volmer plot is quadratic:

$$\frac{I_o}{I} = 1 + (k_d + k_s)[Q] + k_s k_d [Q]^2 \quad (2.5)$$

A plot of $\frac{I_o}{I}$ versus concentration for a competitive case would be expected to be curved, with the magnitude of curvature dependent on which mechanism is dominant. In this experimental case, the lifetime will be dependent on the magnitude of the competitive process, while the intensity will be dependent on the concentration of added acceptor.

2.2 Experimental

All materials were purchased from Aldrich Chemical Corporation. TOPO and alkylamine capped CdSe was synthesized using previously published synthetic techniques[3]. Anthracene was triply purified by sublimation prior to use. For the steady state Stern-Volmer experiments, the emission of the dye was monitored using a Varian Eclipse Fluorimeter as aliquots of freshly prepared CdSe were titrated in. The lifetime studies were performed using an Edinburgh time-correlated single photon counting system consisting of a H_2 -flash lamp coupled to a 1/8 meter monochromator (360nm, 1.0 ns pulse width, 40 kHz) and a Hamamatsu (H5783-02) phototsensor module on a 1/8 meter monochromator for detection coupled to an Becker-Hickl TC-SPC board, for data interpolation. All data calculations were preformed using Mathematica. A sample calculation is shown in Appendix C.

2.3 Results and Discussion

2.3.1 Bimolecular Quenching in a CdSe nanocrystal and Anthracene system

A representative Stern-Volmer experiment is shown in Fig. 2.1, wherein CdSe has been used as a quencher for anthracene in toluene. The five connected peaks on the left (370nm-500nm) belong to photoluminescence of anthracene and diminish with the addition of CdSe nanoparticles. The broad peak at 545nm belongs to the photoluminescence of CdSe. This peak increases with increasing CdSe concentration.

The inset shows the Stern-Volmer plot itself which shows a continuously increasing non-linear trend, which suggests some possible pre-association. The Stern Volmer constant is also much greater than unity, which also infers pre-association. For all the Stern-Volmer experiments performed, these two phenomena always accompanied each other to varying degrees.

From this simple experiment, one can see the potential for this system in detection of organic agents. In the presence of anthracene, there is a predictable change in the fluorescence intensity, which can be correlated directly to the anthracene concentration. The next series of experiments focused on determining the physical phenomena behind the mechanism for this process.

2.3.2 Energy Transfer as the quantum-mechanical quenching mechanism

Undoubtedly, Fig. 2.1 shows that quenching occurs in this system, but gives no indication what the quantum mechanical mechanism for that quenching is, or who the major participants are.

It is well-known that the ligand shell molecules participate in a weak association equilibrium. This dissociation equilibrium may interfere with the anthracene-CdSe association equilibrium in several physically significant ways. The most important one of these would be that the ligand molecules themselves directly quench anthracene. If this is the case, then the energy transfer does not occur between anthracene and CdSe but anthracene and the ligand. The usability of the semiconductor core itself as a detector therefore rests on the quantum mechanical non-interaction between anthracene and the ligand.

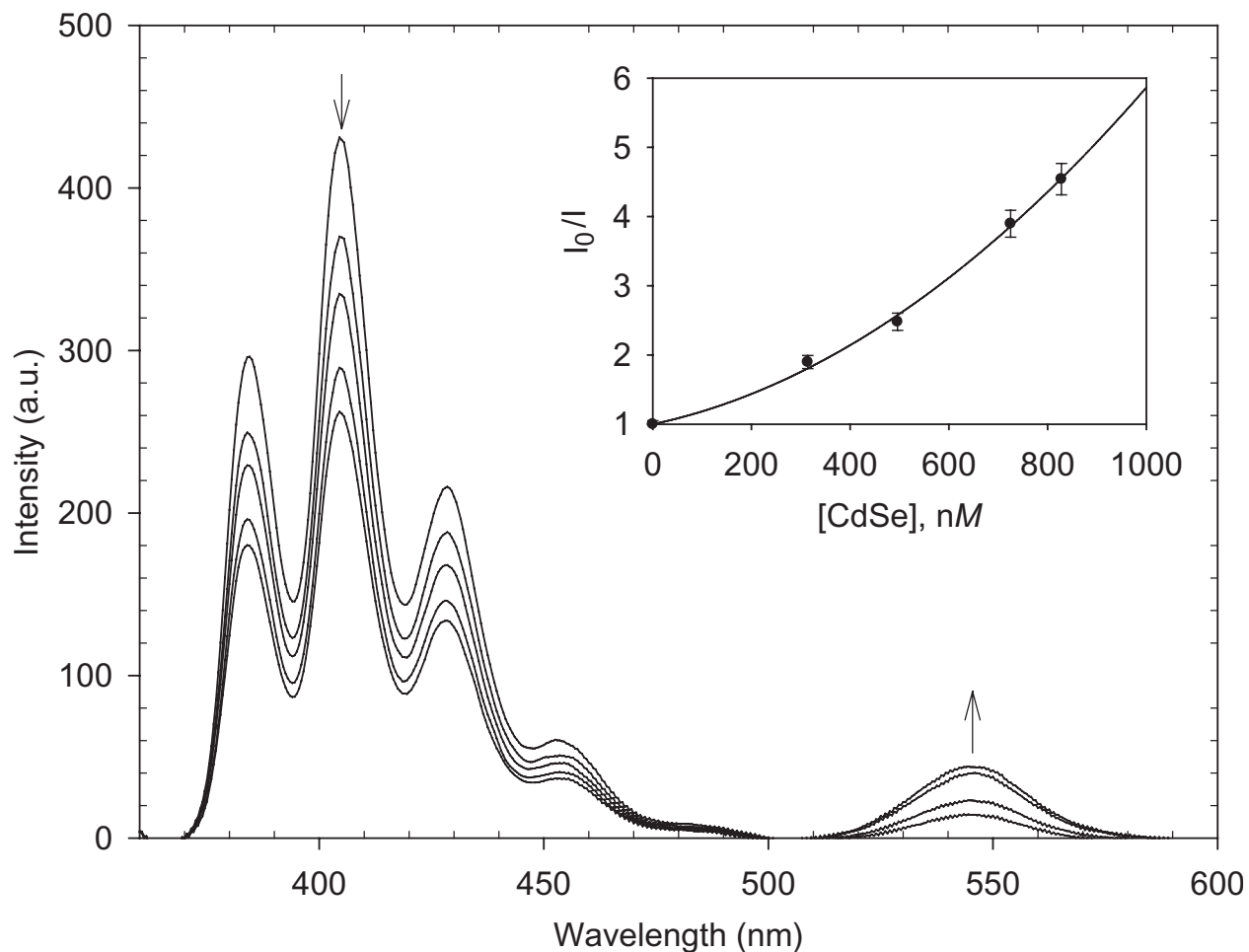


Figure 2.1: Emission spectrum ($\lambda_{ex} = 360$) of anthracene ($1 \times 10^{-5} M$) in toluene at room temperature with 3.5nm DDA capped CdSe quantum dots. Arrows indicate the loss of anthracene emission and the increase in CdSe emission with increasing CdSe concentration. Inset: Stern-Volmer Plot of the steady state quenching data. Data is fit to Eq. 3 as shown by the solid line

Control studies were done, wherein CdSe was replaced with HDA (hexadecylamine) in the role of the quencher. In these studies, anthracene emission remained constant with increasing aliquots of HDA and there was no observed quenching of the anthracene. This experiment, coupled to the loss of anthracene emission and a corresponding increase in the steady state photoluminescence intensity from the CdSe nanoparticles, strongly indicates that not only is the CdSe core responsible for the quenching event, but that the excitation is transferred to it. This transfer of excitation explains the increased photoluminescence.

Of the many possible energy transfer mechanisms, the most likely candidate is the Förster mechanism, which relies on (1) spectral overlap resonance, (2) strong transition dipoles and even has (3) the advantage of long-range transfer. The first two requirements are easily met in this system since anthracene’s emission overlaps the CdSe absorption easily, and both electronic transitions are relative strong. The third feature stands out particularly well in this case. Due to the large size of quantum dots (in the microscopic sense), which can contain hundreds of atoms, there must be a long-range interaction to justify excitation transfers. Additionally, since the ligand itself is not responsible for the quenching, the excitation must be transferred from anthracene across the ligand into the CdSe nanocrystal and only a through-space, non-contact mechanism like Förster can explain this.

The observation of quenching is a Förster[25, 26], wherein the decaying anthracene excited state transition electromagnetically couples to the excitation of the CdSe nanocrystal. The result is anthracene emission shutting off with CdSe emission increasing. Now that the quantum-mechanical quenching mechanism is established, we can divert our focus to the microscopic kinetic mechanism that is dominated by intermolecular forces.

2.3.3 Lifetime Results: Evidence for pre-association

The presence of pre-association is manifested in time-resolved lifetime analysis, and is an excellent way for determining if a static mechanism should be considered. In this single experiment of taking the photoluminescence lifetime decay, both the lifetime and the intensity at a single wavelength can be measured. The intensity is simply the integrated area underneath the decay trace, representing a count of all photons emitted at all times following photo-excitation.

The magnitude of the static process is measurable by investigation of the lifetime studies preformed by measuring the PL decay of anthracene, as shown in Fig. 2.2.

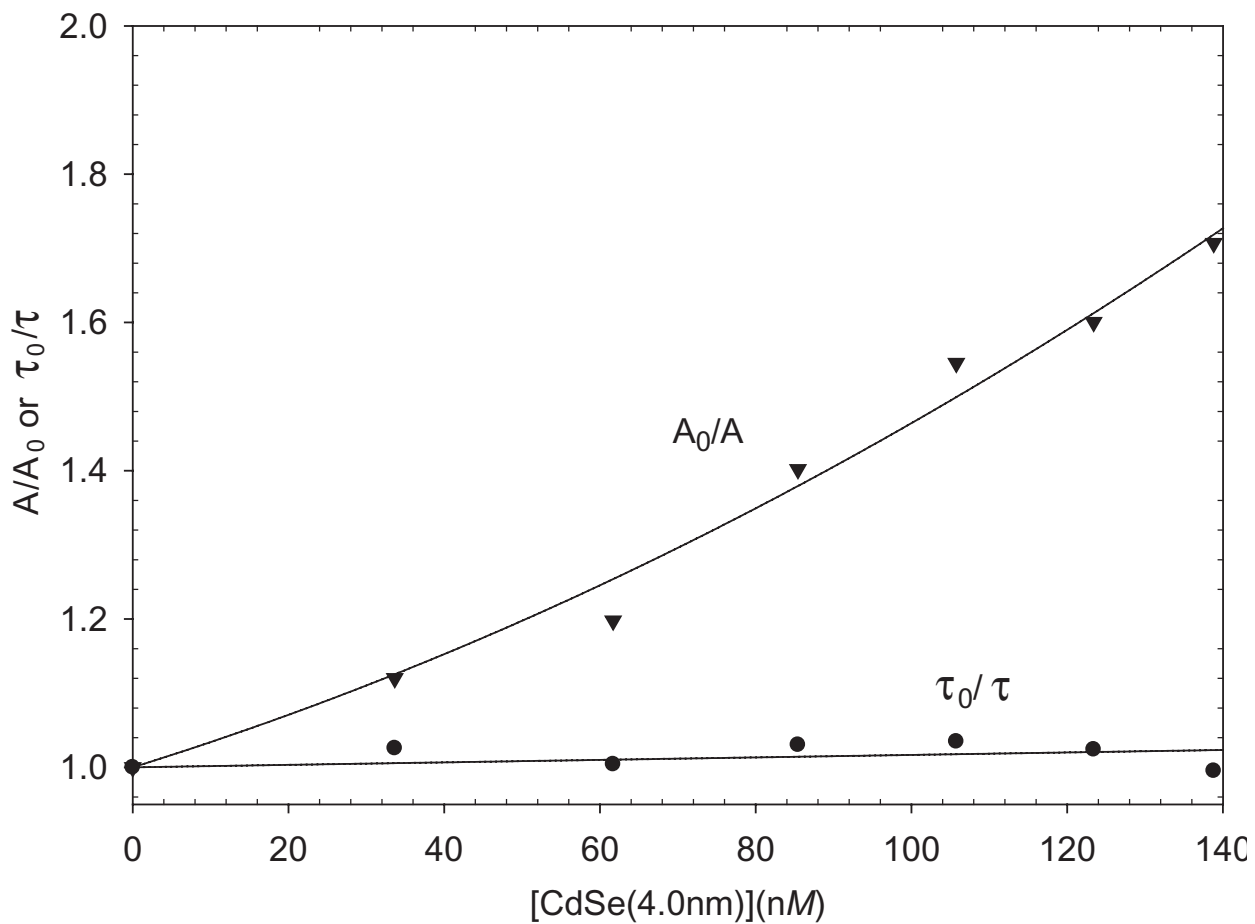


Figure 2.2: Time resolved quenching study of anthracene emission in toluene at room temperature with increasing 4nm DDA-CdSe concentration. Closed circles indicate the change in the lifetime fit to a first order decay. Open circles indicate the change in the total emission intensity as a function of CdSe concentration.

The Stern-Volmer data for anthracene in this experiment was plotted as both $\frac{\tau_0}{\tau}$ and $\frac{A_0}{A}$ vs. $[\text{CdSe}]$, where A and A_0 are the pre-exponential values for a single exponential fit ($I = A_0 e^{-t/\tau}$) of the anthracene lifetime. The intensity data generated from the pre-exponential terms yields equivalent data to the previously measured steady state data since the lifetimes are invariant.

The plot of the time-resolved and steady state intensity (A_0/A and I_0/I) is consistent with the assertion that a static mechanism is influencing the kinetics. The lifetime of anthracene does not change with the addition of CdSe, as shown in Fig. 2.2, which implies the mechanism contains a static pre-association event.

Therefore, we know that there exists a statistical population of anthracene molecules that are adsorbed to the CdSe nanocrystals through association with the ligand shell. These molecules do not contribute at all to the photoluminescence. Only the statistical population of anthracene not associated with CdSe produce observable emission. Therefore we observe their characteristic lifetime, which is in fact at $[\text{CdSe}]=0$. However, the non-emitting anthracene bound to CdSe still effect the intensity since that is a statistical counting of all anthracene, not just the emitting or quenched ones.

At this point, a question that can be asked is: if the number of possible binding locations are increased per dot, will there be a proportional increase in the number of bound (or quenched) molecules? Since this question has to do with the statistical counting of bound versus unbound molecules, it is necessary to return to intensity considerations.

2.3.4 Nanocrystal Size: Changes in binding locations

There exists a very simple way of increasing the number of potential binding donor-acceptor binding locations in a CdSe nanocrystal, and that is through increasing its surface area. Let us consider a hypothetical binding node which occupies a fixed area on the nanocrystal surface. The occurrence of these binding nodes will be directly related to the total surface area if they occur randomly. In other words, binding nodes scale linearly with the surface area. Statistically, we expect that situations where CdSe and anthracene are bound should increase as situations where CdSe and anthracene are unbound decrease. Overall, this causes the equilibrium constant K_S to increase. Therefore increasing surface area increases K_S .

The last consideration will be relating K_S to the simplest way of varying surface area,

and empirically that is through varying CdSe size. If we consider a simple model of a sphere, the surface area (A) is known with respect to its size,

$$A = 4\pi r^2 \quad (2.6)$$

Since the synthesized CdSe nanocrystals have a low aspect ratio and are relatively close to spherical, we expect this relationship to hold in general. If we take all the considerations we have made so far, namely (1) K_S is linearly related to surface area and (2) surface area in a sphere is linearly proportional to r^2 , then the relationship between the static diffusional constant and the nanocrystal size arises naturally:

$$K_S \propto A \propto r^2 \quad (2.7)$$

A plot of K_S vs. surface area should be linear. The data points for these plots are derived from different sizes of CdSe, and their surface areas extracted from their size. A size dependent study as a function of passivant ligand shows the static term is linearly dependent on the surface area of the quantum dot, as shown in Fig. 2.3. Different capping ligands were used, but the trend with respect to surface area for each capping ligand remained linear. The effect of the capping ligand, with respect to the slope of the resulting line will be discussed in the next section.

2.3.5 Stationary Phase Considerations: Varying ligand chain length

If the interaction of the anthracene with the ligand were non-specific (i.e. independent of chemical identity) then it would be expected that all plots of K_S versus surface area should yield the same slope. However, this is not the case. The identity of the ligand affects the slope of these plots.

It has already been said that the ligand shell is analogous to the stationary phase in chromatography. To carry that analogy further, in the same way that different columns cause different analytes to elute at different times, different ligands can cause very different association constants. This property arises from the intermolecular forces existing between the analyte (anthracene) and the stationary phase (ligand), and a simple way of varying the stationary phase is to vary the chemical identity of the ligand. Three different capping

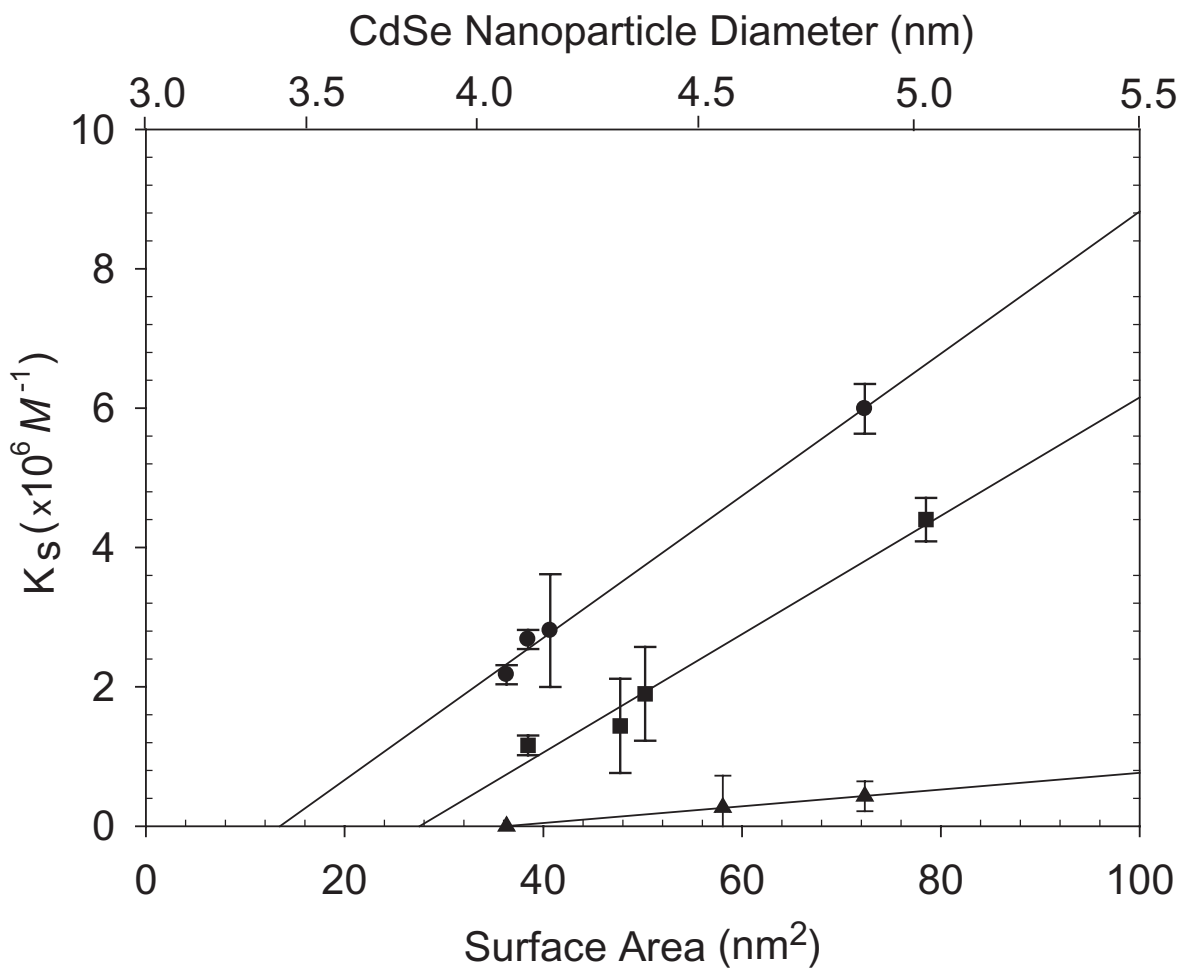


Figure 2.3: The static association constant, as found in Eq 3 was plotted against the surface area, using a spherical model of CdSe, with different sizes and capping ligand of CdSe. Circles represent the dots capped with DDA, squares are capped with HDA, and triangles are the TOP/TOPO capped dots. Lines shown are guides to the eye.

ligands were studied: DDA (dodecylamine), HDA (hexadecylamine), and TOPO (tri-octylphosphine oxide). The first two are both primary amines that form tightly packed monolayers on semiconductor surfaces. These two amines differ only in their chain length with DDA having 12 carbons and HDA having 16 carbons. The last ligand, TOPO, is a tertiary phosphine that does not pack efficiently.

Let us consider the data represented in terms of a constant surface area with different ligands, which would be to consider all vertical lines, or points directly vertical from one another. From this perspective, we can see that K_S for DDA is greater than HDA and is consequently greater than TOPO, and this trend is true for all points on this plot. In other words, it is an important observation that the lines do not cross each other.

Let us compare first the primary amines: there is a stronger interaction of anthracene with DDA than HDA. This can be explained in terms of packing interactions[19]. HDA packs more tightly than DDA, reducing the frequency of regions wherein slotting may “occur.” This is excellent support for slotting as the primary interaction since a motif wherein the planar anthracene molecule lies parallel to the surface would favor the more tightly packed chain since this would create a much flatter, more uniform surface. However, the opposite is true as the looser chains provide a more favorable interaction.

Let us now compare the well packed primary amines to the very loosely packed TOP/TOPO surface. In this case, there is a weaker association with TOP/TOPO relative to the other two. In TOP/TOPO, the angles of the chains do not support a packed structure at all. Without the presence of a packed structure to produce tightly fitting slots, we can expect very little slotting behavior. In other words, when an anthracene molecule slots into the ligand shell, it is less likely to find stabilizing intermolecular forces since there are fewer atoms per given volume in TOP/TOPO than in the primary amine chains.

For the last aspect, we must consider how the static association constant varies with respect to increasing surface area, or in other words: Why do the slopes of the lines differ from one another? First, it should be pointed out that slopes of these lines are no more than an order of magnitude from each other, so that considering the large variance that K_S can have, they are relatively close to each other. The next observation is that the slopes of the primary amines are, within error, identical. The fact that these are so close for similar systems suggests that in a complicated way, these slopes are directly related to the specificity of the ligand shell with respect to screening different sizes of analytes.

The final observation we make for this plot is the independent variable intercept for each line. In this case, we are interested in the surface area wherein $K_S = 0$. The importance of this variable is physically meaningful since it represents the minimum surface area needed to create slots for anthracene to bind into. Looking horizontally along $K_S = 0$, we can see that DDA requires the smallest surface area to create a slot, while TOPO and HDA require increasingly more area. In other words: all nanocrystal sizes to the left of where these intersect the x-axis should produce diffusion-controlled kinetics since there is no pre-association. In fact, the smallest CdSe sizes who the most linear behavior, but unfortunately for DDA and HDA, these sizes are far below the zone in which stable CdSe can be synthesized.

2.3.6 Mobile Phase Considerations: Varying solvent polarity

In the same way that we have altered ligand identity to probe stationary phase-analyte interactions, we can use solvent identity to probe mobile phase-analyte interactions. Before this data is discussed, it is important to note that there is an intuitive inversion of expectations with respect to the K_S variable and our perceptions of “favorable” associations. Namely, lower K_S implies stronger mobile phase-analyte interactions. This occurs because our focus on interactions has shifted from the stationary phase to the mobile phase: as K_S decreases, stationary phase-analyte interaction does not decrease in these experiments since the stationary phase remains constant. Rather, the decrease in K_S is interpreted directly as an increase in mobile phase-analyte interaction.

A mixed solvent system was used for these studies. Differing proportions of a solvent was mixed with toluene. These solvents were hexane, chloroform and acetonitrile. Before examining the data let us consider some aspects of the solvent choices: hexanes are the most nonpolar and are really only miscible in nonpolar organic solvents. Chloroform is more polar than hexanes and has a very similar polarity to toluene. Acetonitrile is much more polar than the other two, and is even miscible in water. Lastly, before we consider the interaction between these solvents and anthracene, it is important to note that organic capped CdSe is much more soluble in toluene and chloroform than the other two solvents.

Anthracene is a relatively polar planar organic, having few regions where aliphatic methylenes like those found in hexane can interact with efficiently. Therefore we expect its interaction with hexanes to be weak, the strongest intermolecular force being dipole-induced dipole. The other two polar solvents have similar sizes and polarities, such that

both would have dipole-dipole interactions. From these very simple considerations, we can form a hypothesis: K_S should decrease as solvent polarity increases, since more polar solvents dissolve anthracene better and will therefore reduce anthracene’s interaction with the ligand shell.

With that in mind, we turn our attention to Fig. 2.4, wherein we see that K_S exhibits a clear dependence on the solvent polarity. For simplicity let us consider only vertical relationships between points and lines, that is only looking at data with the same ratio of solvent/toluene. Like the ligand shell dependence before, it is also important to note that these lines do not intersect, except at 100 percent toluene (as expected). If the hypothesis stated previously was correct, then we should find that hexanes produce higher K_S values than the other solvents, and this is in fact the case. The trend also follows for chloroform and acetonitrile.

2.4 Overview

Mechanistically, the problem of dye intercalation into the nanoparticle surface passivant layer can be described as a competitive equilibrium that lies heavily towards the static process, as shown Fig. 2.5.

The large static component gives rise to a misleading faster than diffusion rate of quenching in Stern-Volmer plots as predicted in the second rate expression in Eqn. 2.5. In fact, the particles are not moving at faster rates, but simply appearing to do so from the high rate of preassociation. The faster than diffusion rate has been previously observed but not fully described for PL quenching at Au nanoparticles[27, 28, 29]. The observed experimental results can be readily described in light of an affinity chromatography problem, where higher affinity of the dye for the organic capping group on the nanoparticle surface as compared to the affinity for the solvent system results in the experimental observation of a larger as seen in Figures 1-4[15]. This assumes that quenching only arises when the anthracene moiety is in close proximity of the nanoparticle surface[20].

As observed in the optical density data, changes in solvent, molecule polarity or passivant type shift the equilibrium process and varies the response in the PL behavior. In fact, this suggests that passivated CdSe nanoparticles can find application in sensor technologies due to the ability to tune the surfaces systematically to influence the affinity for a specific to the nanoparticle surface. The static association constant for anthracene intercalating into

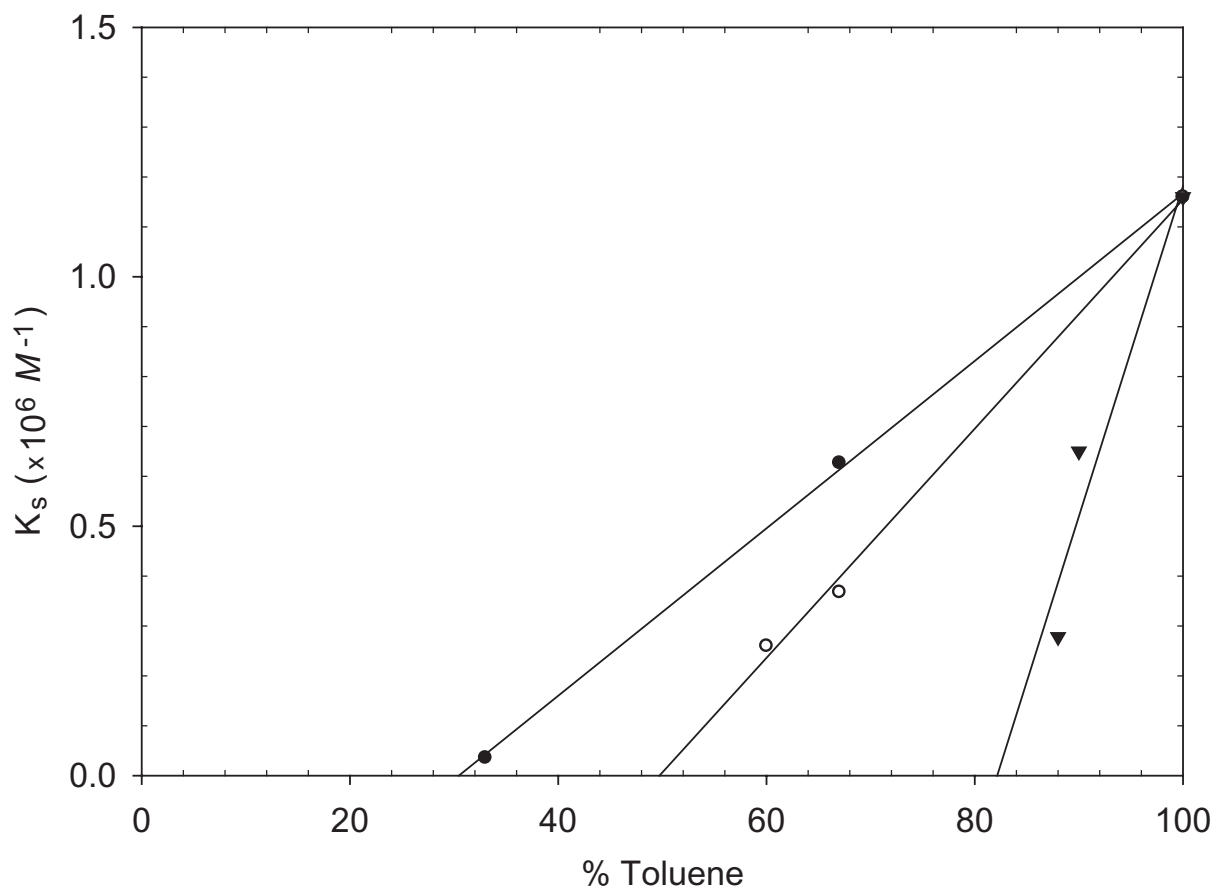


Figure 2.4: The static association constant for anthracene and 3.5nm HDA-CdSe, as found in Eq 3 was plotted against the mole fraction of toluene with different co-solvents hexane (closed circle), chloroform (open circle), acetonitrile (inverted triangle). Lines shown are guides to the eye.

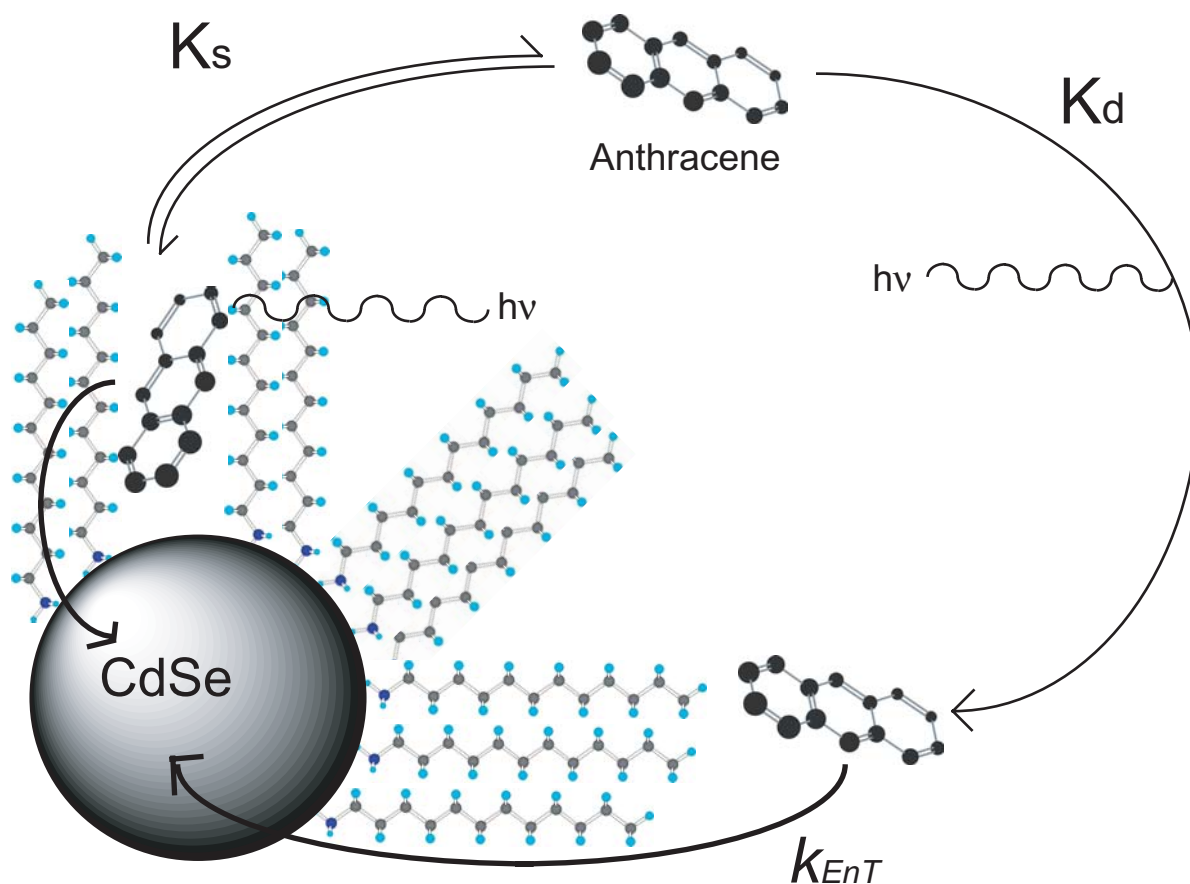


Figure 2.5: Proposed kinetic model for dye interaction with quantum dots. Photoexcitation of pre-associated dye results in instantaneous quenching. There is an equilibrium between the complexed and non-complexed dye that is described by the static association constant, K_s . However, the non-complexed dye still in solution becomes excited and then diffuses to the dot, becoming quenched at a maximum rate of k_d , limited by the solvent type. Proposed quenching mechanism is likely to be resonant energy transfer.

the passivant layer of the nanoparticle is a function of the surface area of the quantum dot. Intercalation of planar organic dyes into self-assembled monolayers of linear organic functionalities is driven by the Van der Waals interactions between the molecule and the passivant layers. In affinity chromatography increasing particle size tends to decrease affinity due to changes in the multiple path term (A) in the van Deemter equation. In the nanoparticle, which is free to diffuse in solution, increasing the surface area of the dot increases the number of potential binding sites for the dyes to slot into which gives rise to the counter intuitive increase in "retention" on the dot surface[30, 31].

Another factor that must be considered in the variation of the capping ligand, is effects that arise due to changes in the packing of the ligands. Previous studies have shown that changing the chain length of a straight chain alkane, affects the overall packing on the surface of the dot[19]. This in turn will affect the association of the dyes with the dots, as the number of potential binding sites will be affected[17]. In fact this explains the drastic difference observed TOPO versus the alkylamines in Figure 3. However, this is a slight over simplification, due to the nature of the nanomaterial used as the acceptor in this experiment. It has been shown that the packing of the surface groups is a function of the type of surface group used to passivate the surface of the material and is affected by the solvent that is used to solvate the system[19]. All the observed effects lend this system to being very adaptable for sensor applications. Modification of the ligands on the surface of the quantum dot and variation in the solvent system used would allow for specific detection of species.

2.5 Chapter Summary

Inspection of the steady state intensity quenching and time-resolved quenching data indicate that the observation of energy transfer can be explained as arising from a competition between static and diffusionally controlled processes[24]. The results suggest strong molecular adsorption of planar aromatic molecules occur on nanoparticle surfaces controlled by the nature of the passivant and nanoparticle size. This is reminiscent to observations in reversed phase affinity chromatography, with the exception that smaller particle sizes yield better resolution due to the increased number of theoretical plates in a packed column. In an analogous manner the number of theoretical plates in a nanoparticle will be controlled by the nature of the passivant and the surface area of the nanoparticle. In light of the anatomy of the

particle, it is a CdSe core with a ligand passivated surface; the ligand used for passivation can be varied, giving the particles different a solubility, changing the magnitude of the interaction with the donor molecules in solution.

The migration of the donor molecule to the nanoparticle in a dilute solution is dominated by an equilibrium process that can be microscopically envisioned as dominated by the affinity of the molecule for the nanoparticle passivant layer. The mechanistic interaction can then be described as a diffusional process if the affinity is low, as a static interaction if there is a strong affinity for the donor molecule for the surface for the nanoparticle, or as an intermediate case between the two, with both static and dynamic quenching taking place.

CHAPTER 3

PHOTOLUMINESCENCE OF QUANTUM DOT EMBEDDED XEROGELS

3.1 Motivation

Silica sol-gels are a well studied group of materials with potential applications in a broad variety of fields, from chemical sensors, chromatography, catalysis, to optical devices. Sol-gel reactions are advantageous in the fact that they are low temperature, solution based reactions that can easily be manipulated to allow for the incorporation of other materials.

Specifically, the sol-gel matrix is an ideal atmosphere to stabilize optically active nanomaterials, and reduce their tendency for decomposition processes like photo-oxidation[32]. In this way, the nanomaterials act as “guests” in the sol-gel “host matrix.”[33, 34, 35, 36] The nanomaterial provides the primary function of the device (i.e. sensing), while the sol-gel provides a stable environment for the nanocrystal.

In this way, the incredible sensitivity of nanomaterial surfaces can be utilized in the field, if encapsulated within a rigid and solid matrix[37, 38]. Additionally the sol-gel provides two important strengths that benefit its guest material directly: (1) it is optically clear and transparent in the visible wavelengths so that the guest material can absorb and emit light without any interference from the matrix, and (2) it is permeable, yet largely inert, to a wide variety of small molecules, allowing these analytes to interact solely with the embedded nanomaterial and does not interfere with direct sensing. An additional benefit is that large impurities cannot penetrate the pores and so the sol-gel provides a size-dependent filtering/screening effect.

3.2 Introduction

3.2.1 The sol-gel family

At the most simplistic level, a sol-gel reaction is a solution phase reaction, where colloids suspended in solution polymerize until a three dimensional, inorganic network is formed[39]. Silicates ($(SiO_x)_y$) are the most common sol-gel building blocks and are representative of what this class of materials can accomplish. These reactions use inexpensive starting materials, proceed in ambient conditions, and because they are relatively insensitive to specific temperatures, show a great deal of reproducibility.

A "sol" is simply a solution of reactants that undergoes hydrolysis and condensation. In a typical reaction, the silicon atoms become linked through oxygen bonds, eliminating an alcohol. As the reaction proceeds for the oxygen bonds on the same silicon atom, a three dimensional silica network gradually builds up. This cross-linked, amorphous structure is called an alcogel. Depending on the types of functionalities that were present on the silicate precursor, there will "pores" of various sizes incorporated inside the alcogel.

In an alcogel there is a three dimensional inorganic network formed, but the matrix is still surrounded by excess water and cosolvents. A final processing step can be taken to remove the excess liquids, and is often necessary to form an optically clear structure. The water and cosolvent will gradually evaporate, leading to a collapse of the pores and the formation of a xerogel[39]. This final structure forms a single, rigid, robust, amorphous solid that is ideal for incorporating materials into.

3.2.2 Sol-gel synthesis

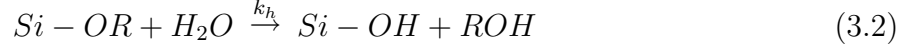
Let us consider the step-by-step synthesis of a silicate-based sol-gel reaction. The overall reaction for a silica sol-gel is:



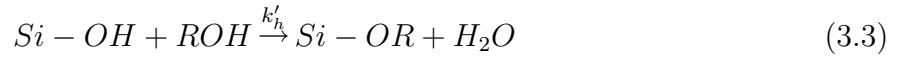
The two major features are (1) the consumption of water and formation of alcohol (2) the conversion of the organic-soluble silicate precursor to the solid-phase silicate. There are a multitude of possible alkoxysilanes that can be used, and the -R group can be as simple as a methyl or a much more complex branched structure.

Hydrolysis

However, the sol-gel reaction actually takes several steps to consume the alkoxysilane precursor. The first step is the hydrolysis for the alkoxysilane as shown in Eqn. 3.2 to form SiOH and the ROH.

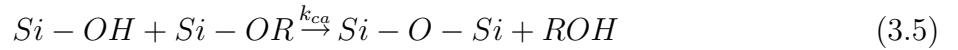
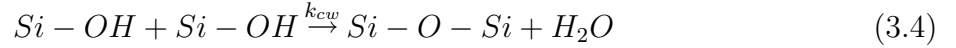


It is important to note that this step is an equilibrium, and as shown in Eq. 3.3, can react again to reform the alkoxysilane precursor.



Condensation

After hydrolysis, condensation occurs. This reaction has two paths that it can follow, either the water producing reaction shown in Eqn. 3.4 or the alcohol production reaction, shown in Eqn. 3.5.



Depending on the reaction conditions used, different reactions are rate controlling. In basic conditions, hydrolysis is the rate limiting step, in acidic conditions it is the condensation reactions that are rate limiting.[40].

Another important aspect of sol-gel chemistry is the fact that the nature of the inorganic network that is made depends on such factors as pH, catalysis, water to Si molar ratio, and temperature. This dependence allows for a large amount of variation in materials made by adjustment of the synthetic conditions.

3.2.3 Incorporating the guest material: CdSe nanocrystals

CdSe quantum dots were prepared using previously published cluster techniques[3]. As prepared, the dots were capped with hexadecylamine (HDA). For incorporation in silica

glasses using tetramethyorthosilicate (TMOS) as the silica precursor, the quantum dots needed to be made water soluble.

Selection of the ligand to recap the quantum dots was critical. Ideally, the chosen ligand needed not only to provide water solubility, but also a group that would facilitate the actual cross linking of the quantum dots in the silica matrix, rather than simply suspending the materials in the pores by trapping it during the condensation process. The ligand also needed a group capable of interacting with the surface of the CdSe, passivating it and displacing the HDA[41].

Interlinking the quantum dots with the silica matrix was an important factor for actually making a hybrid material, rather than just creating a material with the quantum dots as guest molecules and thus potentially displaced from the silica host.

Experimentation with various amino and mercapto silicates showed that the highest quality material was made using aminopropylethoxysilane (APeS). The primary amine in APeS provides a group to bind to the nanocrystal surface, while its silicate end allow for cross-linking with TMOS. This is illustrated in Fig. 3.1. As the reaction proceeds, the CdSe nanocrystals become embedded in the growing sol-gel matrix.

Using APeS as a capping material had an added benefit of catalyzing the sol-gel reaction. The free APeS in the solution acted as an amine to drastically increase the rate of reaction, turning the sol-gel condensation from a process whose time scale is typically measured in days, to an exothermic condensation reaction that occurred in a matter of a few minutes. Adding a large excess of APeS resulted in violent condensation reactions that shattered the forming gels, although the initial luminescence of the quantum dots was unaffected by the violence of the reaction conditions immediately after formation. Adding too little resulted in slow condensation kinetics and poor quality materials.

3.3 Experimental Method

3.3.1 Sol-gel synthesis

Preparing CdSe for incorporation

For sol-gel synthesis, a few hundred milligrams of CdSe-HDA was placed in a test tube and gently heated until the material melted. Several milliliters of methanol were then added, and the solution centrifuged for several minutes. The pellet was then dissolved in 0.25ml

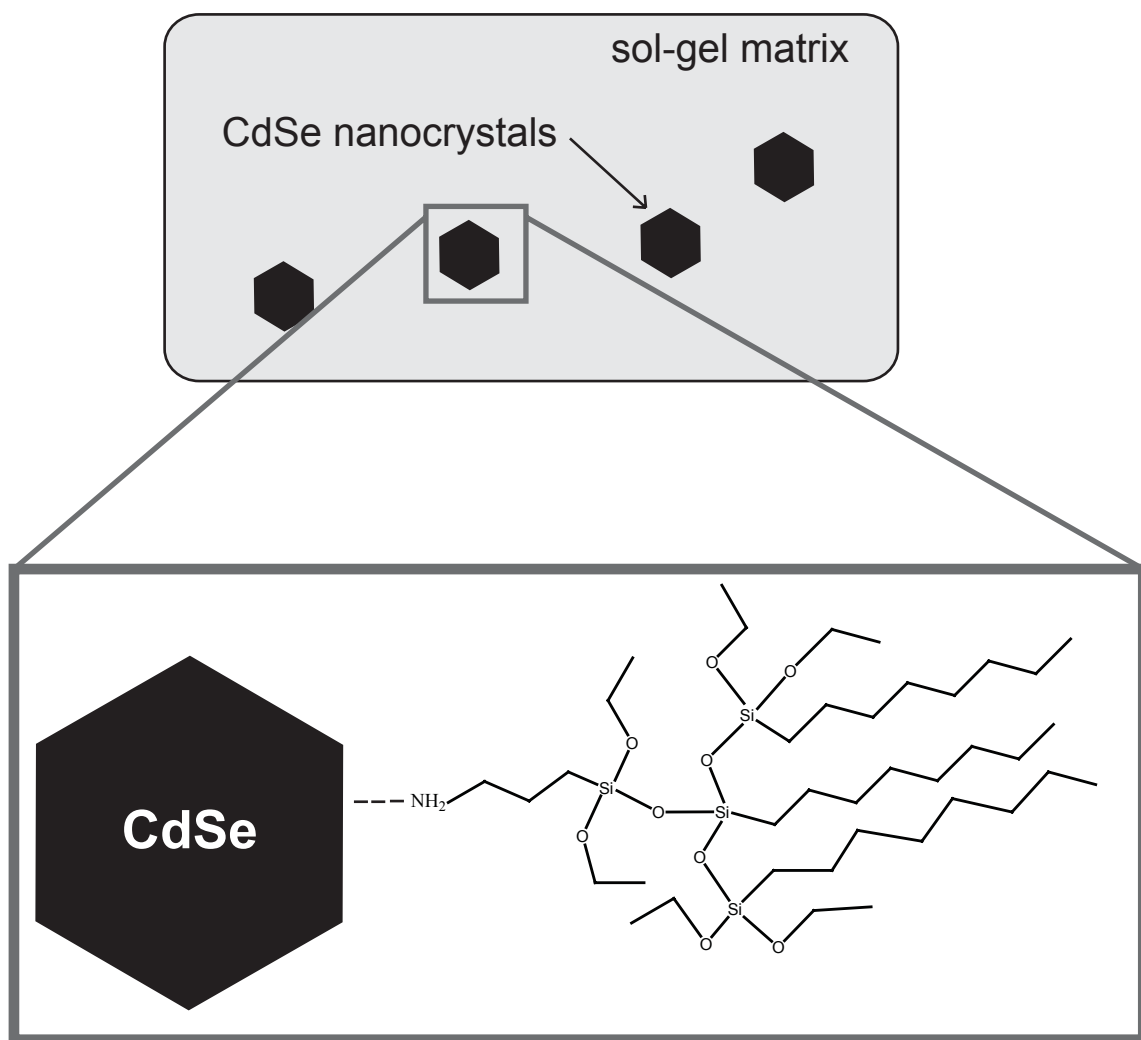


Figure 3.1: Diagram of CdSe Sol. The top diagram shows the CdSe nanocrystals embedded in the sol-gel matrix while the bottom figure is an expanded view to show how the nanocrystals are connected to the sol matrix. The primary amine in APeS binds to the nanocrystal surface while its silicate end has cross-polymerized with TMOS.

of chloroform and several mL of methanol was added again, to precipitate the quantum dots out of solution. This was repeated 2 or 3 more times. After the final wash, the pellet was resuspended in 1 mL of APeS. Before proceeding, the absorbance and emission of the dots was checked to ensure there was no drastic shift in optical properties from the parent material.

Preparing the Sol-gel

After the preparation of the quantum dots, the TMOS solution was prepared which consisted of three compounds: (1)TMOS, (2) methanol, and (3)distilled water. The ratio of TMOS:water:methanol was 3:x:6, where x was varied. For the highest quality sol-gels, the co-solvent needed to be completely dry, and the only water in the reaction carefully controlled by the amount of water added to the TMOS solution. Aliquots of the CdSe-APeS were placed in the desired containers for the sol-gels to form in. The TMOS solution was then added to the molds and the solutions carefully mixed. Depending on the concentration of free APeS in the solution, the rate of condensation was anywhere from 30 seconds to 2 minutes.

3.3.2 Optical Measurements

The emission of the samples was monitored using a Varian Eclipse Fluorimeter. The excitation beam was 90° from the collection path to reduce refracted excitation light of solid samples. The samples were excited at 430nm, with excitation and emission slits set at 5nm, 1200 nm/sec scan rate, 2.0nm data interval, and 0.1s averaging time.

For solid-state photoluminescence, emission was taken in borosilicate test tubes inserted into the excitation path without a secondary sample holder. All samples were measured in the disposable test tubes that they were cast in, in order to limit physical damage to the sample.

3.4 Results

3.4.1 Strong photoluminescence of CdSe in embedded structures

After formation the gels were optically clear, highly luminescent, and completely filled the containers or molds that they were cast in. As the gels began to age, and the solvent

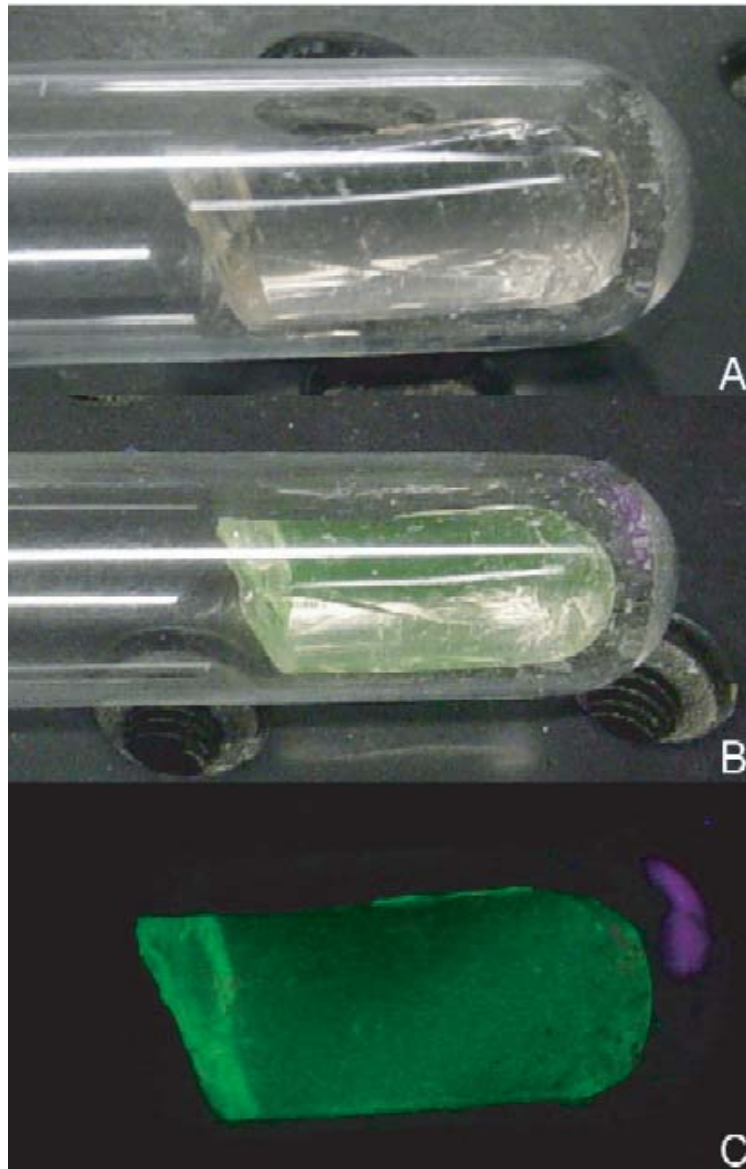


Figure 3.2: Photograph of a representative monolith at room temperature taken with a commercially available digital camera. CdSe nanocrystals (3.5nm diameter) capped with APES (Amino-propyl ethoxysilane) are embedded in a silica based sol-gel. (A) The sol-gel is in the test tube mold that was used to cast the gel in. (B) The sample is illuminated by a UV handlamp at approximately 365 nanometers under room light. (C) The sample is illuminated by a UV handlamp at approximately 365 nanometers with no other light source. The photograph was not digitally enhanced.

evaporated, the gels would pull away from the sides of the mold, however, the original dimensions of the mold were still mirrored on the dried gel.

This can be seen in Panel A in Fig. 3.2. The samples were typically strongly emissive, clearly visible with excitation from a UV handlamp under standard room lights. This is shown in Panel B in Fig. 3.2. The true strength of the emission can be seen in the Panel C of Fig. 3.2, where the sample is excited using a UV handlamp with no other room light.

All CdSe-embedded sol-gels were colorless. It is also important to note that if the concentration of CdSe in the initial reaction was too high, the final condensed dry gel would take on a color that mirrored the color shown by the parent CdSe solution, rather than being completely clear.

Comparison of the emission of the quantum dots in solution to the emission in the newly formed sol-gel show little difference, as shown in Fig. 3.3. Initially, after formation, the dots appeared to be largely unaffected by the sol-gel reactions in terms of wavelength of emission and peak width. The fact that the optical properties remained the same indicates that the CdSe nanocrystals retained the same size and distribution during the sol-gel reaction.

Additionally, the amount of broad defect photoluminescence (found at energies lower than the band gap emission, i.e. 700nm) that is typically seen to increase during reactions that degrade the nanocrystal surface is absent. This is an important point because the presence of defect luminescence is often accompanied with a reduction in the photoluminescence quantum yield. Were such a defect luminescence found to be enhanced after sol-gel preparation, it would have adverse implications for the use of this material as a sensing device. Fortunately, it can be seen clearly from Fig. 3.3 that the defect luminescence has not been altered and consequently, the CdSe nanocrystal surface has remained intact.

One small molecule that can diffuse through the sol-gel matrix and that is known to influence the photoluminescence properties of CdSe nanocrystals is water[42]. Its effect on the photoluminescence is a vital concern to the performance of this device.

3.4.2 The presence of water

Traditionally, the ratio of TMOS:water:methanol for this system is 3:2:6. In order to assess the effect of water on the system, the concentration of water was changed for a series of samples, to: 1, 0.5, 0.25 and 0 (traces B, C, D, and E respectively). The photoluminescence was taken as they were initially formed and appears in Fig. 3.4.

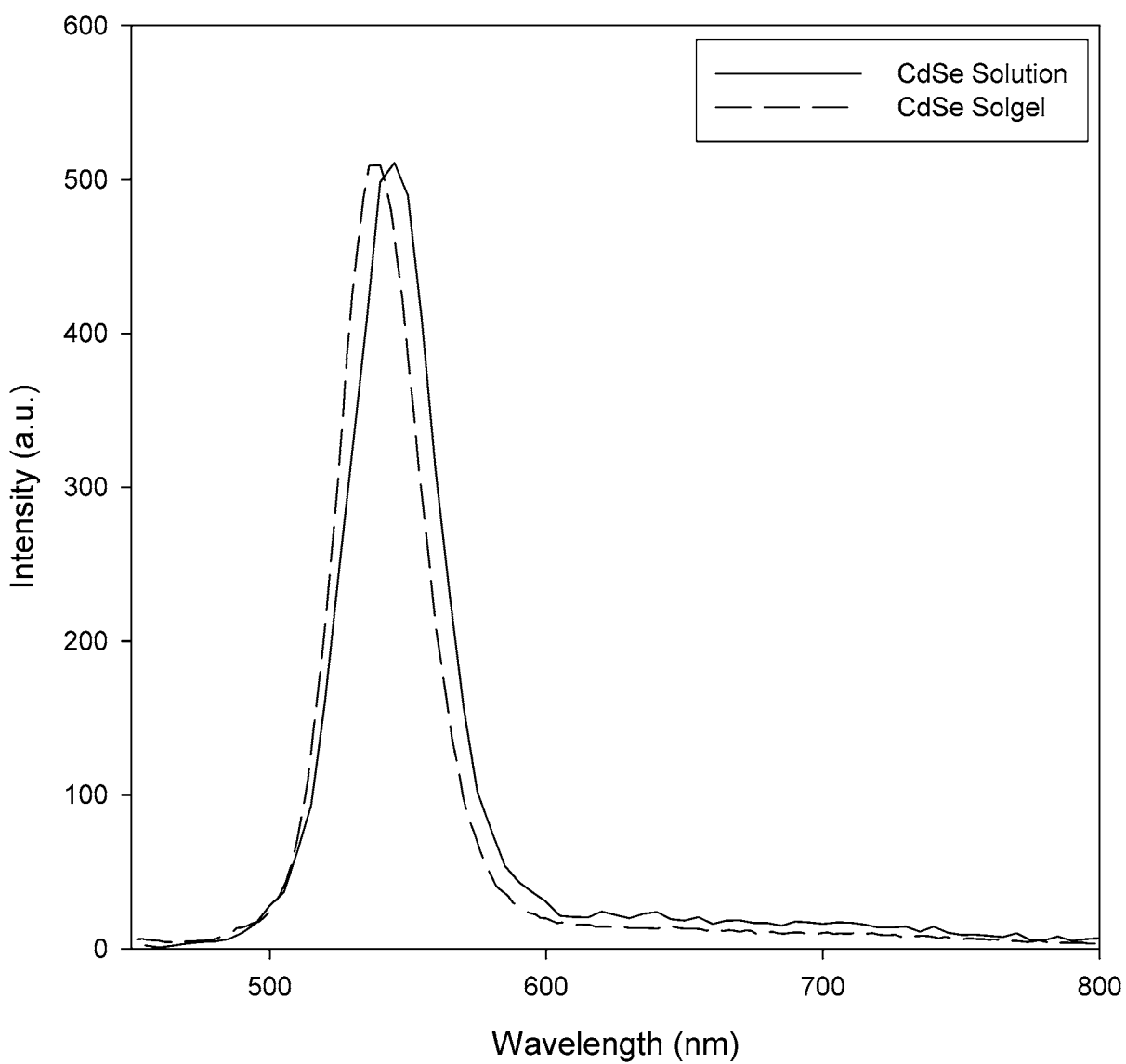


Figure 3.3: Photoluminescence spectra of a CdSe nanocrystal (3.5nm), dissolved in solution (solid line) and incorporated into the sol-gel matrix (dashed line)

The photoluminescence under traditional conditions, shown as (A) is enhanced in intensity as the concentration of water is systematically decreased (B, C, D, E), until the photoluminescence approaches the value it would have if dissolved in solution.

The case of (E) is noteworthy. While, from the overall trend, it matches our expectation that (E) should have the highest intensity, (E) is in fact not a sol-gel. Since water is a reactant of the sol-gel reaction, removing it entirely simply does not slow down the kinetics, but stops the reaction from occurring entirely. Without water the sol-gel does not form. Therefore, the intensity matches that of the CdSe nanocrystal dissolved in solution. As long as a sol-gel reaction proceeds, we can conclude that the higher the concentration of water used to synthesize the gels, the lower the CdSe emission.

The physical reason for this observation most likely stems from the action of water to quench the photoluminescence by direct interaction with its surface through a light-assisted degradation. This effect of water has been well-documented in self-assembled monolayers of CdSe nanocrystals[42]. In that study, the presence of water resulted in irreversible photoluminescence quenching that was linked directly to a light-assisted surface degradation of the CdSe nanocrystal.

The ability of water to interact directly with the nanocrystal surface and cause a change in photoluminescence that is observable within the sol-gel is a beneficial property for using this combination for optical detection of small molecule concentrations. However, for the most sensitive and stable device function, we have learned that the concentration of water must be limited in order for the long-term stability of the device.

3.4.3 Stability under ambient conditions

The stability of a sensor is an important factor in its use in the field, and for this CdSe nanocrystal embedded in a sol gel, it will be the emission intensity that will be the primary factor in the device response. To assess the response of the device over a long period of time, the photoluminescence intensity was tracked over the course of one week. This was performed for all of the samples with differing water concentrations of Fig. 3.4.

After initial formation, the gels were allowed to age on the benchtop, exposed to ambient temperature and humidity. As seen in Fig. 3.5, tracking the emission of the samples over time shows a steady decline in the CdSe nanocrystal emission intensity, although there is no shift in wavelength observed. This behavior has been observed in the literature before, and

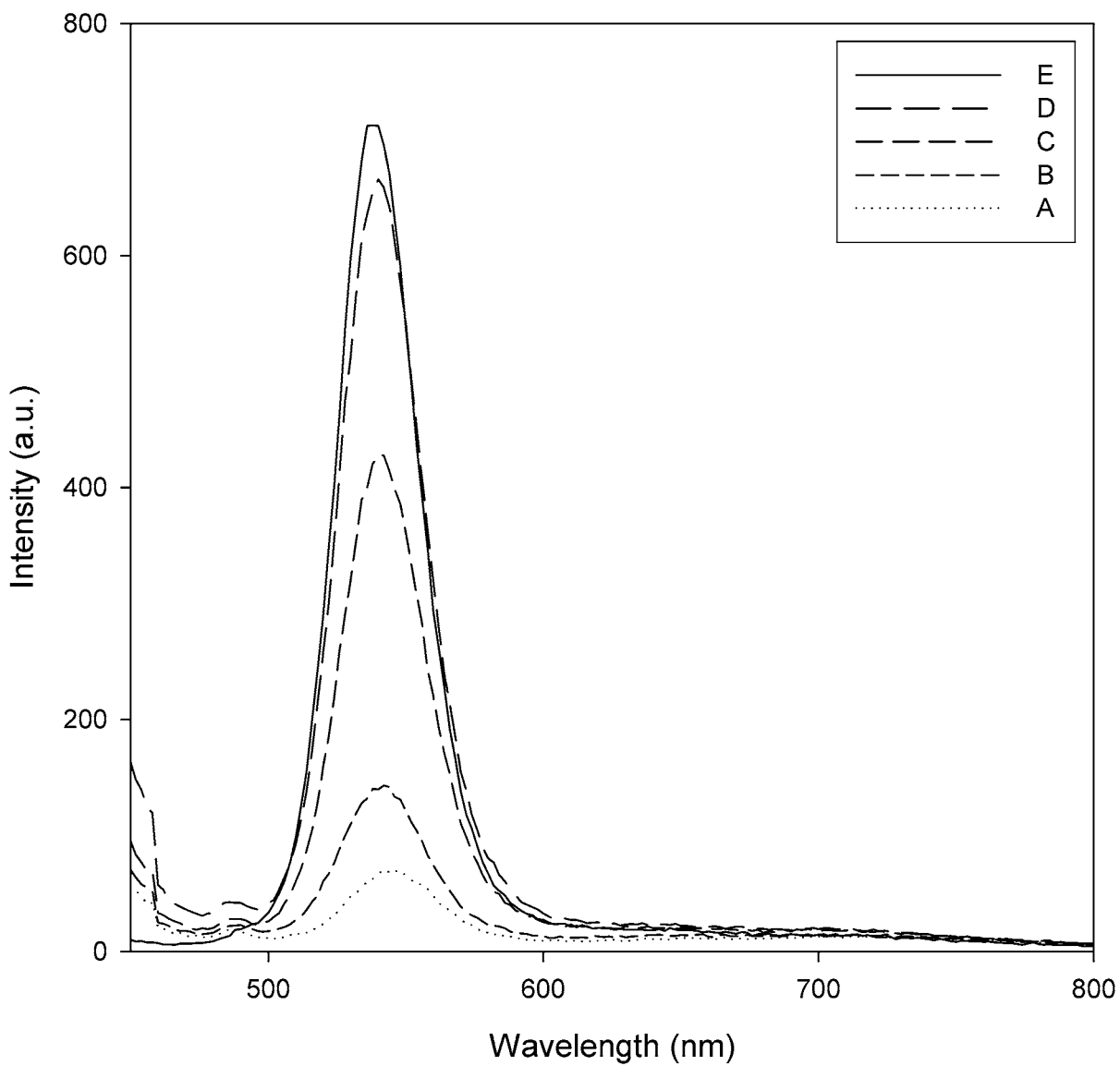


Figure 3.4: Plot of the photoluminescence CdSe nanocrystal (3.5nm) as a function of the concentration of water used in the initial reaction. The traces represent different TMOS:water:methanol ratios: (A) 3:2:6, (B) 3:1:6, (C) 3:0.5:6, (D) 3:0.25:6, (E) 3:0:6

it is largely the reason CdSe has not been widely studied in silica sol-gels.

For each sample tracked over time, two major features are observed in the intensity changes that can be correlated to physical changes in the sol-gel material. First, there is an overall reduction in photoluminescence intensity that likely comes from the aforementioned oxidation of the surface due to water. Second, there is a brief increase in intensity following the decrease in intensity that is due to the formation of the sol-gel.

As the sol-gel cures, the relative concentration of CdSe is artificially increased due to a contraction of the sol-gel volume. Thus, even though the amount of CdSe within the sol-gel remains the same, the reduction in volume increases the relative concentration. Since the concentration of CdSe has been increased within the excitation path, then the number of excited CdSe species increases and consequently so does the observed emission. Therefore an increase in photoluminescence will be observed coincident with the drying of the film, and a peak in the observed emission intensity will be found as the drying process becomes dominant and the oxidation process has run its course. This drying process completes within the first few days, and once again a reduction in intensity occurs due to the remaining oxidation that water produces.

3.4.4 Stability under wet conditions

Tracking the materials in ambient conditions over time showed that the lower concentration water samples lost their emissive properties at a slightly slower rate than samples made with higher amounts of water. If we look at how the concentration of water affects the long term stability of these sol-gels, we find that it is dramatic. While the higher water concentrations (A,B,C) show that their photoluminescence becomes totally quenched after 2.5 days, the lowest water concentration sample last for nearly 3 times that long: over 7 days.

Ideally, the perfect sol-gel system would be one created without the presence of water as this would confer maximum emission intensity as well as the longest stability. However, since water is a constituent of the reaction, some water must be a necessary part of the sol-gel formation. It can be concluded that the optimal synthetic conditions are those that minimize the water concentration required for the gel to undergo hydrolysis.

However, no matter how optimized the initial reaction conditions are, it still does not prevent the inevitable decay in emission when the gels are exposed to ambient conditions. Despite the fact that this device ultimately stopped functioning after a week, having an

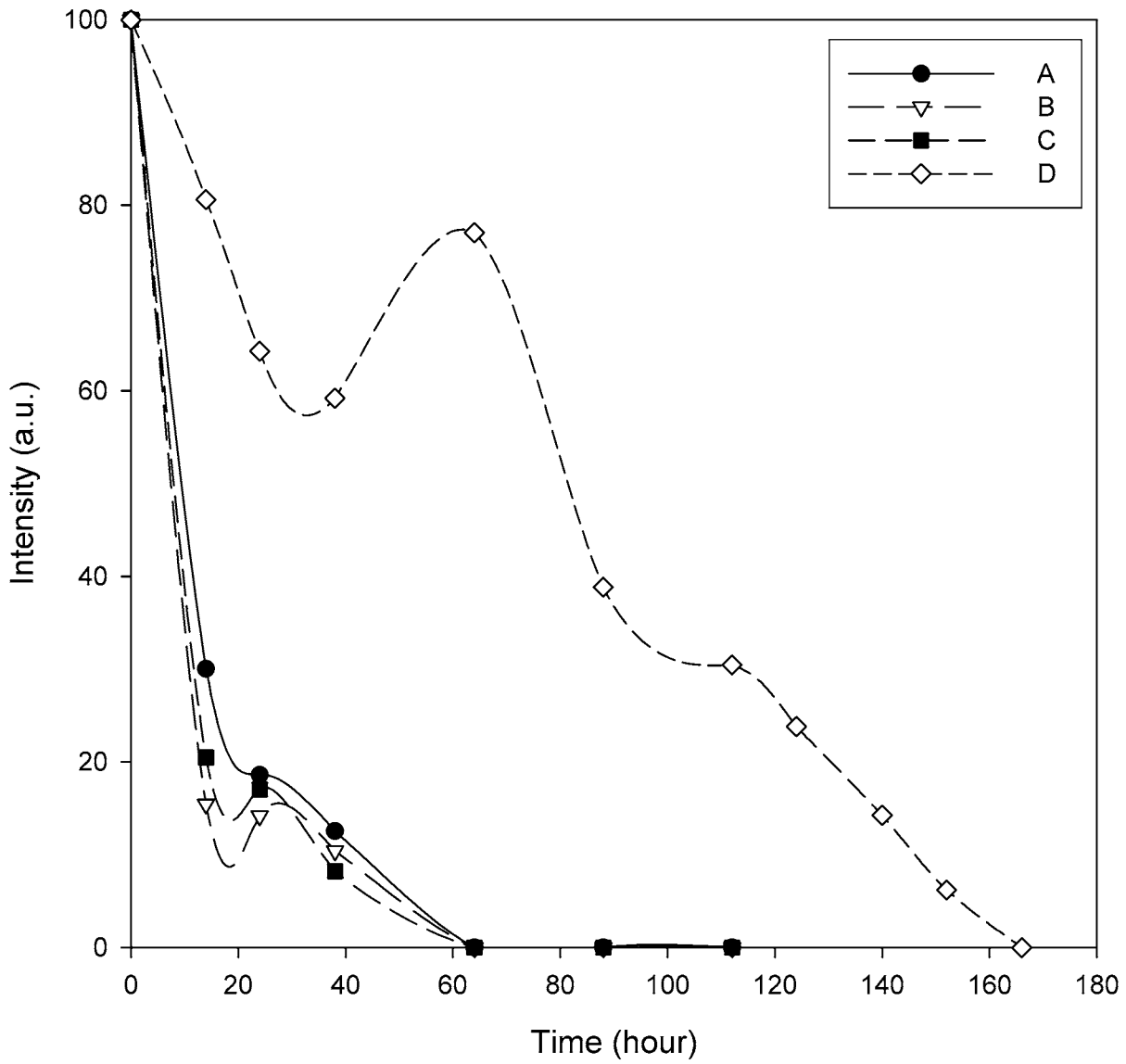


Figure 3.5: Photoluminescence intensity of CdSe nanocrystals embedded in a sol-gel matrix tracked over time for different concentrations of water. The traces represent different TMOS:water:methanol ratios: (A) 3:2:6, (B) 3:1:6, (C) 3:0.5:6, (D) 3:0.25:6

active nanomaterial embedded in a sol-gel for this period of time is unprecedented, and marks the first step in fabricating nanocrystal-based sensing in this particular sol-gel.

3.5 Chapter Summary

The synthesis of stable luminescent sol-gels embedded with CdSe nanoparticles has been developed. Surface passivation of the nanoparticles with aminopropylethoxysilane (APeS) allowed not only for the semiconductor particles to be made water soluble, it allowed for the direct linking of the particles to the sol-gel silica network. Water was shown to play an important role in the initial luminescence properties of the synthesized materials as well as playing a role in the long term stability of the materials under ambient conditions.

Using nanocrystals embedded in a low water content sol-gel, we can now make further modifications to the sol-gel system in order to improve the stability of quantum dot emission. This will be the focus of a later chapter.

CHAPTER 4

IMPROVED STABILITY OF QUANTUM-DOT EMBEDDED XEROGELS

4.1 Motivation

In Chapter 3, the formation of a very stable quantum-dot embedded sol-gel was explored, utilizing a traditional, but slightly altered sol-gel synthesis. The photoluminescence was studied with regard to its synthetic conditions. In this chapter, several factors will be introduced to study the behavior of these quantum-dot embedded xerogels with close attention to (1) long term stability in wet and dry conditions, (2) emission response with solvent variation and (3) variation of quantum dot chemical composition.

4.2 Introduction

4.2.1 Evaporation in sol-gel formation

Closed System: No Evaporation

In a silica sol-gel, forming the gel from the sol involves a slow curing process, during which the solvent evaporates from the solution and the three dimensional silica network fully forms. In addition to this natural evaporation process, the byproducts of the sol-gel condensation reaction (water and alcohol) begin to collect in the solution. Since the sol-gel reaction is an equilibrium, in a closed system gel formation would be dramatically delayed and even halted as products begin to accumulate in the solution. Driving the reaction to completion necessitates the removal of products (Le Châtelier's Principle). Therefore, allowing the water and alcohol formed to evaporate removes them from the sol system, and the sol-gel reactions are driven to completion. Importantly, the rate of evaporation will strongly affect the quality of the sol-gels.

Open System: Rapid Evaporation

If the evaporation proceeds too quickly (i.e. lower pressure, higher temperature) then the slow polymerization process that is necessary for well-formed, monolithic sol-gels will not occur. Consequently, the resulting sol-gel's continuous domain will stretch only a few millimeters and produce a powder rather than a single monolith.

Conclusively, for well-formed sol-gels, no evaporation halts the sol-gel reaction and evaporation that occurs too quickly results in poorly formed sol-gels, such that ideal conditions point to slow evaporation. This is achieved at ambient conditions and typically, no special procedures are implemented since high quality sol-gels can be achieved with little environmental control. It will be shown, however, that in a sol-gel host-guest system that the needs of the guest species (in our case quantum dots) must also be accounted for in addition to the sol-gel host so that proper device function will persist.

4.2.2 Humidity and Quantum Dots

Water production by Sol-gels

As shown in Chapter 3, the presence of water dramatically quenches the quantum dot photoluminescence. This effect is not favorable because for the future use of this device, the emitted light will function as the output signal (if used as a sensor) or as a source of illumination (if used as a phosphor). Preserving strong photoluminescence in the quantum dot is critical.

Unfortunately for the quantum dot, once it is embedded in the host matrix, the sol-gel condensation reaction begins producing copious amounts of water as a by-product of the gel formation. The presence of this water as a quencher and a catalyst for photo-oxidation will impact negatively upon the CdSe quantum dot integrity. Therefore, steps must be taken to remove any unnecessary water from the sol-gel. This will be tackled by controlling pressure and humidity.

Dry Environment is Ideal

Since water is bad for quantum dots, it would be reasonable to assume that total removal of water would produce the highest quantum efficiency and the longest stability. While this is indeed true, there are two aspects relating to sol-gels that must be addressed in order

to provide an ideal quantum dot environment. They are (1) the production of water and evolution of water vapor are critical components to sol-gel formation as discussed in the previous section, and (2) ambient conditions typically involve a non-zero humidity rating depending on climate and geographical location. The former aspect will be addressed here, while the latter aspect will require continued development once these devices are field-ready. To foreshadow the former aspect, we contend that there is a balance between the need for slow and complete evaporation from the host sol-gel and the need for the guest quantum dot to have as little water present as possible. Careful control of the drying rate must be maintained for highest quality quantum dot embedded solgels.

While both the host and guest point to very dry conditions as their ideal environments, it will be shown that the road to preparing a monolithic, optically clear, high efficiency sol-gel requires control of the kinetics of the sol-gel formation process. Pushing the drying limits can be approached with simple humidity control.

4.2.3 Coordinating Solvents

Surface Passivation

Water is not an entirely bad prospect for quantum dot photoluminescence. It has been shown that the presence of water initially acts to increase the photoluminescence efficiency by passivating surface defect sites[42]. The coordinating electron pairs on the oxygen in water have the possibility to temporarily fill electron deficient surface trap sites typically caused by ligand vacancies. Water also has the advantage of being a small molecule so that it may diffuse quickly and efficiently through the ligand shell. As the coordinating electron pair weakly interacts with a trap site, most likely through physisorption, the nonradiative processes involved with carrier trapping are shut down. Consequently, since these darkening processes have been halted, the radiative process becomes more dominant and the quantum yield increases as a consequence.

Photodegradation

However, the negative aspect from water is now that it is interacting with the quantum dot surface, other energetic oxidative reactions may take place. These photochemical or photocatalyzed reactions result in the degradation of the quantum dot surface[42]. Therefore the action of water on quantum dots is a two-fold process: (1) the water molecules increase

the photoluminescence quantum yield by passivating surface traps and (2) the water photo-degrades the CdSe quantum dot surface through oxidation. If the former effect can be exploited and the latter averted, an ideal situation of maximum device efficiency without device degradation can be achieved.

Competitive Reagents

As simple way of achieving strong surface passivation can be obtained by choosing an organic agent that mimics the properties of water that activate the photoluminescence, namely (1) small size and (2) coordinating electron pairs, but avoid the aspect that causes photodegradation, chiefly (3) high reactivity coming from oxygen. Since hydrolysis is an unavoidable step in the sol-gel process, the organic agent must be introduced in the form of a solvent so that a situation may be created wherein it competes with water for trap sites. This approach can be successful with stronger coordination and an excess of the organic agent.

4.2.4 Variations to the Quantum Dot Guest

Another approach of inhibiting the photo-oxidative processes that reduce the quantum efficiency arises from manipulation of the quantum dot chemical composition. This has historically been approached in three different ways: (1) altering the semiconductor makeup of the quantum dot, (2) introducing an inorganic shell that is more resistive to oxidation and (3) modification of the quantum dot shape. Typically, non-spherical shapes tend to increase electron-hole separation and reduce photoluminescence, therefore they will be ignored since they are counterproductive to our aim.

Inorganic Shell

A popular post-synthetic modification to pre-existing quantum dots is the addition of a secondary semiconductor to the reaction solution which results in a shell of the second semiconductor forming on top of the first. This inorganic shell, if chosen wisely, can be utilized for several different purposes. Chief among these is to reduce photo-oxidation with a semiconductor that is less prone to spontaneous oxidation. The most commonly utilized inorganic shell for the CdSe quantum dot system is ZnS, being both less prone to oxidation and being well-matched to the CdSe symmetry and structure.

Since photo-oxidation from water occurs at the quantum dot surface, utilizing a photo-resistive inorganic shell will reduce photo-oxidation. Indeed, this has already been proven in self-assembled monolayers that photo-activation can be achieved while photo-degradation can be avoided[42].

Core Chemical Composition

Similar to changing the inorganic shell, the core chemical composition itself can be altered to inhibit photo-oxidation. The only drawback to this approach is that changing the core elements without careful consideration could produce inconclusive results. To this end, the popular approach in inorganic chemistry of using periodic trends regarding ionization potential and electron affinity to ascertain reaction prediction can be applied to quantum dot surface chemistry.

Specifically, we can consider how the oxidation potential varies as we move across a period or down a group. With regard to our model system of CdSe, the most likely options involve the variance of the anion since varying the cation introduces more complicated synthetic procedures. Logically, going down a group provides the best variance since moving across a period would require drastic changes in the semiconductor composition. The elements downwards in a group are iso-electronic with respect to their valence shells. Looking at Group VI of the periodic table, above and below selenium are sulfur and tellurium, respectively. Not surprisingly, CdS and CdTe quantum dots can be synthesized with procedures not unlike CdSe quantum dots.

Therefore a series comparison of the behavior of CdS, CdSe and CdTe would yield important information of how the stability is affected by the crystal composition. Briefly, we expect the following series of stability: $CdS > CdSe > CdTe$ based upon the oxidation potential $Te > Se > S$ since the stronger oxidation potentials produce more reactive crystals and more reactive crystals will oxidize faster.

4.3 Experimental

4.3.1 Preparation of CdS, CdSe and CdTe Quantum Dots

CdSe, CdS, and CdTe quantum dots were synthesized using previously published synthetic techniques[3]. As prepared, they were capped with hexadecylamine, which for incorporation

into solgels had to be replaced with aminopropylmethoxysilane.

Preparing Quantum Dots for incorporation

For sol-gel synthesis, a few hundred milligrams of quantum dot was placed in a test tube and gently heated until the material melted. Several milliliters of methanol were then added, and the solution centrifuged for several minutes. The pellet was then dissolved in 0.25ml of chloroform and several milliliters of methanol was added again, to precipitate the quantum dots out of solution. This was repeated 2 or 3 more times. After the final wash, the pellet was resuspended in 1 mL of APeS. Before proceeding, the absorbance and emission of the dots was checked to ensure there was no drastic shift in optical properties from the parent material.

4.3.2 Preparing the Sol-gel

After the preparation of the quantum dots, the TMOS solution was prepared which consisted of three compounds: (1)TMOS, (2)co-solvent, and (3)distilled water. The ratio of TMOS:water:co-solvent was 3:0.25:6 unless otherwise noted. For the highest quality sol-gels, the co-solvent needed to be completely dry, and the only water in the reaction carefully controlled by the amount of water added to the TMOS solution. Aliquots of the quantum dots capped with APeS were placed in the desired containers for the sol-gels to form in. The TMOS solution was then added to the molds and the solutions carefully mixed.

4.3.3 Optical Measurements

The emission of the samples was monitored using a Varian Eclipse Fluorimeter. The excitation beam was 90° from the collection path to reduce refracted excitation light of solid samples. For solid-state photoluminescence, emission was taken in borosilicate test tubes inserted into the excitation path without a secondary sample holder. All samples were measured in the disposable test tubes that they were cast in, in order to limit physical damage to the sample.

4.3.4 Exposure of Quantum Dots to Solvents and differing environments

Methanol and Acetonitrile

To determine the effect of solvent on the emission intensity of the materials, the co-solvent was varied. The solgel mixture was prepared as described previously, with the co-solvent being either dry methanol or dry acetonitrile.

Heat, Vacuum, Dessicant

After formation of stable, high quality alcogels, the samples were exposed to a variety of treatments, attempting to both increase the stability of emission from the quantum dots and decrease the rate of time necessary to produce a dry xerogel.

For humidity controlled conditions, the alcogels, still in the test tube they were cast in, were placed in a desiccator. A typical set up is shown in Fig. [4.1](#).

4.4 Curing: Heat, Vacuum, Humidity

To re-iterate what was mentioned in the introduction, typical sol-gel preparations that do not contain quantum dots can be cured under ambient conditions. The resulting sol-gels are optically clear and monolithic. However, since water is a concern for quantum dot stability, the water concentration in the sol mixture will be reduced by controlling the humidity through external means.

Additionally, the stability of quantum dot embedded xerogels was explored under different environmental conditions: ambient, vacuum, heat and humidity. The goal is to produce a super-dry, monolithic quantum dot embedded xerogel with strong photoluminescence and high optical clarity.

Table [4.1](#) summarizes these findings.

4.4.1 Vacuum

As stated before, dry conditions are ideal for both the sol-gel and the quantum dot. To this end, we attempted to remove the water at the earliest step: immediately following the sol-gel reaction, in an effort to prevent as much photo-degradation as possible for the quantum dot.



Figure 4.1: Photograph of a standard gel drying apparatus. Shown in the picture are a desiccator, a sol-gel within the test tube reactor, and a hydrometer. The humidity in the desiccator was monitored by the hydrometer.

Table 4.1: Itemizes the effect of different treatments (left column) on Quantum-Dot Embedded xerogels in descriptive terms of their stability (middle column) and optical clarity (right column). (*) One week was picked as the time scale since this is also the time it takes to undergo the first condensation

Treatment	Stability	Optical Clarity
Vacuum	Crumbles	N/A
Vacuum, aged 1 week	Crumbles(longer than unaged)	N/A
Heat(70°C)	Crumbles	Opaque(small fragments)
Heat(70°C), aged 1 week	Minor cracking	Opaque
Uncovered, DryRite	Cracking	Clear with cracks
Covered, DryRite	<i>Monoliths, very stable</i>	<i>Clear</i>

When placed under a strong vacuum immediately after the reaction, the sol-gel dries very quickly. This incredibly low-pressure environment causes the solvent and water to be lost immediately from the solution. Since water is a necessary component in the hydrolysis step of the sol-gel reaction, the sol-gel reaction is incomplete without it. As a result, the domains in which there is a continuous polymeric structure is very limited, resulting in very small fragments. Even after the solution has been allowed to cure for a week under ambient conditions prior to exposure to the vacuum, the end result remains the same: crumbling sol-gels. However, since the sol-gel was given time to cure slowly in that week, the crumbling takes place on a much slower scale.

4.4.2 Heat

In a similar approach to applying a vacuum (lowering pressure), heat was applied (increasing temperature), to promote solvent evaporation. With mild heat (70°C), the rate of evaporation would be slower. This would still allow polymerization through hydrolysis to continue while slowly reducing the presence of water.

Some success was achieved in this method, in comparison to the vacuum treatment, in that crumbling of the sol-gel was reduced. The resulting larger fragments, however, were opaque and therefore not suitable for use in optical measurements. Even when allowed to cure for a week prior to heating, the sol-gel remained opaque. Notably though, the sol-gel was monolithic through this process, with some small visible cracks appearing in the structure.

4.4.3 Humidity

The heat treatment, while milder than the vacuum, still produces unusable opaque gels. To attempt a milder approach, the freshly prepared sol-gel mixtures were placed into a dessicator.

Under these conditions, the sol-gels resulted in the same monolithic structures as in the cured/heated version discussed above, but with one important distinction: they were transparent. The sol-gel solution placed directly in the dessicator eventually produces some cracking in the large structure. This, too, can be avoided by covering the reaction test tube with parafilm and using a pin to produce a very small hole. This small hole limits the rate at which water can be drawn out of the sol-gel and captured by the dessicant. Therefore, the overall reaction rate has been kinetically slowed down.

The final result is clear, uncracked, monolithic sol-gels embedded with quantum dots, achieved by slow evaporation in a dessicator.

4.5 Super Dry Xerogels

4.5.1 Photoluminescence Under Dry Conditions

The photoluminescence of the well-formed, super-dry quantum dot embedded xerogels cured in the dessicator in Table 4.1 was monitored over the course of its curing. The emission intensity is plotted in Figure 4.2 over the course of three weeks.

Time zero in this experiment was the moment the reactants were combined, with the entire test tube reactor being placed in the desiccator immediately after. It is important to note that photoluminescence measurements were taken rapidly, removing the test tube reactor from the desiccator for as little time as possible then immediately replacing it, so that the sol-gel was exposed to very dry conditions over the course of the entire experiment.

Very Stable Photoluminescence

Interestingly, the photoluminescence of the quantum dot responds to the curing process, showing drops (water oxidation) then rises (gel shrinking), before finally settling into a stable photoluminescence. The curing process for this particular sol-gel can be seen to take about 4 days ($\sim 100hrs$), at which point all structural changes have completed. It is beyond this curing point that the quantum-dot embedded sol-gel shows its most striking feature:

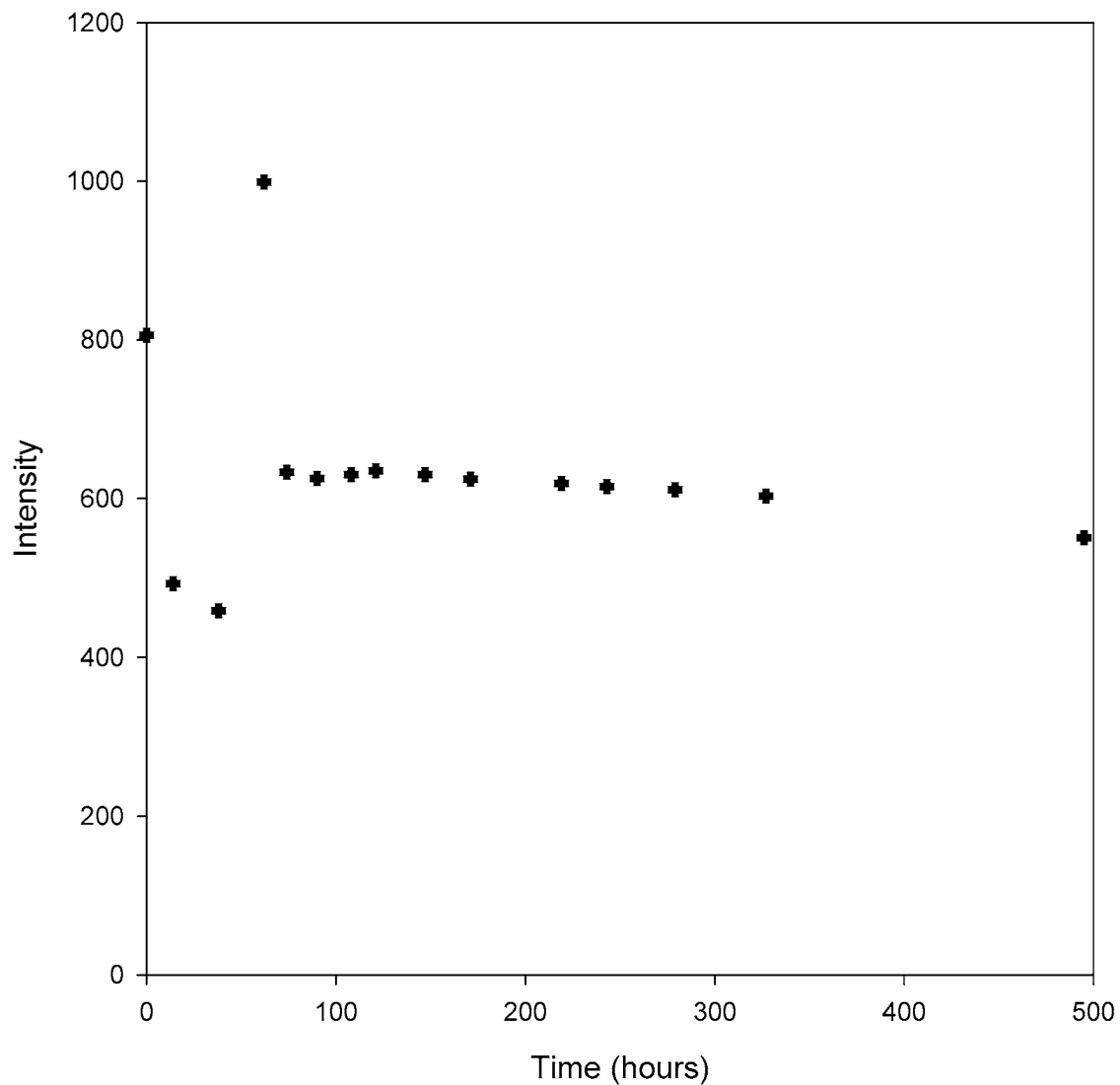


Figure 4.2: The photoluminescence intensity of a 3.5nm CdSe embedded sol-gel sealed in a desiccator was monitored during its curing phase and beyond. The sol-gel remained in the dry dessicator environment over the course of the entire experiment. The line connecting the points is a guide to the eye.

the photoluminescence intensity remains extraordinarily stable over the course of the next 14 days, dropping less than 10 percent of its original intensity.

This strong, stable photoluminescence from this material makes it a bright prospect for use as a lighting material, as long as its immediate environment can be controlled. As will be shown in the next section, ambient conditions produce a more reduced photoluminescence efficiency.

4.5.2 Photoluminescence under Ambient Conditions

With the creation of super-dry, monolithic, high photoluminescence quantum dot embedded xerogels, the next logical step is to determine their performance in ambient conditions. The well-formed xerogels created in Table 4.1 were removed from the desiccator after two weeks of curing and the photoluminescence was monitored. This data is shown in Figure 4.3.

Water Absorption

Along with the photoluminescence intensity, the mass of the sol-gel was also monitored. Time zero corresponds to the moment the sol-gel was removed from the desiccator. As the sol-gel moves from a very dry environment (desiccator) to a wet environment (ambient), there will be some water absorption by the sol-gel since it is very hygroscopic. In less than 12 hours after its removal from the dessicator, the sol-gel will have absorbed enough water vapor that it will be in equilibrium with its environment.

It can be seen in Figure 4.3 that the mass of the sol-gel increases rapidly until it reaches a fixed value after 12 hours or so. This mass gain remains unchanged for the next 5 days and longer, and is directly proportional to the water gained from the atmosphere.

Photoluminescence Quenching

Looking at the photoluminescence from the quantum dots, it can be seen that it drops substantially as water is gained. Over the course of the next three days, the photoluminescence drops slowly to zero, such that after 90 hours, the photoluminescence is completely quenched. The resulting sol-gel, although optically clear and monolithic, has entirely lost its quantum dot emission. The reason for this reduction in photoluminescence intensity comes from the oxidation of the quantum dot surface in the presence of water[42].

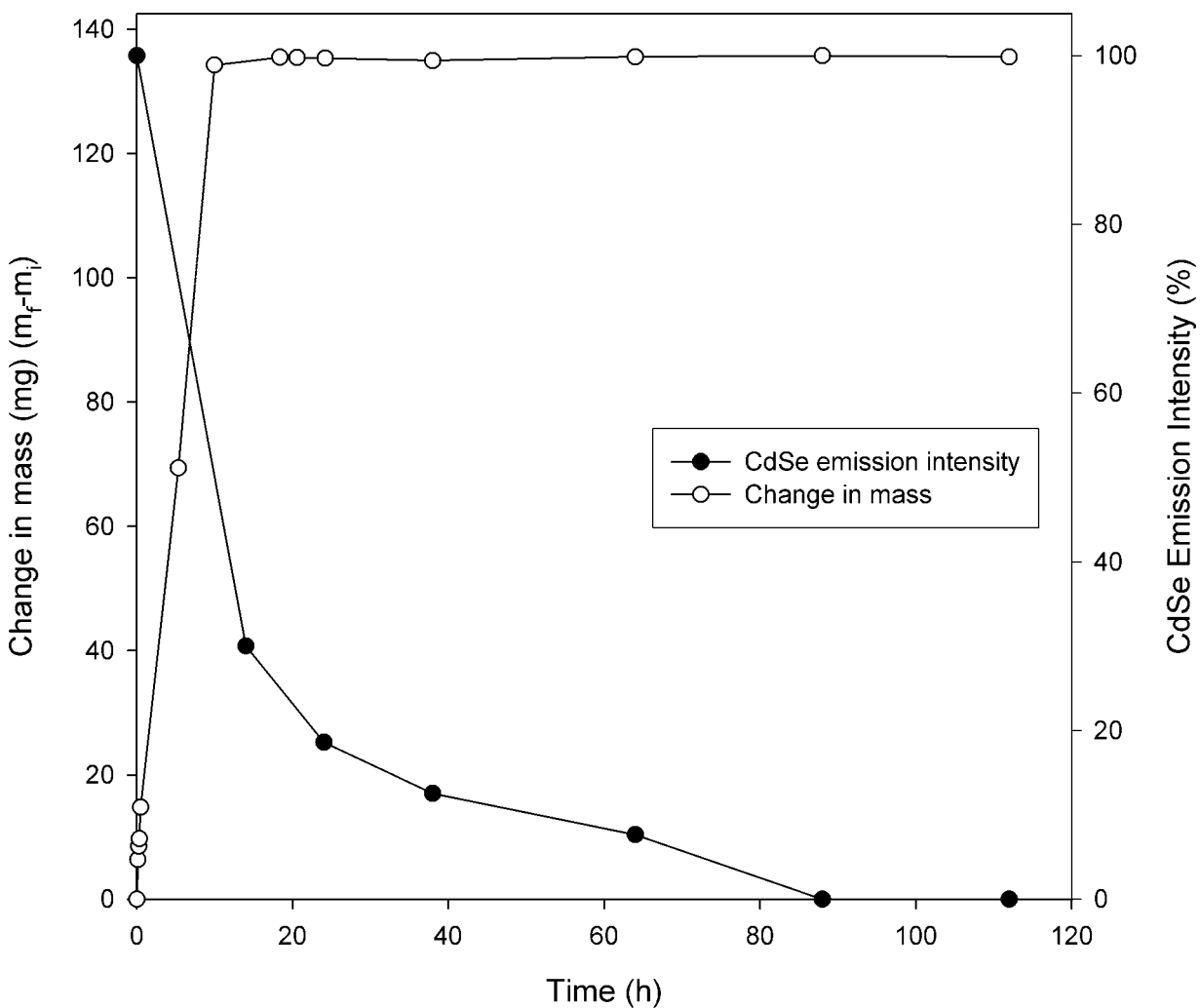


Figure 4.3: The emission intensity of a gel that had been carefully dried for 2 weeks in a humidity controlled environment was monitored when it was exposed to ambient conditions. This data is plotted as a percent change, with the max intensity at time zero being 100. At the same time, corresponding measurements of the samples mass were recorded.

The presence of water is absolutely lethal to the function of a stable quantum dot embedded sol-gel. With water present, the half-life of the photoluminescence is on the order of hours, while without water, the photoluminescence stability may be on the order of months (extrapolated).

4.6 Solvent Effects

As stated in the introduction, the use of a small, coordinating solvent to competitively fill the electropositive trap sites on the quantum dot surface, can increase quantum dot emission without resulting in oxidation. This organic agent must be (1) small, (2) coordinating, (3) relatively unreactive and (4) miscible in water. There are few reagents that fit these restrictions, and acetonitrile is the most readily available one.

Experiments forming clear, strong photoluminescence quantum dot embedded xerogels were performed with the replacement of methanol with acetonitrile as the solvent. The resulting photoluminescence from the sol-gel is plotted in Figure 4.4. Note that each sol-gel compared has identical amounts of quantum dots, such that the emission intensity should be directly proportional to the average population quantum yield.

As can be seen in Figure 4.4, the photoluminescence intensity of the acetonitrile treated quantum-dot embedded sol-gel is much greater than the methanol treated sol-gel. This increase in photoluminescence comes from the reduction of quantum dot surface oxidation from water, which occurs more frequently in the methanol case than the acetonitrile case.

4.7 Different Quantum Dot Guests

To ascertain how periodic trends affect the stability of quantum dots embedded in xerogels, a series of synthetic modifications were made. Two aspects were varied: (1) the identity of the Group VI anion (S, Se, Te) and (2) the presence of an inorganic capping shell, namely ZnS.

4.7.1 CdS and CdTe Quantum Dots

Xerogels were simultaneously prepared containing either CdS, CdSe or CdTe quantum dots. The photoluminescence intensity was monitored over the course of their curing time and appears in Figure 4.5.

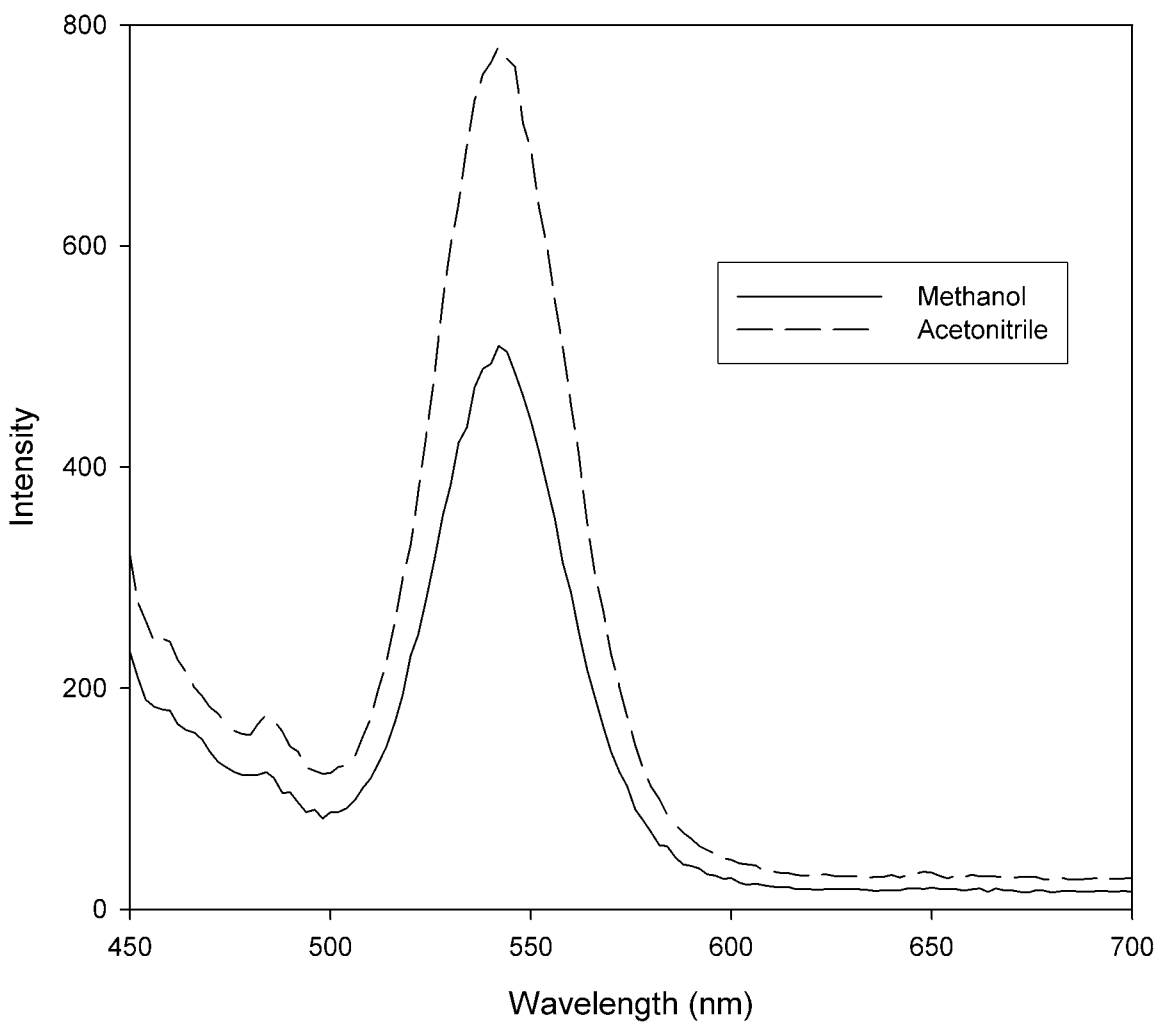


Figure 4.4: Two 3.5nmCdSe embedded sol-gels were created under identical synthetic conditions, with the only variation being the solvent used. The initial emission from the gel synthesized with aceto is almost double the emission intensity of the gel created using methanol as a co-solvent.

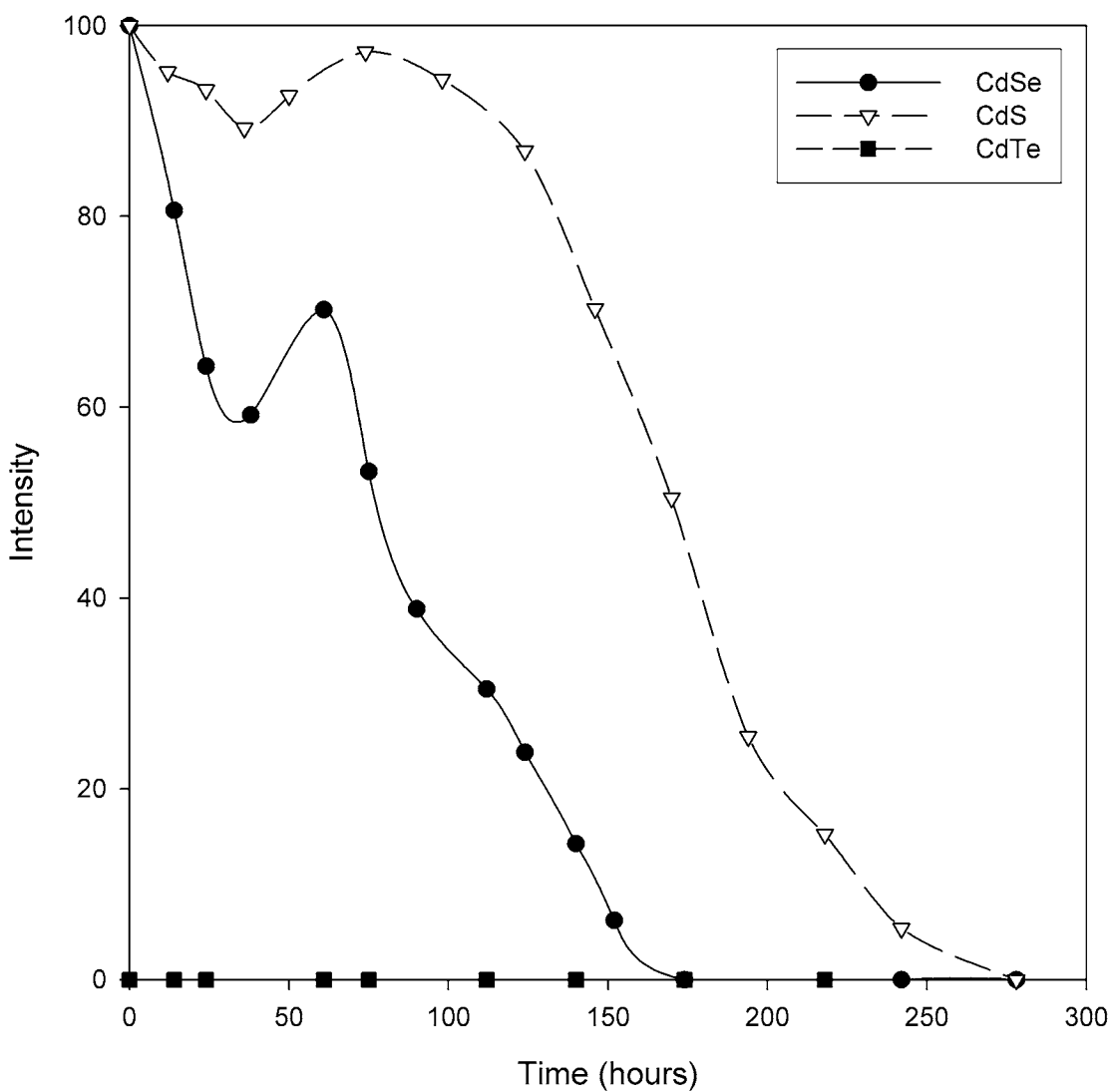


Figure 4.5: The photoluminescence intensity of xerogels containing either: CdS, CdSe or CdTe quantum dots. monitored over the course of gel curing. Time zero corresponds to the addition of the reaction mixture. Curing took place under ambient conditions.

The CdTe emission was entirely quenched, even from the outset of the experiment, despite having similar concentrations to the CdS and CdSe counterparts. CdS and CdSe embedded gels both show the typical drop in photoluminescence (onset of oxidation) along with the rise (gel contraction), then subsequent decline toward zero photoluminescence (resulting from continued oxidation and degradation).

Notably, the photoluminescence from the CdS embedded gel persists for significantly longer a time period than the CdSe version. While the half-life of the photoluminescence of CdSe is only 3 days, the half-life of CdS lasts for over a week, and while the emission from the CdSe version expires in 175 hours, the CdS emission lasts for another hundred hours longer (275 hours). The overall trend for the half-lives can be seen as $\text{CdS} > \text{CdSe} > \text{CdTe}$.

As mentioned in the introduction, the primary effect of moving down a group is that the oxidation potential should increase, and we therefore expect that CdTe should oxidize more easily than CdSe, and the CdSe should oxidize easier than CdS. Following this trend, we would consequently expect that CdTe should degrade faster than CdSe and CdSe faster than CdS. As a result, the rate of loss of emission activity should follow this degradation trend and we expect CdTe should decay faster than CdSe and CdSe should decay faster than CdS. This prediction is exactly what we observe. CdS is the most stable of the three, lasting an unprecedented duration in ambient conditions (11 days) and most dramatically, CdTe is completely quenched at the moment of the reaction.

4.7.2 Core-Shell Quantum Dots

Adding an inorganic shell that is resistant to oxidation has the benefit of filling any ligand vacancies that result in trap sites and consequently reduce oxidation frequency, with an added benefit that the native photoluminescence quantum yield is also improved. These so-called core-shell quantum dots have historically proven to be remarkably stable as well as remarkably bright.

CdSe quantum dots overcoated with ZnS were added to a sol-gel reaction to produce a high quality, strongly emitting xerogel. To determine how the presence of water would affect these xerogels, several samples with varying water concentrations were prepared. The TMOS:water:dry methanol for the samples were: A: 3:2:6, B:3:1:6, and C 3:0.5:6. After initial alcogel formation, there was no difference in wavelength or intensity of emission from the three samples. They were then allowed to age under ambient conditions for two months.

Bright Core-Shell Xerogels

After two months, the emission spectra were taken; these are shown in Figure 4.6 as well as a representative spectra of the initial alcogels.

After two months, the ZnS-coated CdSe quantum dot embedded xerogels remain strongly emitting, and are the most bright and the most stable quantum-dot embedded xerogel variant made so far. Whereas the emission of the best uncapped quantum dot embedded xerogels lasted on the order of weeks, the emission of these core-shell dots last for months. A photograph showing how strong the photoluminescence is to they eye is shown in Figure 4.7.

Water Impervious Photoluminescence

Interestingly, the trend with respect to the concentration of water is counterintuitive with respect to the results of the uncapped quantum dots. In those experiments it was found that samples with higher water concentration tended to produce weaker emission. In the core-shell gels, it is the samples with higher concentration that produce the stronger emission. From Figure 4.6, we can see that the highest water concentration (A) also has the strongest emission, followed by (B) with an intermediate water concentration and finally the lowest emission coming from (C) having the lowest water concentration. If anything, it seems that water has improved the photoluminescence without affecting the stability.

This observation is consistent with a situation wherein water increases the photoluminescence due to trap site passivation (on the ZnS surface) which would result in stronger emission. This passivation would occur more frequently with higher water concentrations (which is what is observed). However, since the ZbS is less prone to oxidation, water does not reduce its long-term stability, allowing it to remain photo-active for months. Therefore, these core-shell dots benefit from the advantages of water (increased emission) without suffering from the disadvantages (photo-degradation).

Conclusively, the most highly efficient and stable quantum-dot embedded xerogels can be achieved if the quantum dots themselves are capped with ZnS. Conveniently, these can be prepared under ambient conditions and do not require the use of any curing treatments.

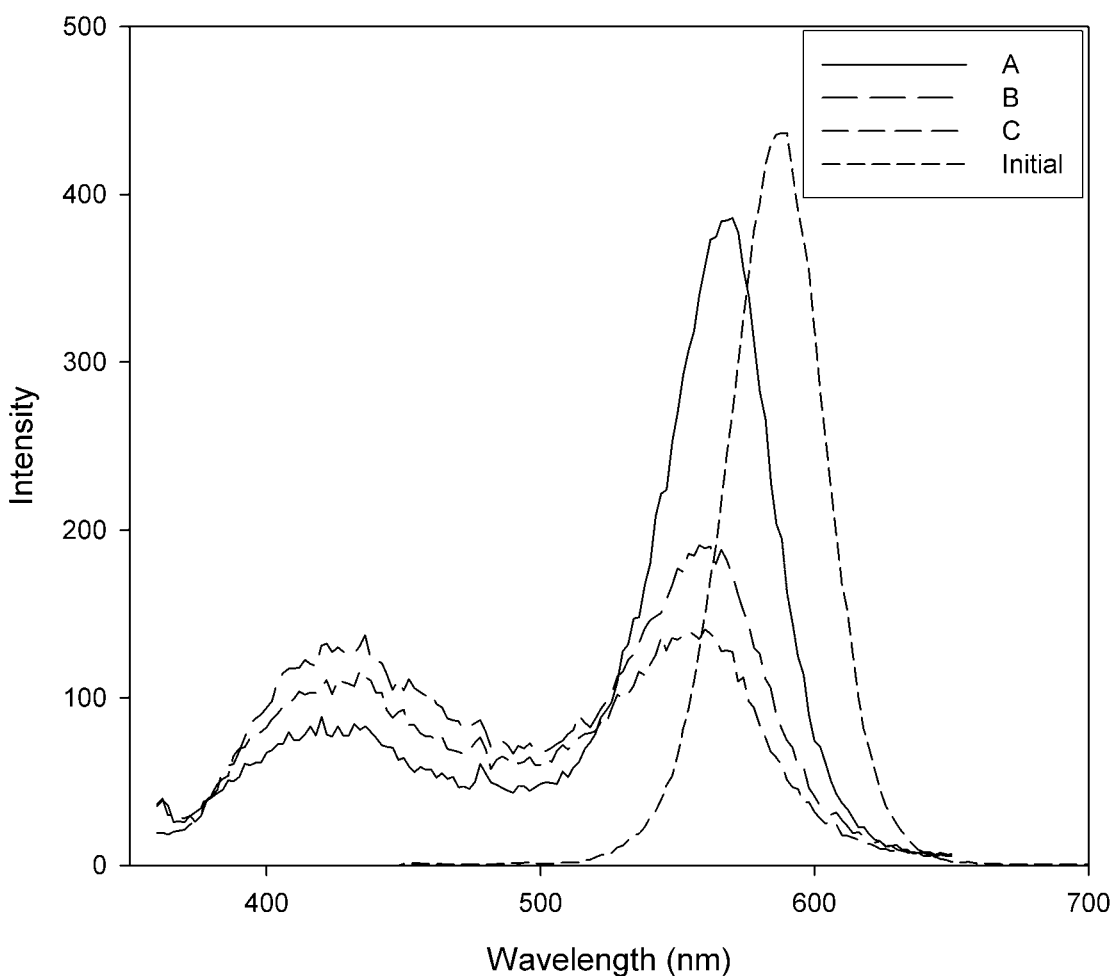


Figure 4.6: Photoluminescence spectra of ZnS-coated CdSe quantum dots embedded in a silica xerogel, with different starting water concentrations (A,B,C). All quantum dots showed identical emission spectra at the moment of reaction (represented by the curve called Initial). Two months after curing, the emission spectra changed depending on water concentration: 2 parts water (A), 1 part water (B) and 0.5 parts water (C).

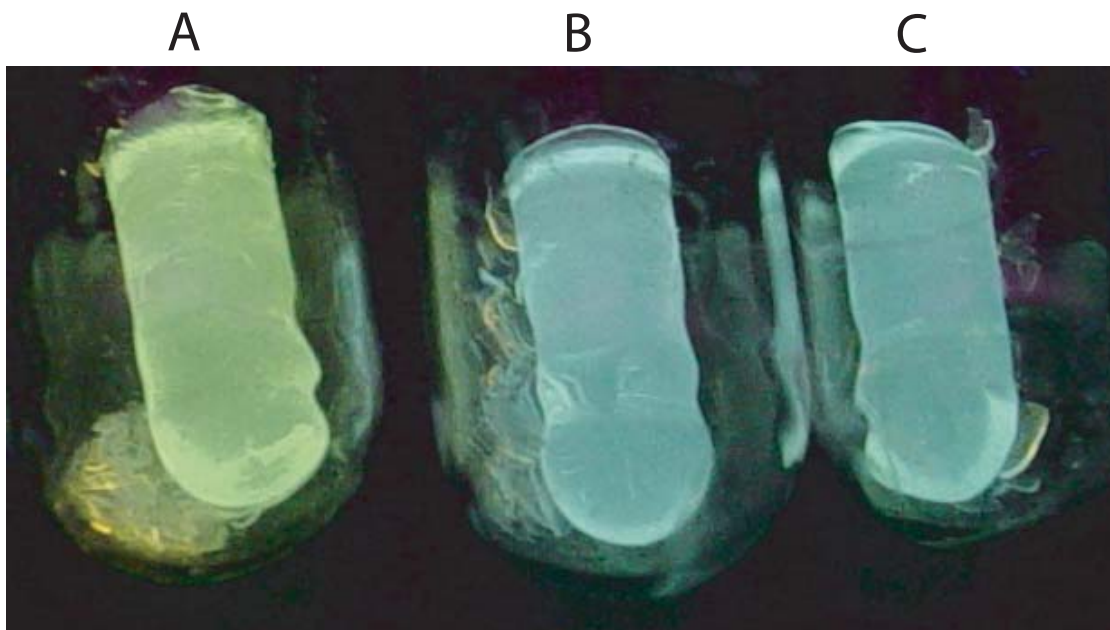


Figure 4.7: Digital photograph of three ZnS-coated CdSe quantum-dot embedded xerogels inside their reaction test tubes, illuminated with a UV light after two months curing in ambient conditions. The labels (A), (B) and (C) correspond to their respective spectra in [Figure 4.6](#)

4.8 Chapter Summary

Long term stabilization of CdSe embedded sol-gels was achieved by: (1)carefully controlling the water used to synthesize the gels, (2)limiting environmental exposure to ambient water, and (3) controlling the oxidative potential on the surface of the quantum dot. For the highest quality materials, all of these factors need to be carefully optimized. For example, a material that has a low oxidative potential (i.e. CdSe-ZnS) is more forgiving to water exposure, while one with a higher oxidative potential (i.e. CdSe) needs to have much more stringent environmental conditions for production of high quality materials.

We have shown that long term stability for CdSe sol-gels is possible under controlled conditions (low water content used for sol-gel creation and limited environmental exposure to ambient water).

CHAPTER 5

CDSE QUANTUM DOTS EMBEDDED INTO POROUS GLASS

5.1 Motivation

5.1.1 The Problem with Sol-gels

Although the incorporation of quantum dots into silica matrices like sol-gels has yielded promising results, the primary issue with these materials remains the susceptibility to water, which drastically affects the photoluminescence intensity through photo-oxidation. Two fundamental flaws plague silica sol-gels: (1) the necessity of water in the hydrolysis step of gel formation and (2) the hygroscopic nature of the resulting sol-gel that forces uptake of water under ambient conditions. Regarding long-term stability, the large pore sizes in these silica sol-gels can be problematic, trapping water and other small molecules in close proximity to the quantum dots.

5.1.2 Using Pre-formed Glass

An alternative approach to creating transparent, rigid, malleable structures is embedding quantum dots into a pre-formed glass rather than forming the glass around the quantum dots[43]. This will be the focus of the current chapter, wherein stable, porous glasses were exposed to quantum dot solutions so that they may be incorporated into the glass through simple diffusion and adhesion. Because the glass is already formed, there are no reaction steps that involve water that will unnecessarily expose the quantum dots to moisture. For these reasons, it is expected that this approach will yield stable, bright, glasses embedded with quantum dots.

5.2 Introduction

5.2.1 VYCOR[®]: a porous glass

VYCOR[®] is a silica glass produced by Corning and is composed of 96 percent silica. Unlike other silica products, it can be formed into a variety of shapes, although sheets or rods have been historically preferred. VYCOR[®] is made in a multi-step process. First an alkali-borosilicate glass is formed into the desired shape. It is then heat treated to produce two distinct phases. The first phase is boric oxide and alkali rich; the second phase is silica. Afterwards, it is soaked in hot acid, which dissolves the first phase. After washing, only the silica phase remains. At this point, the material is highly porous and possesses a high affinity to water and organics. On average, VYCOR[®] has an internal pore diameter between 4 and 6 nanometers, which may be an issue for QD embedding, particularly in limiting the incorporation of larger sizes of quantum dots (where the dot diameter is greater than the pore diameter)[44].

5.2.2 Synthetic Manipulation

Immersion

Since VYCOR[®] was purchased directly from Corning, pre-shaped into rods, the only issue manipulated is the incorporation of quantum dots. This process can be achieved by simply immersing the VYCOR[®] in solutions of quantum dots. It is expected that the quantum dots will encounter and collide with the pores on the VYCOR[®] surface, and become trapped[45]. Relying on only the statistical encounter of empty pores with quantum dots, this process is expected to take some considerable time[46].

A Sticky Ligand

Alternatively, to improve the embedding process, some the HDA ligands present on the quantum dots were exchanged for APeS, the goal with this modification being that the quantum dots would be more likely to stick to the silica glass surface if the surface of the quantum dot was itself composed of silica. This modification was expected to improve quantum dot adhesion and glass formation.

5.3 Experimental Methods

5.3.1 VYCOR[®] Preparation

The VYCOR[®] glass rod was cut using a diamond blade into thin wafer disks (approximately 1 to 3 mm in thickness). The water used on the saw made the material wet and increased the opacity of the material. After the disks were cut, they were placed in a 100C oven overnight to dry. After drying the discs were once again transparent.

5.3.2 Embedding Quantum Dots

A solution of CdSe quantum dots was prepared by taking a few hundred milligrams of CdSe-HDA and was placed in a test tube and gently heated until the material melted. Several milliliters of methanol were then added, and the solution centrifuged for several minutes. The pellet was then dissolved in ~ 1 mL of toluene. The dry VYCOR[®] disk was then placed in the CdSe-toluene solution and the container sealed. The VYCOR[®] was allowed to soak in the quantum dot solution for 48 hours. The disk was then removed from the solution and allowed to dry. Upon initial removal from the CdSe solution, the disks were extremely opaque. However, once they were allowed to dry, they returned to the translucence of the original dry material.

5.3.3 Ligand Exchange

A few hundred milligrams of CdSe-HDA was placed in a test tube and gently heated until the material melted. Several milliliters of methanol were then added, and the solution centrifuged for several minutes. The pellet was then dissolved in ~ 0.25 mL of chloroform and several milliliters of methanol was added again, to precipitate the quantum dots out of solution. This was repeated 2 or 3 more times. After the final wash, the pellet was resuspended in 1 mL of APeS. Before proceeding, the absorbance and emission of the dots was checked to ensure there was no drastic shift in optical properties from the parent material.

5.3.4 Optical Measurements

The emission of the samples was monitored using a Spex Fluorolog Fluorimeter. Excitation was achieved with a Xenon arc lamp coupled to an excitation monochromator. All emission

was measured using front-face excitation of the sample and collected using an emission monochromator coupled to a PMT detector.

5.4 Results and Discussion

5.4.1 Quantum Dot-Embedded VYCOR[®]

Two different sizes of CdSe quantum dots were successfully embedded into VYCOR[®], namely 3.5nm and 5.0nm, both overcoated with HDA. A photograph of these two glasses is shown in Figure 5.1, under UV illumination. As can be seen, the quantum dot-embedded VYCOR[®] glasses strongly luminesce, and possess the distinctive colors representative of their solution-phase luminescence; the 3.5nm CdSe embedded glass glows green while the 5.0nm glass glows orange. Additionally, the transparent nature of the glass remains intact in these samples. The orange luminescence of the 5.0nm glass emitting through the 3.5nm CdSe-embedded glass sample can be clearly seen.

5.4.2 Ligand Exchange: APeS

Interestingly, although the exchange of the organic ligands present on the CdSe quantum dots (HDA) with a silica based ligand (APeS) was expected to improve quantum dot uptake into the porous glass, the opposite observation was noted. Despite long term immersion of VYCOR[®] into solutions of CdSe quantum dots capped with APeS, no embedding occurred. Specifically, when the VYCOR[®] disc was removed, it was colorless, and the quantum dot solution retained its strong color. None of the quantum dots in solution embedded into the VYCOR[®].

Currently it is unclear why this particular strategy failed to work. Several explanations can be put forth. For example, trace amounts of water present may have catalyzed gel formation, allowing some quantum dots to aggregate into small, soluble clusters. The aggregation of only a few quantum dots would inevitably lead to their inability to embed into the silica pores. For example, if a water molecule catalyzed the addition of two quantum dots to form a bound pair, then that total pair diameter would be greater than the pore diameter, and subsequent encounters with the silica pore would prevent it from physically fitting into the pore.

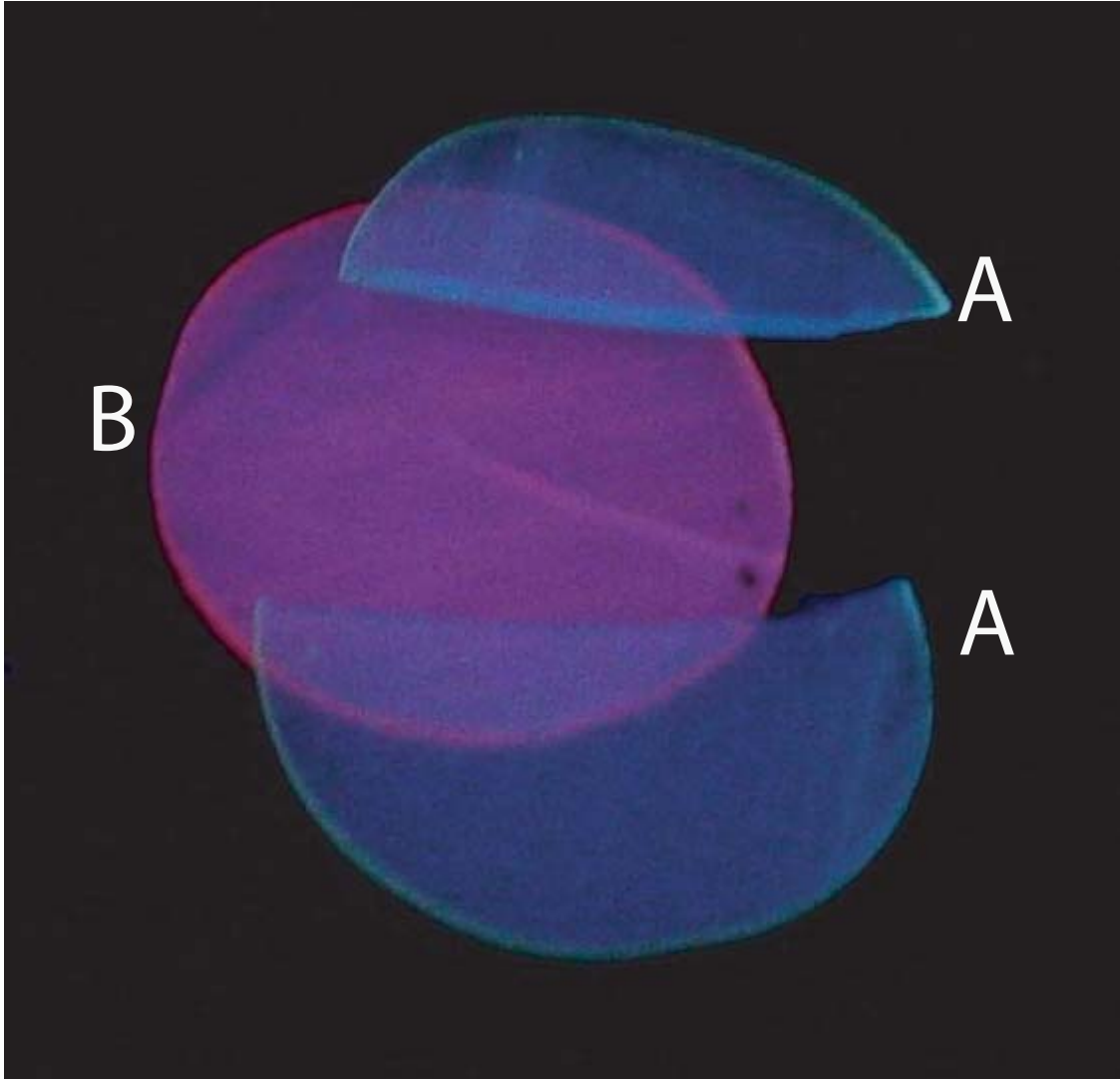


Figure 5.1: Photograph of disks of VYCOR[®] embedded with CdSe-HDA, under UV illumination. The fractured disk (both halves are labeled A) is embedded with 3.5nm CdSe-HDA. The disk labeled B is embedded with 5nm CdSe-HDA. The VYCOR[®] disks emit brightly and are translucent to the eye.

5.4.3 The Kinetics of Assembly

The photoluminescence was tracked starting immediately after VYCOR[®] was immersed in the quantum dot solution. From here, all the following results will deal exclusively with HDA-capped quantum dots since (as mentioned above), the APeS exchanged dots were resistant to embedding. Figure 5.2 shows the photoluminescence taken over a period of 48 hours, wherein the VYCOR[®] disc was removed from the quantum dot solutions briefly during measurements. The lower wavelength region of the quantum dot luminescence was not measured due to the presence of reflected excitation light, which can be considerable since this experiment was performed using front-face excitation. No valuable data in this region was lost: as can be seen from the figure, the photoluminescence traces have identical profiles and differ only in their relative intensity.

Despite this, it can be seen that the photoluminescence of the VYCOR[®] disc (peak wavelength=575nm) rises slowly with time over that 48 hour period. The reason for this increase is that the photoluminescence is directly proportional to the quantity of CdSe quantum dots embedded in the VYCOR[®] pores. Therefore the climb in photoluminescence mirrors the increased number of quantum dots embedded in VYCOR[®] as time progresses. At approximately 48 hours the uptake of quantum dots has reached its maximum: all the pores are filled and the fabrication of a quantum dot embedded porous glass is complete. Testing of this new material can now begin.

5.4.4 The Robustness of the Quantum Dot Embedded Glass

Redissolving into Solvent

Now that a quantum dot embedded porous glass has been successfully formed, the next logical question would be to address how strongly the quantum dots are bound to the silica surface. For device incorporation, it is important to know if this quantum-dot embedded VYCOR[®] can be exposed to further chemical treatments during a typical device fabrication process, particularly solvents. Essentially, the strength of this association can be tested by exposing the quantum dot embedded glass to a medium that is favorable for the quantum dots, particular an organic solvent they are strongly soluble in. When exposed to that medium, the quantum dots embedded in the pores may dissociate and become free within the solution. The resulting photoluminescence of the VYCOR[®] disc would be reduced due

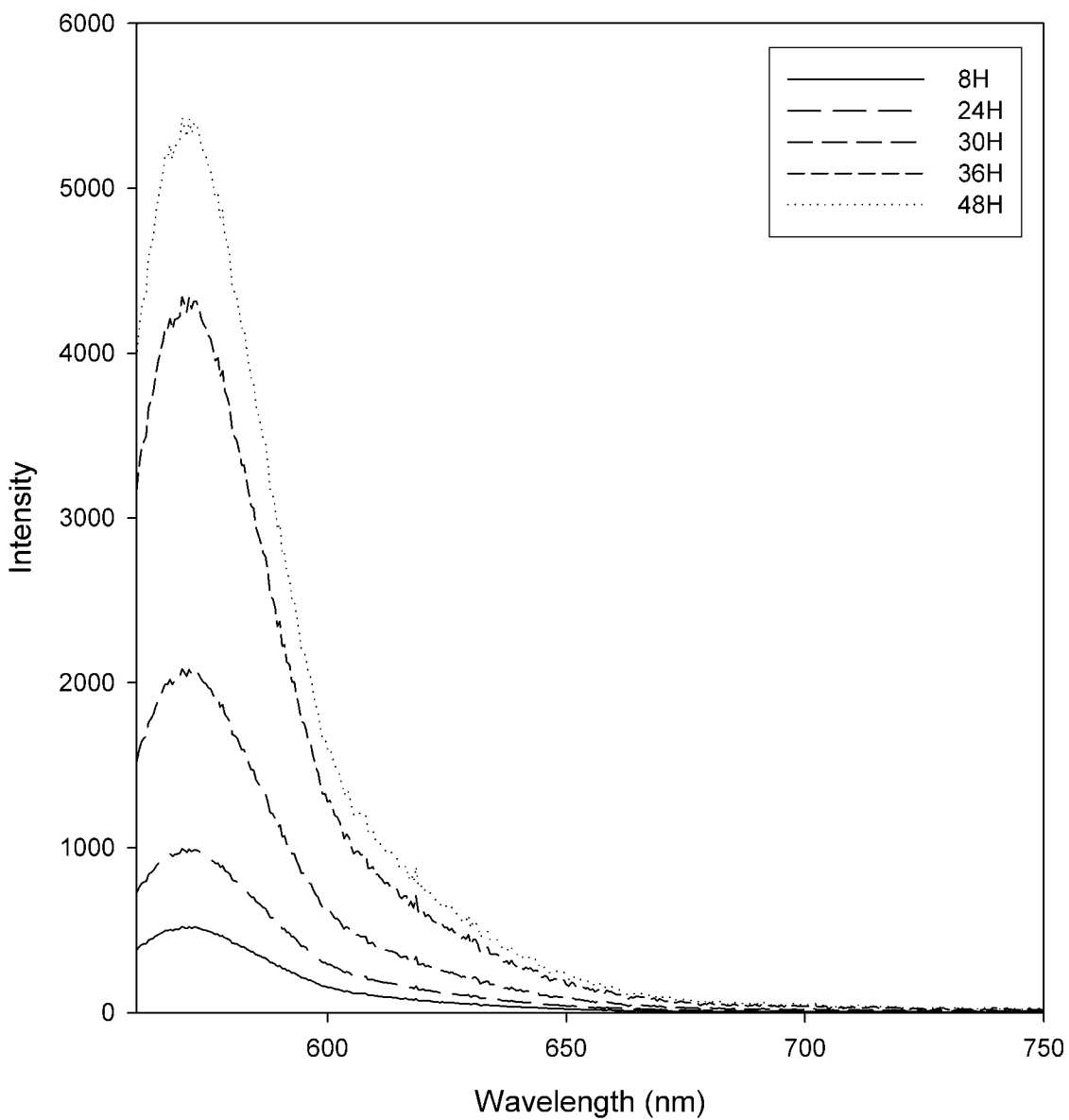


Figure 5.2: Photoluminescence spectra of a VYCOR® disk soaked in a solution 5nm CdSe-HDA/toluene is shown at different time intervals. There is a steady increase in emission intensity over a 48 hour period of immersion.

to the smaller population of embedded quantum dots.

Immersion in Pure Toluene

Following the complete implantation of quantum dots into the VYCOR[®] disc, the disc was immersed in a solution of pure toluene; no quantum dots were present in that solution. Even after a period of 8 hours, the quantum dot embedded disc retains its photoluminescence intensity. This is shown in Figure 5.3. As can be seen, the intensity and emission profile varies less than 1 percent before and after 8 hours of continuous immersion in pure solvent. Since the intensity and profile are unchanged, this strongly implies that little to no quantum dots have departed from the host matrix. They are all strongly bound to the VYCOR[®] surface.

5.4.5 Long-term Photoluminescence Stability

Comparison to Sol-gels

An important aspect for this material's long term use as either a sensor material or an illumination source rests in its stability under ambient conditions. Whereas quantum dots embedded in sol-gels demonstrated that quantum dot-embedded glasses possess strong photoluminescence under dry conditions, under ambient conditions the photoluminescence decayed rapidly due to the presence of water. To determine how this material performs under ambient atmosphere, identical conditions as performed with the quantum dot embedded sol-gels were utilized. The photoluminescence under these conditions was monitored, and the intensity as a function of time appears in Figure 5.4.

Stability Under Wet Conditions

Despite the presence of water in the atmosphere under ambient conditions, the photoluminescence remains remarkably stable. As stated, the period of photoluminescence intensity increase found in the first 48 hours after implantation is a result of the VYCOR[®] gradually uptaking the quantum dots. The time after this 48 hour period, when embedding is complete, reflects how stable the quantum dots are in this environment. As can be seen, the photoluminescence does not decrease and remains stable within 2 percent of variation despite a remarkably long 8 days of exposure. This increase in stability is a significant improvement upon the sol-gel variant.

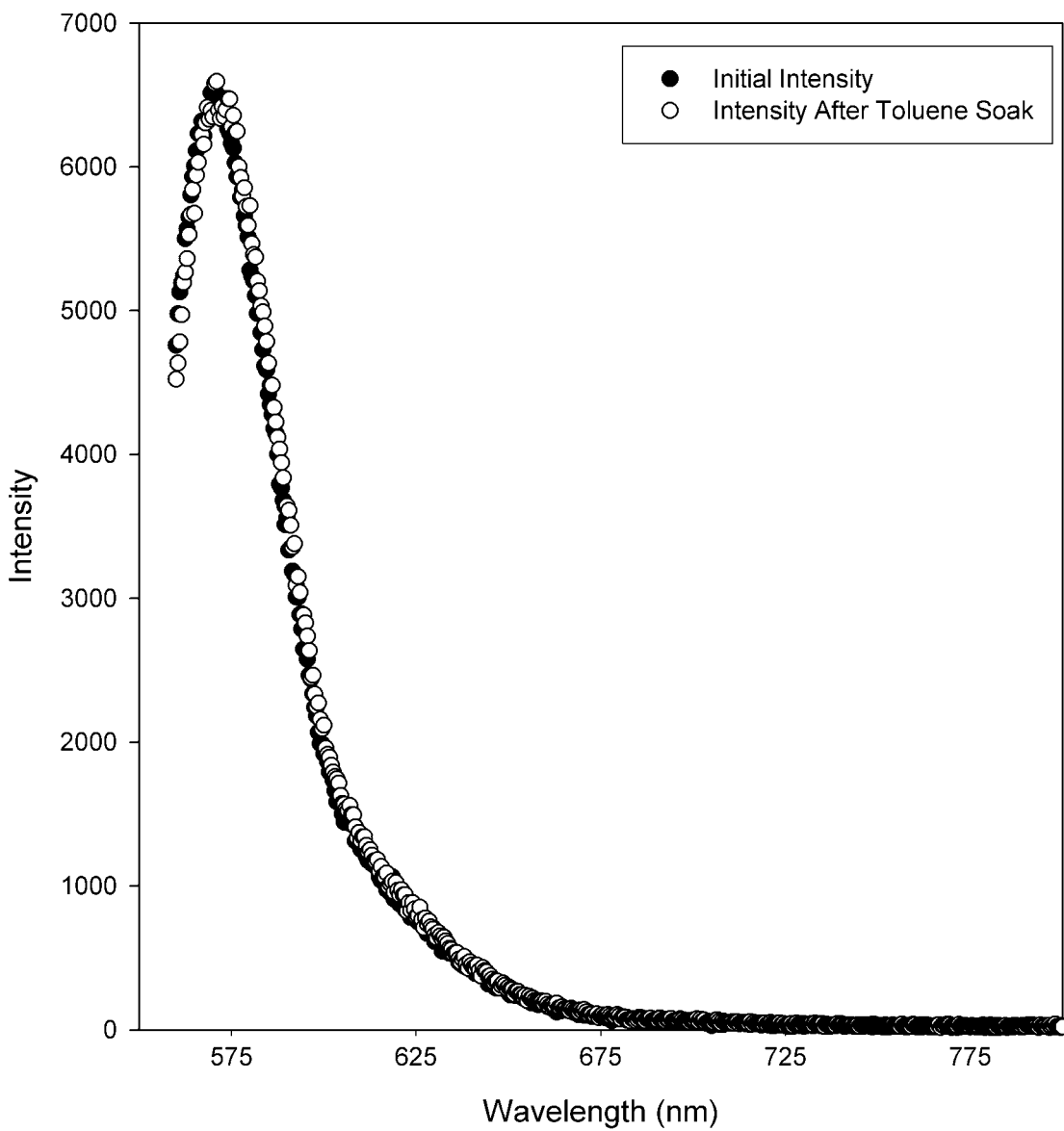


Figure 5.3: Photoluminescence spectra of a 5.0nm CdSe embedded VYCOR® disc before and after (8 hours) immersion in pure toluene

Explanations for Long-Term Stability

This preservation of long-term stability under wet conditions is somewhat surprising, considering the open nature of the porous glass, and that particularly no post-fabrication treatment was used to seal out ambient moisture. Moreover, VYCOR[®] is itself hygroscopic so that over the course of time, the uptake of water from the atmosphere would be a natural process. The strong similarity in chemical composition to sol-gels is also striking; both sol-gels and VYCOR[®] are amorphous silica-based glasses. Arguably the only fundamental structural difference between the two lies in the pore size: VYCOR[®]'s are much smaller than the sol-gels

Indeed, it is the pore size that presents itself as the most likely candidate for explaining this newfound stability. The very small pore sizes are just big enough to accept these quantum dots and little else. Their small size may explain their exclusion of other accompanying materials. For example, as a quantum dot embeds itself into one of these pores, it prevents further access of water into the pore since it is physically blocking the path. Therefore the uptake of water into the VYCOR[®] itself can be limited due to this. If water cannot get around the quantum dot embedded in that pore, then it can only attack the exposed side: the side pointing away from the VYCOR[®] surface toward the environment. This geometric effect should itself reduce the process of photo-oxidation.

5.4.6 Quantum Dot Implantation Depth

The incredibly small pore diameter of the VYCOR[®] matrix was expected to impose serious complications in the degree of penetration that the nanomaterial can make into the porous glass. Because the quantum dots utilized are comparable in diameter (3.5nm, 5.0nm) to the VYCOR[®] pore size (4-6nm), then blocking of the entrance deeper into the VYCOR[®] is expected. Therefore, a complication in the embedding nature of these quantum dots is that only the surface of the VYCOR[®] (in direct contact with the immersed quantum dot solutions) will be populated with quantum dots. Quantum dots cannot penetrate into the core of the VYCOR[®] material, and thus the quantum dots are a solely surface phenomenon.

The application of a file to the VYCOR[®] surface verifies this expectation. Filing down the top 1-3 millimeters of the VYCOR[®] disc surface reveals a colorless region of VYCOR; the characteristic quantum dot color, and consequently quantum dots themselves have been

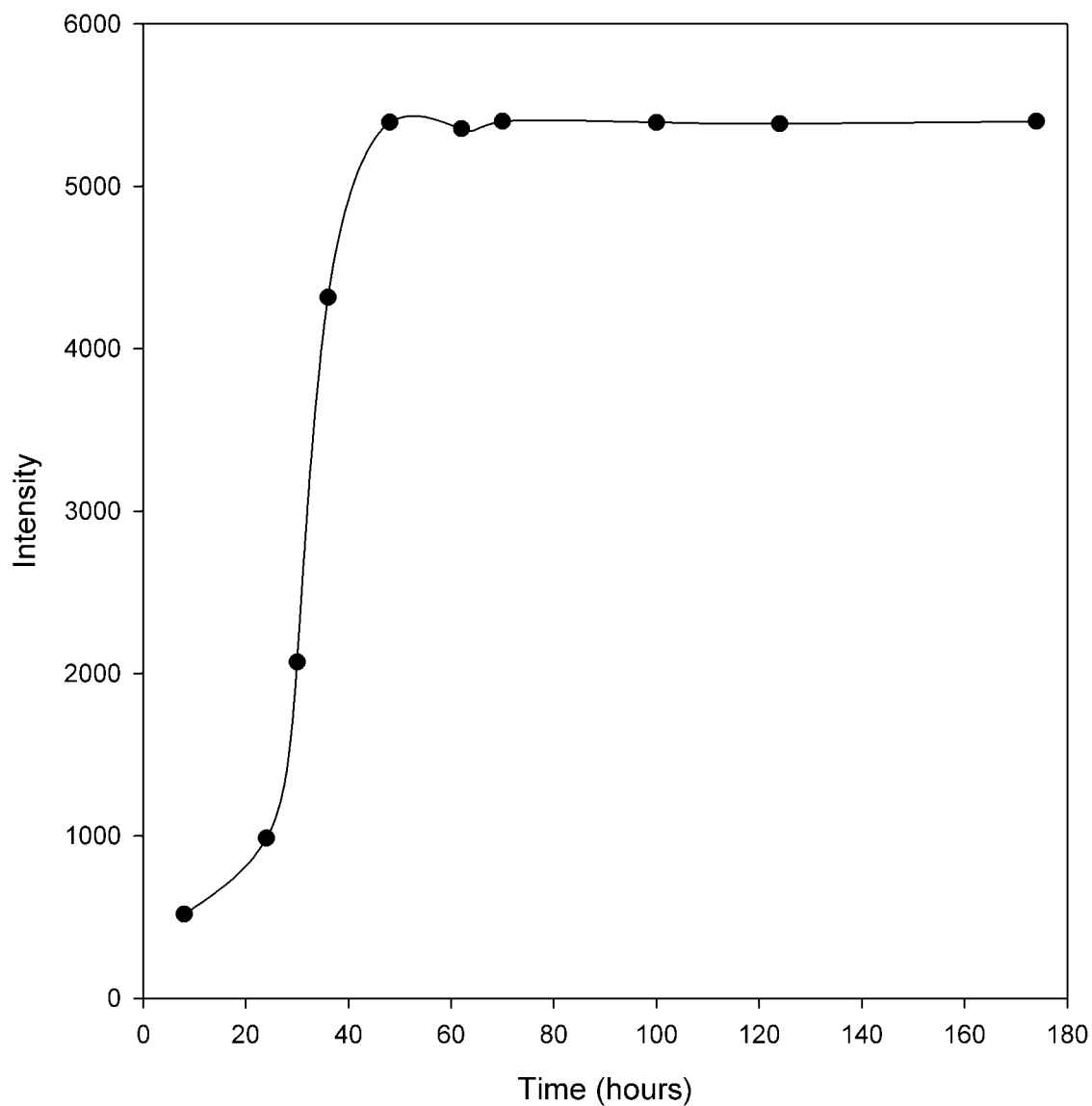


Figure 5.4: The maximum photoluminescence intensity of a sample of VYCOR® embedded with 5nm CdSe quantum dots was monitored over time. After 48 hours the sample was removed from the quantum dot soak and allowed to dry under ambient conditions. The emission intensity remained steady over time.

removed. Under UV illumination, this exposed fragment is no longer photo-active.

5.5 Chapter Summary

Despite the desirable qualities of quantum dots for device applications, their poor stability under ambient conditions, particularly in the solid-phase has made them difficult to incorporate. The development of a host material that confers stability has been a major goal in the incorporation of these quantum dots into various devices.

This chapter documents the production of CdSe quantum dots embedded into the commercially available porous glass, VYCOR®. These structures are transparent, strongly luminescent and very stable under ambient conditions. As such, they hold much promise for their utilization in devices for the purposes of sensing and lighting. However, since the glasses are pre-formed, the implantation of quantum dots deep into the VYCOR® matrix could not be achieved, and only superficial penetration of the nanomaterial was realized. Despite this limitation, combination of the easy access of the host matrix (VYCOR® is commercially available and inexpensive) and the ease of preparation (simple immersion), still make this material not only a viable, but strong candidate for further investigation for device incorporation.

CHAPTER 6

NANOCRYSTALLINE SENSORS: VAPOR SENSING IN GLASS, FILM, PLASTIC AND LIQUID

6.1 Motivation

6.1.1 Advantages and Disadvantages of Nanomaterial Sensors

A rapidly growing area for nanomaterial applications has been the field of sensors and detectors, particularly of chemical agents[47]. Possessing significant advantages of conventional sensors, such as increased surface area, greater sensitivity and microscopic integration, nanomaterials have been characterized as next generation sensors. However, along with these strengths come directly related weaknesses. While greater surface area may increase the contact interface between sensor and analyte, the larger higher energy surface makes the sensor more prone to degradation through simple usage. Though nanomaterial sensors have proven to be greatly sensitive to a variety of chemical agents, their selectivity among those requires more complicated design.

6.1.2 Device Integration

Most importantly to this chapter, is the question of integration of these nanometer-sized sensors into macroscopic designs, which comprises the bulk of their application. While their incredibly small size makes them advantageous into incorporation into microscopic environments such as biological cells, their size also poses a problem into their incorporation into larger systems such as integrated circuits. In other words, while attachment of individual nanocrystals to structures such as DNA and proteins is elegant and straightforward through chemical functionalization, their incorporation into bulk structures raises more questions, such as: How can these nanocrystals be interrogated and addressed from a bulk system?

How can they be made robust and stable for long term use in ambient or thermally stressed environments? How can they be physically incorporated into hand-held devices, manipulated with electrical signals and their optical reports detected?

To summarize, there must be an equally elegant way of bulk incorporation that mirrors the microscopic incorporation that has been the primary focus of this field. This will be the focus of the current chapter, as solutions to these issues will take the form of utilizing inert, durable, transparent matrices to facilitate the first stages of device integration.

6.2 Introduction

6.2.1 Explosives Detection

In recent years, the need to be able to reliably detect and identify the presence of explosive threats has become increasingly important. Despite recent technological advancements in detection, which include immunoassays and fluorescent polymers, the best sensor for inexpensively searching large areas at a time remains the canine nose. Most sensitive techniques, such as GC-MS, are limited by the requirements of extensive sample preparation or large amounts of instrumentation that are not practical in field settings. Most explosive materials exhibit extremely low vapor pressures (typically less than 10ppm under standard conditions), making detection much more difficult. The ideal sensor is one that is portable, robust, requires no complex sample preparation, has specificity between different explosives, and is low cost to produce.

6.2.2 The Photoluminescence as an Optical Report

It is natural to take advantage of the strong photoluminescence found in CdSe quantum dots as the signal monitored for detection. While the Stern-Volmer data detailed in Chapter 2 has revealed the interaction between CdSe quantum dots and anthracene, the primary change in photoluminescence that was quantitatively monitored was the reduction in anthracene intensity. Not all organic reagents have a fluorescence or phosphorescence that can be monitored, so the photoluminescence of the nanomaterial will be the report that is monitored. Moreover, while resonance energy transfer was found to be the primary action between anthracene and CdSe, that interaction may not be found between CdSe and other organic reagents; in fact, it is unlikely if those organic reagents are not optically active.

Despite this absence of energy transfer, a significant number of interactions are still possible between the CdSe and the organic reagent, including energy transfer, surface passivation, and interaction with the capping ligands. All of these interactions should produce changes in the photoluminescence intensity or profile.

6.2.3 Trinitrotoluene

Historically, trinitrotoluene (TNT) while not the most powerful explosive, was the standard that all other explosives were measured against[48]. With its relative stability under ambient conditions and the low vapor pressure common to most explosive materials, it makes an excellent material to begin investigations on explosive detection.

6.2.4 Solution-phase sensing

Determining CdSe Quantum Dot Sensitivity to TNT

Solution phase studies are critical to help examine the interaction between the quantum dot and the explosive. The kinetics equations developed for solutions (i.e. Stern-Volmer) strongly aid in determining the fundamental question of whether or not CdSe quantum dot photoluminescence will be affected by the presence of TNT, and if so: is this effect predictable, understandable and most importantly, quantifiable. The simple approach will then be to track the photoluminescence intensity as a function of controlled amounts of TNT dissolved in an organic solvent.

Advantages

Aside from the ease of preparation, a freely dissolved nanocrystalline sensor possesses the advantage of being inserted in microscopic environments that a solid-phase bound sensor cannot enter. Biological cells, capillary tubes, and molecular electronics are all popular examples of nanocrystals utilized in this way.

Disadvantages

Perhaps the simplest and simultaneously the most complicated nanocrystalline sensor is that dissolved freely in an organic solution. While this type of sensor requires no preparation except for solvation, the reagent selectivity is much more complicated due to the very large variety of organic soluble reagents that can quench the CdSe photoluminescence. To

overcome this, a chromatographic/separation step can be performed prior to analysis to isolate the presence of the analyte. Alternatively, a multi-channel analysis can be performed to obtain the “fingerprint” of the analyte, utilizing several reporters whose sensitivity to the same organic reagent varies. The electronic nose (ref) is a classic example.

6.2.5 Thin Evaporated Films

Thin Film Deposition Styles

A simple and straightforward approach to device integration is the simple evaporation of a concentrated nanocrystal solution (typically dissolved in a volatile organic solvent) directly on the sensing platform. While elaborate ways of creating this densely packed, thin, solid film have been utilized (such as spin-coating, spray-coating, etc...) their primary focus has been the uniformity and homogenization. Simple drop-casting can be utilized provided that the accumulation of evaporation rings does not become problematic to the sensing function.

Advantages

This particular fabrication has some unique advantages and disadvantages. Among the advantages is that this particular fabrication produce the highest density: greatest number of sensors in the smallest volume, along with the easiest fabrication method: simple evaporation. Additionally, since there is no barrier between the quantum dots and the analyte, these should provide the fastest response time and arguably the greatest sensitivity. Moreover, the application of thin films directly onto the sensor can be done easily with this method. Drop-casting a thin film over the top of a photo-sensor or an integrated circuit or printed circuit board, directly into the measurement instrumentation is a unique and advantageous style for incorporation. This allows for greater signal detection since it will be unperturbed by intervening elements that may scatter the photoluminescence for example.

Disadvantages

Several disadvantages are also notable. For example, the lack of a protective matrix means these materials are the most susceptible to photo-oxidation. Moreover, since the quantum dots are so densely packed, the layers of dots beneath the top analyte-facing layer will be exposed to less analyte due to physical obstruction by the top layer. Therefore, only the top layer is utilized and the underlying layers are wasted. Significantly, this fabrication is not

robust, and must be covered with an external enclosure in the field. It cannot, for example, be exposed directly to organic solvents since it will dissolve into the organic solvent and cannot be filtered out efficiently.

6.2.6 Encased in Plastic

Advantages

Another simple technique for device incorporation is to embed the quantum dots in a dense, transparent plastic. Such an environment provides several advantages. By encasing the quantum dot so thoroughly, it provides a significant robustness to stressful conditions. Additionally, since the plastic is transparent, the optical properties should not be impacted by its presence. Finally, the concentration of quantum dots in the plastic can be arbitrarily controlled by simply altering the ratios of the starting mixture. Specifically, the approach taken will be to dissolve a commercially available plastic in an organic solvent then mix in a scalable amount of quantum dot, followed by drying of the formed plastic.

Disadvantages

While drop-cast films provide the least amount of protection, encasing quantum dots in a dense plastic produces the exact opposite: it provides the greatest amount of protection, but that protection comes at a cost. Since the plastic is dense, it certainly prevents uncontrolled oxidation of the quantum dot surface. However, this protective barrier acts to (1) impede the analyte diffusion through the plastic and (2) restrict access to the quantum dot. The primary effects of this drawback may be the increased response time and decreased sensitivity, respectively.

6.2.7 Revisiting VYCOR[®]

The fabrication of a VYCOR[®] disc embedded with CdSe quantum dots has already been addressed in a previous chapter. To summarize the important points, the VYCOR[®] discs were strongly photoluminescent, incredibly stable to water-based photo-oxidation, and accepted quantum dots only on their outer surface, produce a very thin layer (possibly monolayer) of quantum dots in their pores.

Advantages

The advantages of this system are the proven robustness of VYCOR[®] as a protective matrix to water-based oxidation, its cost effectiveness, and ease of preparation. VYCOR[®] has so far proven to be the categorically best way to embed quantum dots in the solid state, and as will be shown in this chapter, also presents itself as a useful and important sensor.

Disadvantages

Since the VYCOR[®] samples are pre-formed, if there is a need for unusual shapes, then the cost effective, commercial availability advantage of VYCOR[®] are ignored. The small pore-sizes of VYCOR[®] may make detection of large, macromolecular entities much more difficult as they will be physically excluded from entering the material. This would limit its effectiveness only to small molecules. Notably, this may not be an undesirable effect, since size exclusion may represent the first step in selectivity, which is equally important in sensor design as sensitivity.

6.3 Experimental

6.3.1 CdSe Quantum Dot Preparation

CdSe-HDA was synthesized via the cluster route[3]. However, as the material contained excess HDA left over from the synthesis, it was cleared up prior to use. A portion of the CdSe was placed in a test tube and gently heated until the material melted. Several milliliters of methanol were then added, and the solution centrifuged for several minutes. The pellet was then dissolved in chloroform and several mL of methanol was added again, to crash the quantum dots out of solution. This was repeated 2 or 3 more times. After the final wash, the CdSe pellet was processed depending on the final material that was being made, as detailed below.

6.3.2 Solution-Phase measurements

For solution phase measurements, the CdSe was resuspended in toluene. A concentrated TNT solution was prepared, and added to the standard CdSe quantum dot solution in measured aliquots. The quantities of all aliquots were tracked as a change in mass with

an analytical balance, then converted to volumes using solvent density, and finally volumes recalculated to determine effective concentration.

6.3.3 Drop-cast Films of CdSe Quantum Dots

For the preparation of drop-cast films, the CdSe pellet was resuspended in hexane. The absorption and emission of the material was then checked, and then the material was drop-cast onto clean microscope slides. The solvent was then allowed to evaporate under ambient conditions.

6.3.4 VYCOR[®]

For embedding into VYCOR[®], the CdSe pellet was then dissolved in ~1 mL of toluene. The dry VYCOR[®] disk was then placed in the CdSe-toluene solution and the container sealed. The VYCOR[®] was allowed to soak in the quantum dot solution for 48 hours. The disk was then removed from the solution and allowed to dry.

6.3.5 CdSe Quantum Dots Embedded in Polystyrene

Polystyrene beads were dissolved in toluene to form a viscous solution. The CdSe pellet was then dissolved in toluene, and added to an aliquot of the polystyrene/toluene solution. After careful mixing, the mixture was used to cast the plastic films.

6.3.6 Photoluminescence Measurements

For the steady state Stern-Volmer experiments, the emission of the dye was monitored using a Varian Eclipse Fluorimeter as aliquots of TNT were titrated into a solution of CdSe.

For all the solid state samples, the emission was monitored using a Spex Fluorolog Fluorimeter. Excitation was achieved with a Xenon arc lamp coupled to an excitation monochromator. All emission was measured using front-face excitation of the sample and collected using an emission monochromator coupled to a PMT detector.

6.3.7 TNT exposure

All the solid state samples were exposed to TNT for 24 hours by enclosing them in a sealed environment with several milligrams of crystalline TNT.

6.4 CdSe Quantum Dots Dissolved in Toluene

6.4.1 Stern-Volmer Quenching

The photoluminescence of the CdSe quantum dots was tracked as a function of TNT concentration. These results appear in Figure 6.1 in the form of a Stern-Volmer plot. The actual photoluminescence observed is tracked in the inset, from which we can see that as the concentration of TNT increases, the photoluminescence decreases. As the photoluminescence decreases, the inverse ratio of the changing photoluminescence (which is the dependent variable of the Stern-Volmer equation) increases.

The Stern-Volmer plot reveals that this relationship is linear. Moreover, analysis of the Stern-Volmer constant shows that the quenching observed is diffusion controlled. It is important here to recall the results of the previous quenching studies involving anthracene, wherein identical experiments to these were performed. The fundamental difference is that the photoluminescence of anthracene was tracked with increasing CdSe quantum dot concentration, while for these studies, it was the CdSe photoluminescence that was tracked with increasing TNT concentration. While in the anthracene experiments, strong pre-association was found due to interaction of anthracene with quantum dot ligands causing a nonlinear Stern-Volmer plot, no pre-association is found in the TNT experiments, and the Stern-Volmer plot remains linear and well-behaved. By extension, we can conclude that TNT has little to no interaction for HDA (the ligands bound to the CdSe quantum dots).

6.4.2 The Mechanism for Quenching

The quantum-mechanical quenching mechanism for anthracene and CdSe quantum dots was straightforward: resonance energy transfer. The quenching mechanism for CdSe quantum dots by TNT is more complicated. Resonance excitation energy transfer can be ruled out, however. This is primarily due to the fact that the emission profile of CdSe is not resonant with the absorbance profile of TNT. Without this resonance condition, resonance energy transfer cannot take place.

The most likely candidate for the quenching is an electron transfer. In this case, an electron from TNT or CdSe is transferred from one entity to the other. This electron carries the excitation energy, which is subsequently released in various nonradiative pathways. The entity that donated the electron is effectively quenched since charge recombination cannot

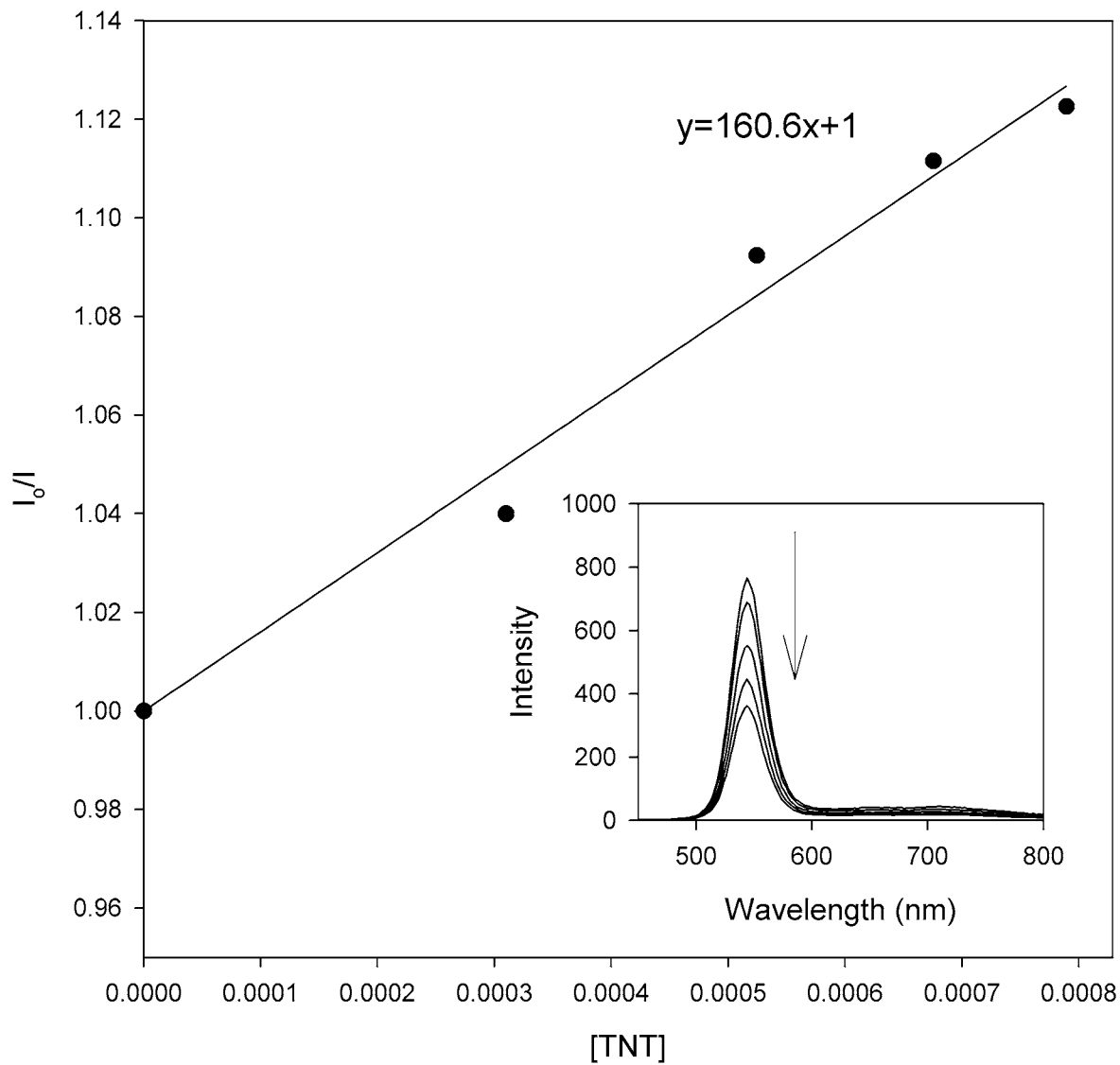


Figure 6.1: Stern-Volmer plot of 3.5nm CdSe-HDA quantum dots being quenched by TNT. Inset: Corresponding photoluminescence spectra of CdSe quantum dot photoluminescence at different concentrations of TNT. As TNT concentration increases, photoluminescence intensity decreases (as indicated by the arrow)

occur if one of those charges have been removed. Here, the remnant charges are typically normalized by interaction with the solvent or other bath states, exchanging and carrying charge until the charge difference is indirectly balanced for the two entities.

6.4.3 Prospects for Improvement

Two important results were found based on the Stern-Volmer study: (1) TNT quenches CdSe in a systematic, predictable way, and (2) TNT has very little interaction with the ligands on the CdSe surface. While the former result is promising for using CdSe quantum dots as sensors for TNT detection, the latter result fits into the undesirable category, but is not surprising since no effort was made to change the quantum dot surface to interact with TNT. Clearly, to improve the TNT detection, further modification of the surface ligands must be made. Attaching ligands that interact strongly with TNT would translate into a significant improvement to the low-level detection limits of this method. “Sticky ligands” would be able to bind trace amounts of TNT, which would result in a quenching of the quantum dot photoluminescence. This is certainly the best prospect for improving sensitivity, and fits along the lines of engineering functionalized surface ligands for quantum dots that has become popular in this field.

6.4.4 The Need for a Solid-State Sensor

However, the solution phase can be an inconvenient medium for incorporating into a bulk sensor. For example, the CdSe quantum dots in the solution will be difficult to recover and re-use for further TNT detection once they have been exposed, primarily due to their difficulty in separating from the analyte solution. This is typically done with precipitation, from which the CdSe quantum dots can withstand a limited number of cycles before massive ligand loss makes them no longer soluble in any solvent. To achieve incorporation into a solid-state sensor, solid-state alternatives need to be explored.

6.5 Thin Evaporated Films of CdSe Quantum Dots

6.5.1 Dramatic Quenching upon TNT Exposure

Thin, evaporated films of CdSe quantum dots were prepared by drop-wise addition and drying onto microscope slides. Figure 6.2 shows these slides before and after exposure to

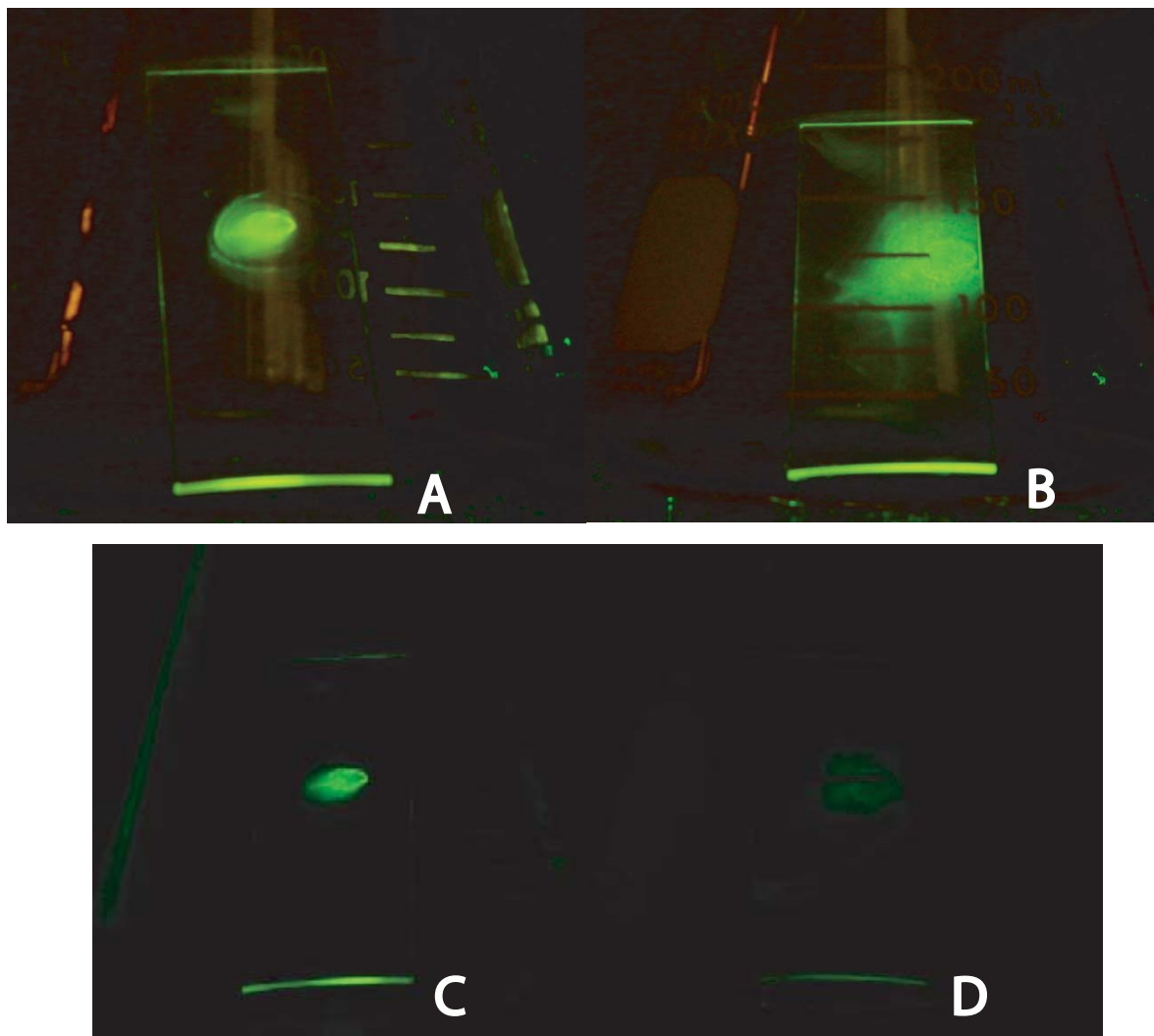


Figure 6.2: **A** and **B** are two drop-cast films of 3.5nm CdSe-HDA quantum dots. **A** was used as a control while **B** was exposed to TNT for 24 hours. After 24 hours Film **A** is shown in Panel **C**, and Film **B** in **D**.

TNT vapor for 24 hours. The change in the photoluminescence efficiency is dramatic. Side-by-side are shown two photographs under UV illumination of these drop-cast films. The left-hand sample (A,C) serves as the control (identical between the two photographs), while the right-hand sample (B,D) was exposed to TNT for 24 hours. While the control shows little to no variation in its photoluminescence intensity, the same cannot be said for the sample exposed to TNT. The photoluminescence coming from this sample is so dramatically quenched that there is little to no photoluminescence left after exposure.

6.5.2 Complications to Direct Sensing

Although this material was exposed to TNT vapor, the question still remains of the sensitivity of this particular method. Notably, the photoluminescence of thin evaporated films of quantum dots has a strong tendency to degrade over time, primarily arising from its photo-activated oxidation with ambient molecules by water. Since the photoluminescence is not stable over time, the only way of directly sensing the presence of TNT would be through a difference comparison with an unexposed, but temporally identical sample (as has been done for the control experiment above). So although the photoluminescence response was dramatic, exact quantitation becomes complex since the photoluminescence intensity cannot be reliably trusted to be invariant.

6.6 CdSe Quantum Dots Embedded in Polystyrene

6.6.1 Integrating into the Polystyrene Matrix

Figure 6.3 shows the photoluminescence spectrum before and after incorporation of the quantum dots into the polystyrene matrix. As can be seen, the photoluminescence profile shifts to higher wavelengths and broadens once it is incorporated into polystyrene. Such a change is not unexpected. Optical properties of molecular chromophores are dependent on a variety of internal and external factors, the most relevant of which are environmental rigidity and dielectric constant. Moving from toluene to polystyrene causes the dielectric constant to shift, which will certainly affect the photoluminescence energy (since all light emission is inherently electromagnetic, and consequently electrical). Additionally, the rigidity imposed by polystyrene will reduce the number of degrees of freedom and additionally bath dissipation of excitation energy.

However, a unique quantum dot change may also be interpreted from this slight wavelength shift. It is possible that the exciton wavefunction (composed separately of an electron and hole) has penetrated further than the solvated form, such that some portion may extend itself into the polystyrene matrix. The greater separation between the hole and electron wavefunctions and the resulting large exciton wavefunction would naturally give rise to a red-shifted emission on the basis of quantum confinement: larger dots (less confinement) have lower band-gaps (lower energy, higher wavelengths).

6.6.2 Photoluminescence Profile Change Upon TNT Exposure

TNT undetectable

While TNT was found to produce quenching of the CdSe photoluminescence when thin evaporated films were formed, when embedded into polystyrene, little to no photoluminescence quenching is observed. Figure 6.4 shows the photoluminescence spectra of these quantum dot embedded polystyrene films before and after exposure to TNT.

The photoluminescence intensity does not change, but the profile has become slightly narrower and slightly shifted toward the red (higher wavelengths). This change is so gradual, however, that it is not suited for use for detection. The narrowing in the peak profile is within the slit-width limitations of the emission monochromater, as is the case with the shift in peak position. Instrumentally speaking, these spectra cannot be reliably distinguished.

The lack of photoluminescence quenching is highlighted in Figure 6.5, which is a digital photograph of the polystyrene films studied in this experiment. Comparing the left-hand (unexposed) and right hand (exposed to TNT) images, there is little noticeable variation in the strength of the emitted light. Moreover, the wavelength shift observed is not noticeable; if it were, the emitted light would have a redder color (possibly appearing yellow rather than green).

Closed Framework

The lack of photoluminescence quenching is a strong indication that this material is not sensitive to TNT. The obvious reason is that the polystyrene is too densely packed around the quantum dots, and inhibits the penetration of TNT into its matrix. Without TNT present near the quantum dots, the photoluminescence remains unaltered. The problem

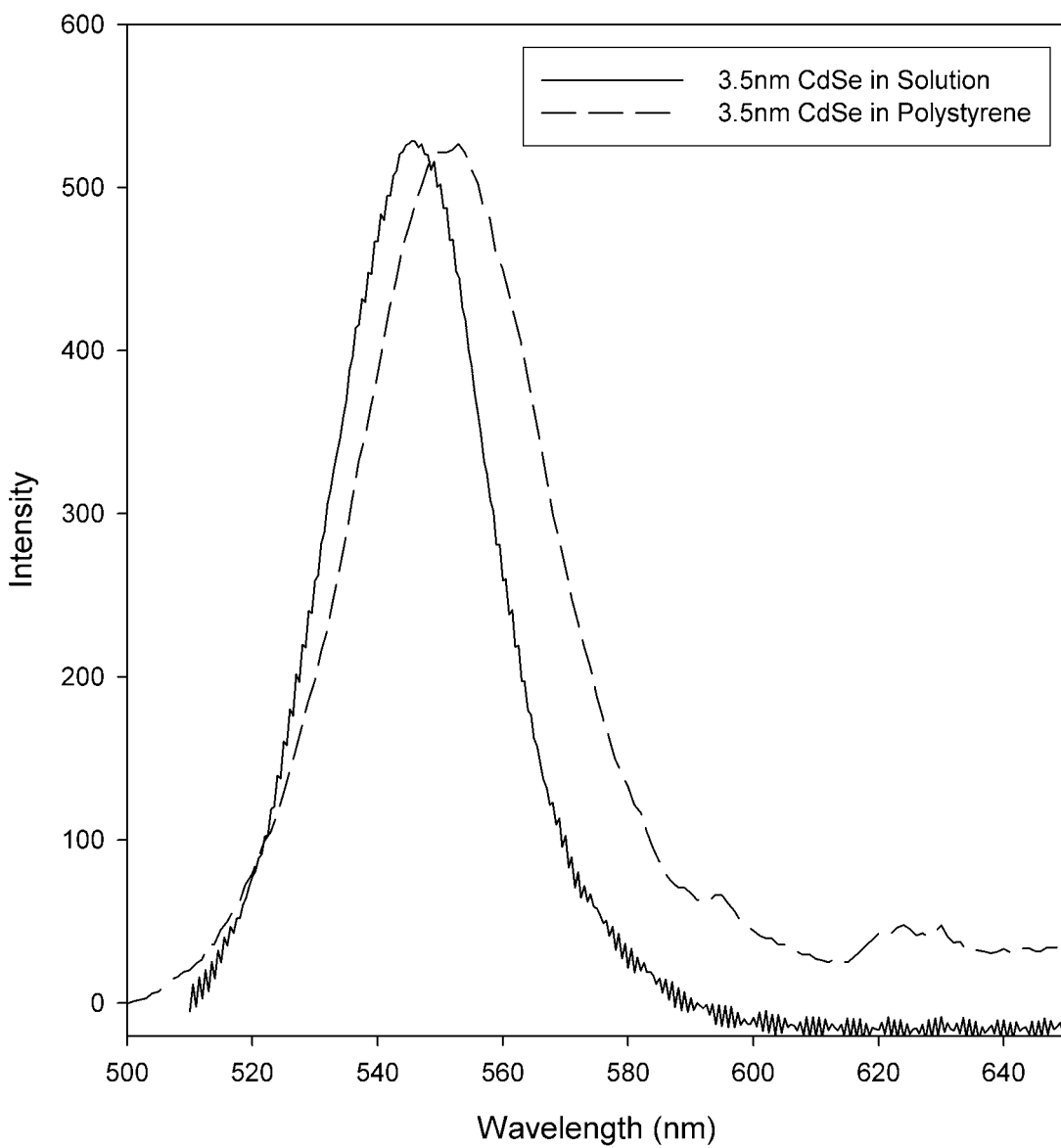


Figure 6.3: Photoluminescence spectra of 3.5nm CdSe quantum dots embedded in a polystyrene film compared to its parent solution (in toluene)

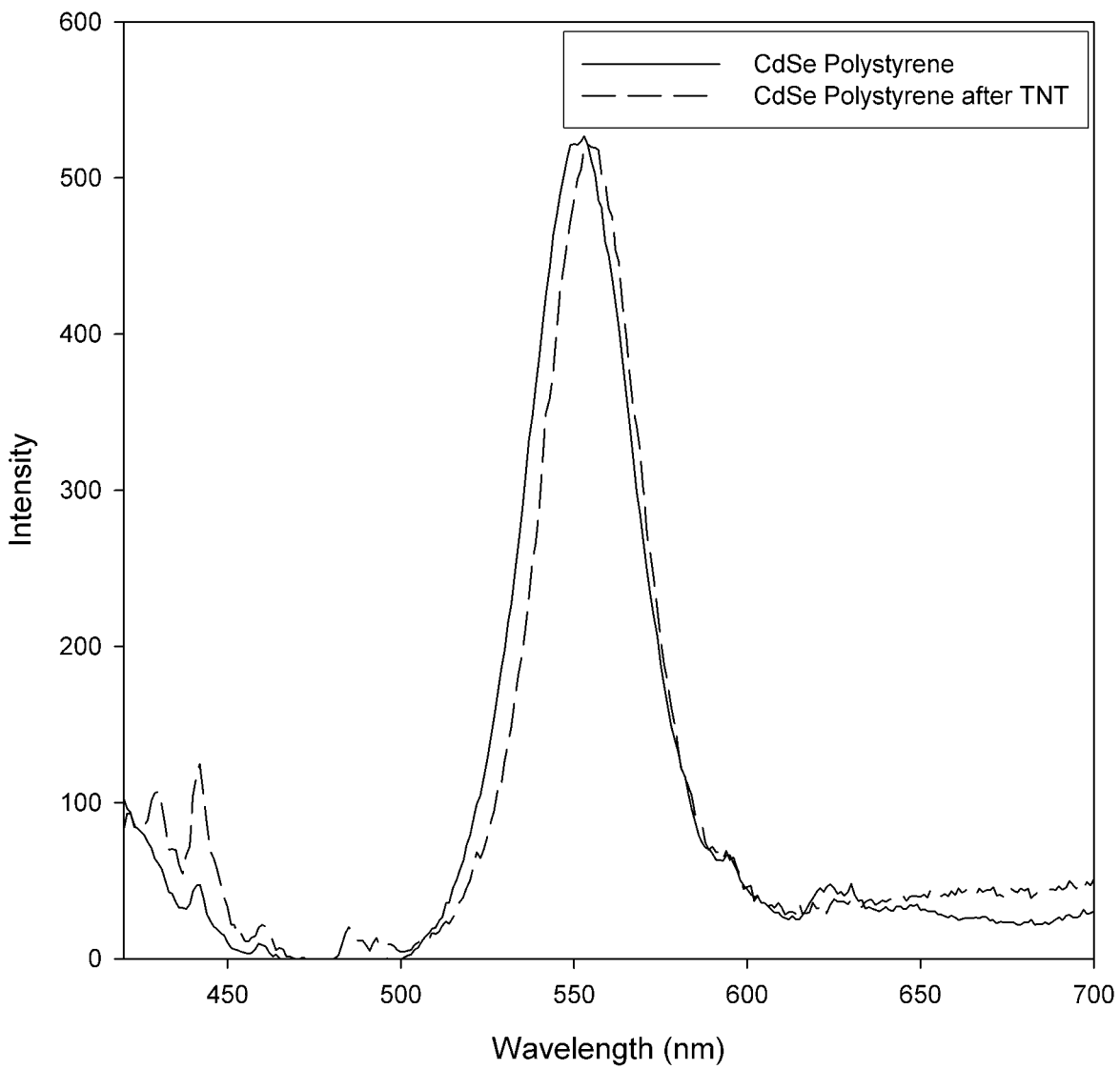


Figure 6.4: Photoluminescence spectra of 3.5nm CdSe in a polystyrene film after TNT exposure for 24 hours

with this system is intrinsically a failure of delivery of the analyte to the sensing system. Clearly, a more open, possibly porous framework would yield better results.

It is useful, at this point, to compare the photographs of the thin films generated by drop-casting with those generated with polystyrene. Both cases represent the opposing ends of a spectrum of encapsulation. At one extreme, the quantum dots are left open and exposed to TNT, which diffuses to them with no intervening material. The photoluminescence in this case is fully quenched. At the other extreme, the quantum dots are sealed tightly in a dense matrix and TNT cannot diffuse through the intervening materials. As a result the photoluminescence is unquenched. While the photoluminescence within the polystyrene is incredibly stable, it is totally insensitive to TNT. While the evaporated film is incredibly sensitive to TNT, it is also the least stable over time. The goal, then, must be a balanced mediation between these two extremes: a situation where CdSe is long-lived and photo-stable and where it is also very sensitive to TNT.

6.7 CdSe Quantum Dots Embedded in VYCOR®

6.7.1 Dramatic Quenching upon TNT Exposure

Exposing the CdSe quantum dot embedded VYCOR® discs to TNT produced a significant decrease in photoluminescence, as shown in Figure 6.6. The photograph comparing the discs, shows how dramatic the quenching is. The photoluminescence has completely disappeared from the entire disc when it is exposed to TNT. Alternatively, the disc that was unexposed still continues to glow brightly. Just like the thin evaporated films, TNT acts to strongly quench the quantum dot photoluminescence.

While the small pore size may have been an obstruction to water to photo-oxidize the quantum dot surface, it clearly does not affect the accessibility of the quantum dot surface to TNT. Figure 6.7 shows the photoluminescence spectra of the discs in Figure 6.6. Here, we can clearly see the same bright photoluminescence that is characteristic of quantum dots embedded in VYCOR® is present in the unexposed control sample, while the exposed experimental sample is completely non-luminescent. It has been completely quenched by TNT.

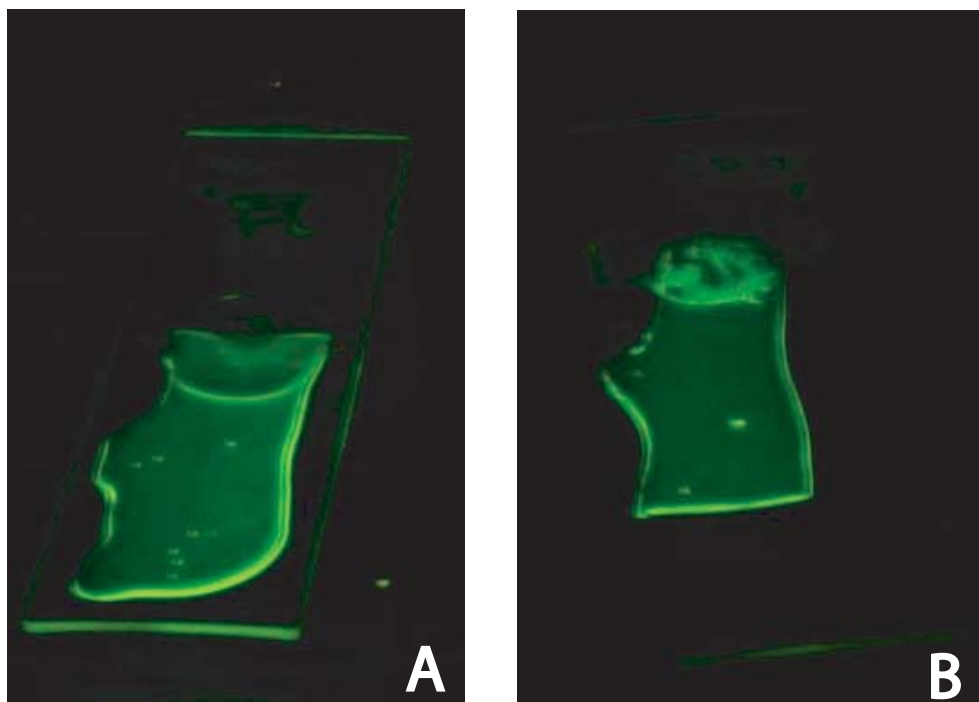


Figure 6.5: Digital Photographs of 3.5nm CdSe quantum dots embedded in a polystyrene film, illuminated with a UV handlamp. Image **A** is the (unexposed) control while Image **B** has been exposed to TNT for 24 hours

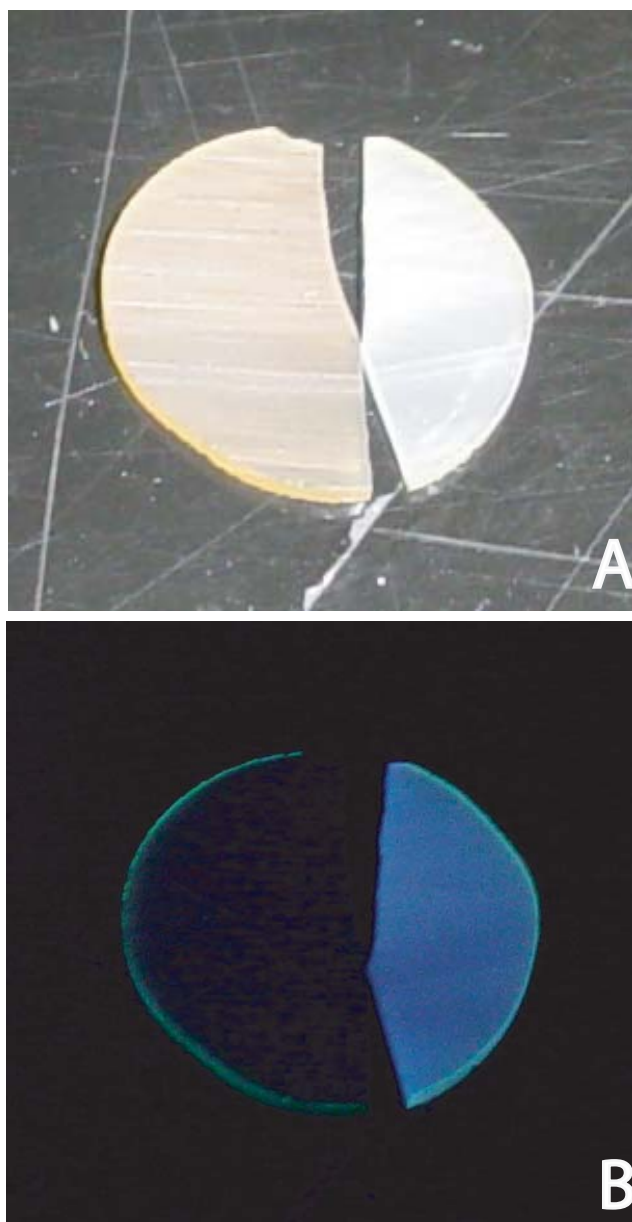


Figure 6.6: Photograph of CdSe quantum dots embedded into VYCOR[®] discs. Disc on the left has been exposed to TNT, disc on the right has not. Note that only the surface of the left disc was TNT exposed, thus the edge is still emitting

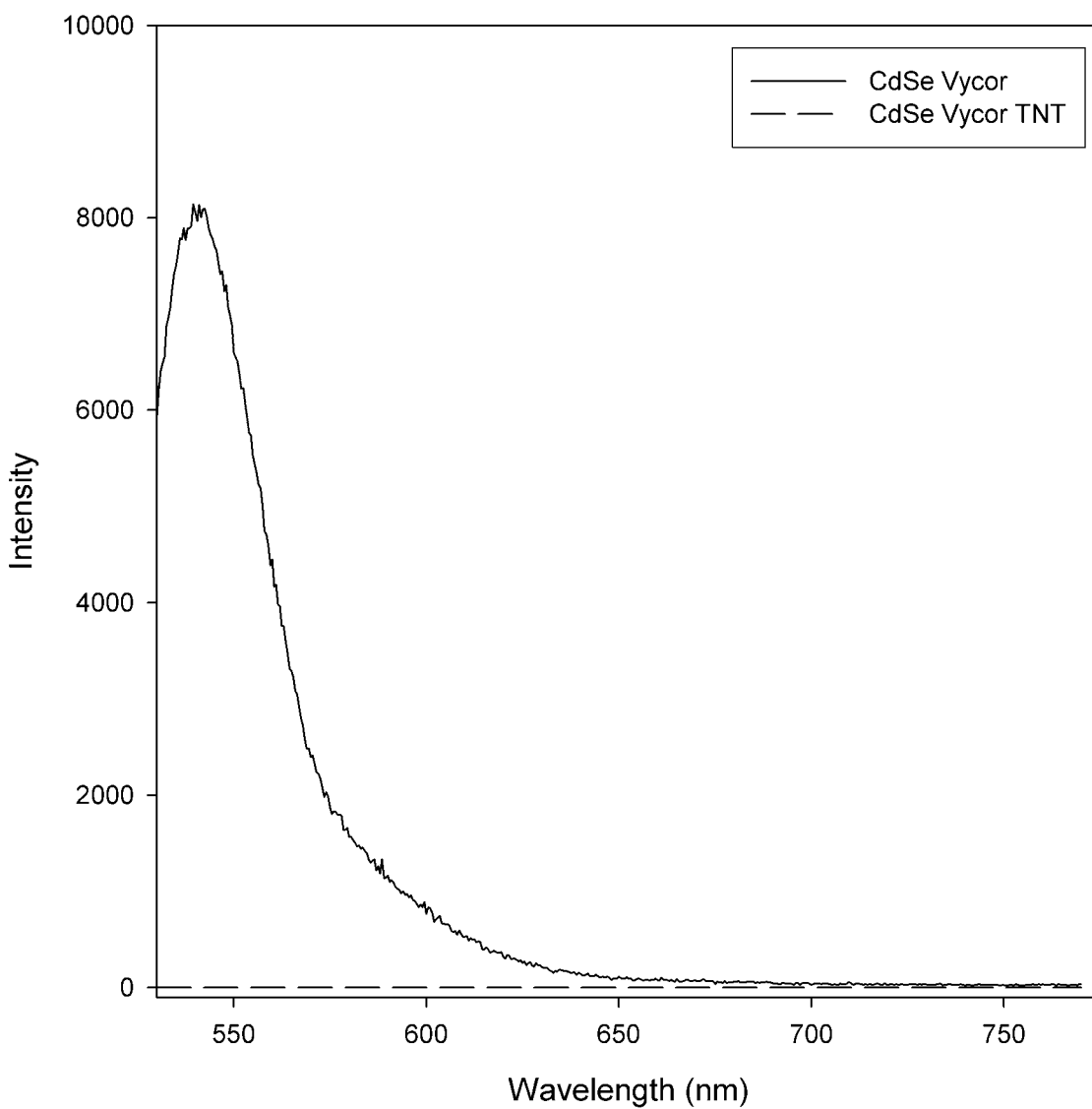


Figure 6.7: Photoluminescence spectra, before and after exposure to TNT, from 3.5nm CdSe quantum dots in in VYCOR[®]

6.7.2 A Stable, Sensitive, Solid-state TNT Detector

The goal of achieving a solid-state sensor based on CdSe quantum dots has been realized. The VYCOR[®] matrix provides a stable environment that protects the quantum dot from oxidation by water, but still allows TNT to diffuse and make contact with the embedded CdSe quantum dots. This situation is somewhat assisted by the fact that CdSe quantum dots are unable to penetrate into the core of the porous glass, and are trapped in the glass surface. Since TNT does not need to diffuse into the glass in order to interact with CdSe, then the bulk of the photoluminescence signal comes from the CdSe quantum dots at the porous glass surface. This situation improves the response time and is also an efficient use of material.

Possible Future Developments

A sensing package utilizing this technique would require three primary components: (1) an excitation source to excite the CdSe quantum dots, which can be achieved with a low-power LED, (2) a photo-detector of some kind, most likely a photodiode or CCD, and (3) the quantum-dot embedded porous glass. This glass can optimally be mounted onto the photo-detector, and its counts can be correlated to the TNT vapor pressure. For greater sensitivity an external standard of known TNT vapor pressure exposed to identical quantum dot embedded glasses can be integrated into the sensor package.

This sensor package can easily be hand-held, light and portable, and it is not inconceivable that integration into a micro-electronics package may even make it wearable (i.e. badges). For threat and explosives detection, such a low footprint and concealable device would find great application in a variety of areas, not the least of which is counterterrorism. Although the final sensitivity will ultimately be based also on the instrumentation, the strong sensitivity of CdSe quantum dots to TNT make this a promising alternative for TNT detection.

6.8 Chapter Summary

The incorporation of CdSe quantum dots onto various substrates and matrices has yielded a large variety of possible TNT-based sensors. Of these, the only non-functional one was based on a densely packed plastic, polystyrene, from which we learned that a porous framework is

important to detection.

The solution-phase studies showed that TNT does systematically quench CdSe quantum dots and that the photoluminescence quenching is a predictable function of the TNT concentration, suggesting that CdSe quantum dots will make good TNT detectors. The thin evaporated films will unlikely be developed further for vapor sensing since their long term stability under ambient conditions is poor. The strongest candidate to emerge from these different incorporation schemes is the porous glass VYCOR[®], which provides the ideal combination of CdSe quantum dot stability coupled to a strong sensitivity for TNT. This is achieved by the small pores within the material that allows TNT to diffuse into the CdSe without obstructing its passage.

CHAPTER 7

EXCITED STATE THERMALIZATION OF CDSE QUANTUM DOTS WITH THE DETAILED BALANCE METHOD

7.1 Motivation

The relaxation of photo-generated charge carriers in quantum confined systems has recently received attention due to the developing technology of using quantum dots[1, 49, 50, 51, 52] for solar energy conversion. A fundamental understanding of the electron dynamics of these low-dimensional systems would advance the engineering possibilities by directing the capture of this electronic energy to do electrical work and improve conversion efficiency. Understanding carrier relaxation processes is critical to manipulating the excited state, particular light-emitting processes.

7.2 Overview of Excited State Processes

7.2.1 Thermalization

When a chromophore absorbs a photon of light, it enters into an excited electronic state. This new electronic geometry imposes several consequences. One of these is the vibrational relaxation that results from the atoms in the chromophore migrating to new positions based on the new electronic geometry. Essentially, the excited state will find itself in a higher energy vibrational level, and will slowly relax down to lower and lower vibrational levels and rotational levels, all the while releasing the excess energy as heat. Finally, it returns to the lowest energy vibrational and rotational state where it transitions back to the electronic ground state. Typically the chromophore ends up in a higher lying vibrational state, and more thermal relaxation occurs in order to reach the lowest energy electronic and vibrational

ground state. The reasons that higher lying vibrational states are invoked has primarily to do with electronic transitions becoming more favorable when the excited state and ground state geometries are similar, which is the case only in highly distorted (high vibrational energy) states. Since the excited state electronic geometry and the ground state electronic geometry are rarely the same, it follows that their atomic geometries should not be the same either.

7.2.2 Cool States

Minimum Distortion

For simplicity, let us consider the situation in which little to no thermalization occurs during an electronic excitation. This case is a very specific event and has very strong restrictions. The first of these is the nature of the excited state relative to the ground state. A molecule that undergoes little to no thermal relaxation will inevitably have an excited state that is very similar, electronically, to its ground state. Because their electronic distributions are so similar, little to no molecular distortion occurs and consequently, very little relaxation is needed for the excitation or emission process. The vast majority of molecules do not fit into this situation because the excited states are typically comprised of combinations of anti-bonding orbitals, all of which have opposing geometries to the bonding orbitals that compose the electronic ground states.

Maximum Distortion

There is a second situation where little or no excited state thermalization can occur. This occurs when the excited state is formed in its lowest energy vibrational state; it has already reached the point of relaxation and no more relaxation can occur, therefore no thermalization is necessary. In order for this situation to occur, the ground state must distort itself an extraordinary amount, adopting the atomic geometry of the excited state in its lowest energy vibrational configuration. When it has done this, it can absorb light to form the excited state. Thus, the ground state must absorb quite a bit of energy from its surroundings to reach a high energy vibrational state.

Therefore, cool states wherein there is little excited state thermalization tend to be the exception rather than the rule when it comes to studying the excited state.

7.2.3 Hot States

Most scenarios end up with the excited state being formed in high energy vibrational states. The exact energy and probability of forming each state is directly reflected in the absorbance manifold. For simplicity we consider only electronic transitions beginning in the vibrational ground state of the electronic ground state and reaching various vibrational states of the excited state. This is a good assumption if the ambient heat energy does not significantly exceed the vibrational energy spacing. Organic chromophores at room temperature fit into this category.

Excitation Energy

The energy needed to reach the electronic excited state will be the difference between the ground and electronic state energies plus an integer multiple of the vibrational energy spacing, which is directly related to the vibrational energy level that is initially formed. Therefore, the energy actually consumed in an electronic transition is greater than the difference between the electronic energy levels because it contains a component for vibrational excitation. This component is directly related to the heat it releases. Consequently, higher excitation energies produce higher energy excited states and therefore release more heat to their environments. Therefore in an absorbance spectrum, bluer wavelengths of light produce hotter states.

Excitation Intensity

The next factor for producing hot states comes directly from the overlap in likelihood of finding the electronic and vibrational ground states in a similar atomic geometry. Just as in the case discussed above regarding cool states, wherein it was said that producing these is unlikely due to the necessary ground state distortion, the molecular geometry becomes important for determining the probability of transitions to specific electronic vibrational states. Thus, electronic vibrational states with similar atomic positions to the ground state tend to be the most likely formed states. In an absorbance spectrum, this probability appears as the intensity; more intense peaks reflect the most statistically favored transitions.

7.2.4 Bath States

No Bath States

So far, it has been said that energy has been released from thermal relaxation though no mention has been made of where. For a molecule in a vacuum (or a vapor under low pressure), thermal relaxation is inefficient and hot states can persist for a very long period of time. The only method of heat dissipation comes from the release of an infrared photon as the excited state vibrationally relaxes.

The Solvent Bath

For the majority of condensed phase spectroscopy, there is a large variety of states that can accept the thermal energy released. These states are typically called “bath states” because their energy spacings are nearly continuous and they do not saturate (there are a lot of them). Thus, these bath states regulate the temperature and accept almost any quantity of energy released by the system. Realistically, the solvent acts as the thermal bath for the majority of condensed phase chromophores. By far, it outnumbers the chromophores dissolved in it, and the liquid nature of the solvent produces a continuous energy spectrum. Thus, thermal energy is transferred by physical collision of the solvent molecules with the excited chromophores, leaving the solvent molecules in a higher energy vibrational and rotational state and the chromophore in a thermally relaxed state.

7.2.5 Semiconductors

Semiconductors, though very different from molecular chromophores, bear many functional similarities. The excited state processes are similar; thermal relaxation occurs in both, and everything is identical except for the following changes in terminology and definition.

Exciton

A chromophores lowest energy excited electronic state is analogous to the exciton in a semiconductor. Both states have relaxed, and both contribute directly to the photoluminescence profile. While terms like fluorescence and phosphorescence are well-defined in molecular chromophores, they are harder to pin down for semiconductors, so the blanket term of photoluminescence is typically applied. By definition, an exciton consists of a bound electron

and hole pair, and while that may seem very different from an electronic excited state, two important considerations can be made.

First, consider that the conduction band is formed from the anti-bonding orbitals of the atoms comprising the semiconductor, in the same way that the excited state is comprised of combinations of anti-bonding orbitals. Additionally, an electron in an exciton is energetically located at the bottom of the conduction band in the same way that an electron is placed into the LUMO during electronic promotion in a chromophore.

Secondly, if we consider that as chromophores are electronically linked to each other as in the case of conjugated polymers, the excited states begin to behave very closely with semiconductors. As the chain length of conjugated polymers increases, defining their excited states as excitons becomes both more commonplace and more accurate. Solid-state polymers produce other species derived from excitons such as polarons and polaritons, clearly showing how related these are to their semiconductor cousins.

Carriers

There is an important distinction that is usually made between chromophores and semiconductors that inevitably leads to two terms that are closely related, but refer to different processes. In a semiconductor, the electron and hole are formed in their respective bands with high vibrational energy. Slowly, they relax toward the bottom (top for the hole) of their bands and form the exciton. Intrinsically, the existence of holes and electrons that separately relax in energy leads to the term “carrier relaxation” as opposed to “excited state relaxation.” Though physically different, the terms mean the same thing: the initially electronically excited species relaxes toward a lower energy state by emitting thermal energy.

Phonons

For solid-state materials, vibrations and rotations are not intrinsically defined and their closest counterparts are phonons, of which two varieties exist: optical phonons and acoustic phonons. Of these, optical phonons tend to be of higher energy and as implied in their name, tend to be more involved in higher energy processes such as optical excitation. Optical phonons are classically depicted as the “breathing” motions of a crystal, visually imagining the crystal expanding and contracting. Acoustic phonons are a different variety, involving translating elements that are more like crystal vibrations, visually imagining the crystal to

“shake.” Both of these phonons replace the solvent in acting like the thermal bath. They are pathways from which thermal energy can be transferred from the excited carriers to the crystal structure itself.

7.3 Thermal Relaxation in Quantum Dots

Quantum dots form a unique intermediate situation between the solid-state crystal and the molecular chromophore. They are larger than most chromophores but smaller than most bulk crystals. The small size of quantum dots (less than the exciton bohr radius) means that the thermal relaxation will pursue a more molecular-like behavior, while the presence of the semiconductor crystal lattice implies vibrational relaxation will occur through phonons. Unlike the semiconductor crystals, the quantum dots are dissolved in a solvent, which provides an efficient thermal bath, not to mention a ligand shell whose vibrations also help to relax the excited state.

7.3.1 The Phonon Bottleneck

Specifically, the large quantum-confinement induced energy splitting between hole energy levels was thought to impede carrier relaxation, resulting in the so-called phonon bottleneck wherein only multi-phonon processes could result in efficient hole relaxation. Thorough ultrafast experiments[53, 49] have shown that a competitive pathway, Auger electron-hole energy transfer, induces rapid thermal relaxation of the hole states[54, 55]. After carrier thermalization, relaxation occurs wherein the carriers dissipate their excess kinetic energy through collisions with phonons (carrier-phonon coupling[56, 4]), followed by the dissipation of this energy to a continuum of bath states (phonon-bath coupling). While the phonon bottleneck controversy primarily involves internal relaxation (hole-phonon coupling), external relaxation (phonon-bath coupling) is a largely unexplored issue. In addition, the carrier temperatures on colloidal QDs have been studied only under pulsed laser excitation producing non-equilibrium states. Continuous-wave irradiation should produce a photon mediated thermal equilibrium between the excited state and ground state.

7.3.2 Thermal Relaxation

Another issue that is characteristic to quantum dots is how efficiently the lattice acts as a thermal bath with pseudo-continuous energy levels. In bulk semiconductors, which have thousands of atomic planes, the lattice is the thermal bath. However, since quantum dots possess only a dozen or so planes, we clearly cannot make the assumption that the lattice alone will dissipate the heat effectively. Molecular vibrations are not efficient solvent baths and consequently, these vibrations must couple to the solvent bath to release thermal energy. In colloidal quantum dots, the presence of the ligand passivating layer, and more importantly, the presence of the solvent can act as thermal insulators and thermal baths. For example, long-chain alkyl ligands form crystalline domains that may impede efficient carrier or lattice phonon thermalization with the continuum of energy levels in the solvent bath. Even if carrier-phonon relaxation is fast, without efficient heat dissipation into a thermal bath, the excess energy will remain trapped in the resulting carrier-phonon equilibrium, and the carriers will remain hot. The inability of the quantum dot lattice to act as a thermal bath coupled with the insulating effect of the ligand shell results in poor thermal relaxation and consequently hot carriers and eventually hot luminescence.

7.3.3 Detailed Balance Approach

For the first time we are applying a method to quantum dots that has accurately determined excited state temperatures for both organic molecular and bulk semiconductor systems[57]. Bolton and Archer have demonstrated the usability of this technique with both bulk GaAs and Rhodamine-6G molecules, wherein they obtain carrier temperatures (295K) within a few degrees of the lattice temperature (297K) of GaAs and slightly warmer excited state temperatures (325K) for R6G compared to the solvent bath (296K). This approach is called the detailed balance method, requiring only the absorption and continuous-wave emission spectra to be analyzed. We briefly discuss this method of analysis, and its application to quantum dots as a function of excitation energy where we find surprisingly high carrier temperatures. We propose that hot carriers arise in a QD from quantum-confinement induced incomplete internal relaxation as revealed by probing external equilibration behavior by the detailed balance method.

Since Auger electron-hole energy transfer induces hole relaxation to its lowest energy

excited state without phonon participation to dissipate the excess energy, we can expect the hole to arrive at the band-edge as a hot carrier. The remaining kinetic energy in the hole can be dissipated through collisions with phonons, which subsequently dissipate the heat to the bath (organic ligand shell or solvent). If this secondary cooling process is fast, then the hole and electron will recombine in completely cooled states and possess an excited state temperature similar to the bath. However, if the excited state temperature is much higher than the bath temperature, then the coupling efficiencies of carrier-phonon and phonon-bath must be very poor. Measurement of the carrier temperature provides insight into the coupling process.

7.4 Experimental

CdSe QDs with an organic shell of hexadecylamine (HDA) were synthesized using colloidal chemical methods(ref). After precipitation with methanol, they were redispersed in a n-hexane solution. The CdSe solutions were placed into sealed 1-cm quartz cells, and degassed with dried Argon gas. Photoluminescence and UV-Vis Absorbance spectra were taken on a Varian Eclipse Fluorimeter and Varian Cary 50 Bio UV-Vis Spectrophotometer, respectively. The excitation and emission bandwidth was kept at 2.5nm, with a slow scan rate (200nm/min), producing a digital resolution of 0.5nm (~ 1 -5meV). Intriguingly enough, it is also possible to extract the radiative lifetime (τ_r) from the intercept.

7.5 Overview of the Detailed Balance Method

7.5.1 The Bolton-Archer Equation

The equation developed by Bolton and Archer for the graphical analysis of the excited state temperature is:

$$\ln \left[\frac{f(\nu) / \int_0^\infty f(\nu) d\nu}{\epsilon(\nu) \eta(\nu)^2 \nu^2} \right] = \left(\frac{-h}{k_B T} \right) \nu + \left[\ln \left(\frac{8\pi \ln(10) \tau_r q_g}{10c^2 N_A q_u} \right) + \frac{E_g}{k_B T} \right] \quad (7.1)$$

The variables are: q_g =ground state degeneracy, q_u =excited state degeneracy, N_A =Avogadro's Number, c =speed of light, $f(\nu)$ =fluorescence spectrum, $\epsilon(\nu)$ =extinction spectrum. A full derivation of the Bolton-Archer equation utilized in this chapter appears in Appendix D.

The Left-hand Side

The two most important features are the extinction spectrum and the fluorescence spectrum, which are both empirically measured. Their ratio, combined with an energy squared factor, makes up the argument of the logarithm on the left side of Equation 7.1. The extinction spectrum is a direct reflection of the ground state population, including the ground state temperature. In the same way, the fluorescence spectrum is a direct reflection of the excited state population, especially the temperature. Since the electronic structure varies from compound to compound, the excited state temperature cannot be readily extracted solely from the fluorescence spectrum. In order to eliminate contributions from the electronic structure, the two spectra appear as a ratio.

The Right-hand Side

The independent variable on the right-hand side is the photon frequency (or photon energy, which will be utilized later for convenience). The temperature appears with the Boltzmann constant and together reflect the statistical distribution of states based on available heat energy. The most important variable here will be the temperature, which is the factor that will be graphically extracted.

7.5.2 Data Fitting: Utilizing the B-A Equation

Equation 7.1 is expressed as a straight line ($y=mx+b$) such that a plot of the logarithm of the emission spectrum divided by the absorption spectrum (and divided by an energy squared factor) will produce a straight line whose slope is the inverse temperature of the thermalized excited state. Specifically, $y=\ln \left[\frac{f(\nu)/\int_0^\infty f(\nu)d\nu}{\epsilon(\nu)\eta(\nu)^2\nu^2} \right]$, $x=\nu$, $m=\left(\frac{-h}{k_B T} \right)$ and $b=\left[\ln \left(\frac{8\pi \ln(10)\tau_r q_g}{10c^2 N_A q_u} \right) + \frac{E_g}{k_B T} \right]$.

7.5.3 Important Assumptions

The Boltzmann Approximation

The use of the Boltzmann distribution to approximate the excited and ground state populations is valid in the neighborhood of high temperatures. At low temperatures, the statistical nature changes and becomes dependent on the exchange interaction, producing either Fermi-Dirac statistics or Bose-Einstein statistics. At high temperatures, these become

Boltzmann statistics. Room temperature is considered under this definition to be well within the high-temperature limit. Since all of the experiments were performed at room temperature, this is a valid and accurate approximation.

Steady State Approximation

Another approximation used is the steady state approximation, which implies that the number of excited and ground state species does not drastically increase or decrease over time; their rates of formation are the same and there is no excessive build-up of one species over the other. Since there is a continuous beam of light that stimulates the production of the excited state and the excited state decays to the ground state spontaneously, this situation is satisfied. If these experiments were performed with a pulsed laser however, this approximation would be invalid. Population inversion in a laser cavity to produce stimulated emission would also not satisfy this condition. Since all the experiments were performed in a dilute solution with weak continuous illumination, this approximation has been satisfied.

7.6 Typical Molecular Fluorophores

7.6.1 Anthracene

For comparison, we have performed the same analysis on a well-studied organic molecule, anthracene in absolute ethanol, and we obtain an excited state temperature of 315K, as show in Figure 7.1. As expected, this is less than 20 degrees from the bath temperature. Similar observations were found in R6G and bulk GaAs[57]. The accuracy and versatility of this method on such dissimilar materials as R6G (a molecular chromophore) and GaAs (a bulk semiconductor) indicate a valid applicability to quantum dots, which is an intermediate regime between these two extremes.

7.7 CdSe Carrier Temperatures

7.7.1 Hot Carrier Temperatures

In Figure 7.2 we show the detailed balance fit of Eqn. 7.1 derived from the absorbance and photoluminescence of 3.5nm HDA passivated CdSe excited at 320nm (3.875eV). As can be seen, excellent agreement is obtained between the data and the model. The slope of this line (-20.3 eV^{-1}) is inversely proportional to $k_B T$ and yields a temperature of 570K, which is far

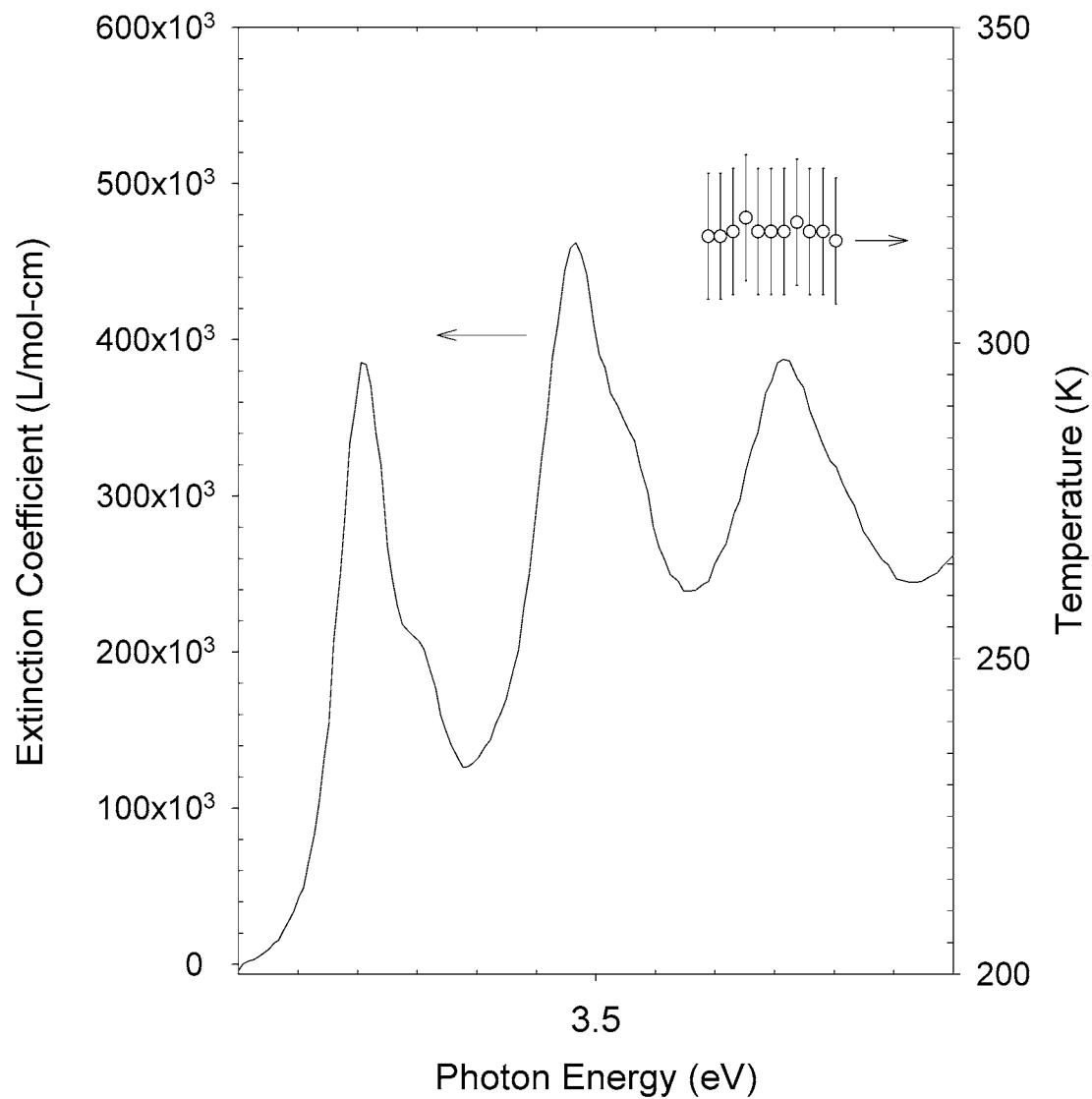


Figure 7.1: Excitation spectrum of anthracene in ethanol (solid line), overlaid with the excitation-energy dependent excited state temperatures as determined with the Bolton-Archer method (open circles with error bars).

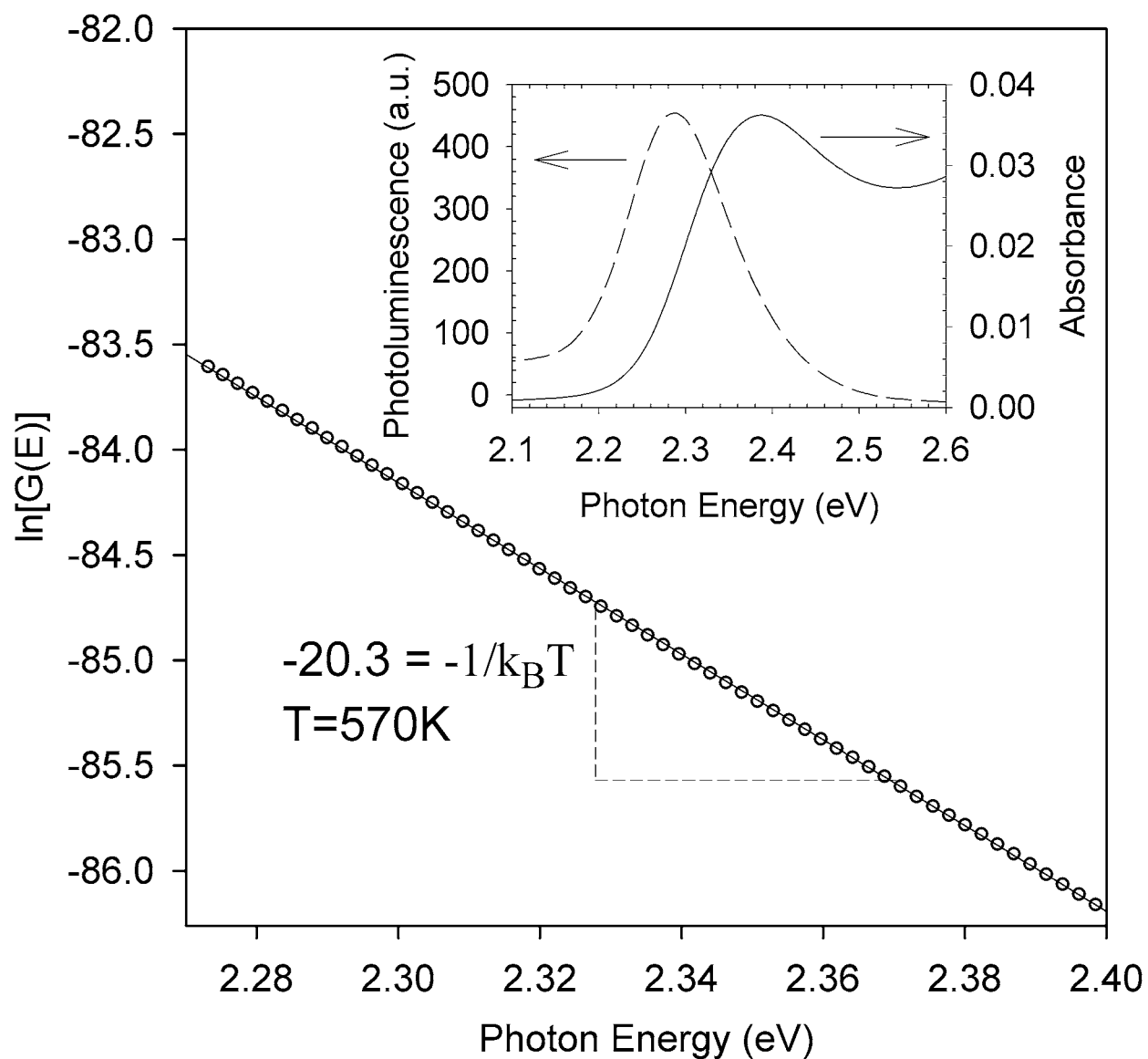


Figure 7.2: Fit (solid line) of Eqn. 7.1 (open circles) for CdSe(3.5nm)-HDA/toluene excited at 320nm. The fitted slope of the line is -20.3 which corresponds to a temperature of 570K by solving for the temperature in Eqn. 7.1. Inset shows the absorbance spectrum and the emission spectrum of the sample at 320nm.

above the temperature at which the experiment was performed (295K). The large disparity in temperature between the analyte (CdSe QD) and the bath (solvent) is surprising and suggests that thermal energy is not efficiently released from the CdSe QD to the solvent bath via carrier-phonon coupling.

7.7.2 Excitation-Energy Dependent Carrier Temperatures

To further explore the effect of the initially formed electronic state on the temperature of the emissive state, the carrier temperatures were determined at different excitation energies as shown in Figure 7.3. Over the excitation range studied, we see that the carrier temperatures are always very high and vary from 500K-750K. By comparison, experiments that probe excitation energy on anthracene/ethanol reveal a stable carrier temperature (Figure 7.1 inset).

7.7.3 Correlation with High Energy Exciton States

Underlying Structure

In addition to the high temperatures found for CdSe QDs, an underlying structure is observed in the carrier temperature data. When overlayed onto the absorption spectrum (Figure 7.3) it appears that these features correlate to the discrete electronic features for 3.5nm CdSe QDs[8]. As can be seen, the peaks obtained in the carrier temperature spectrum correlate directly to higher-lying CdSe exciton states, specifically the sharp peak at 2.85eV correlates to the $1P_{3/2} - 1P_e$ transition and the broad peak at 3.15eV corresponds to the $1P_{1/2} - 1P_e$ transition. In fact, direct comparison of the linewidths obtained for the $1P_{3/2} - 1P_e$ in Bawendi's[8] low-temperature PLE and our room-temperature carrier spectrum show that they are very similar ($\sim 80meV$). More importantly, examination of the absorption spectrum (Figure 7.3 shows that the $1P_{3/2} - 1P_e$ and $1P_{1/2} - 1P_e$ transitions are not spectrally resolved at all due to size-broadening, while the carrier temperature spectrum (Figure 7.3) has linewidths that correspond closely with transient differential absorption studies[58] ($82meV$).

High Exciton Energy State Relaxation Differences

Additionally, the difference in peak temperatures between the $1P_{3/2} - 1P_e$ and $1P_{1/2} - 1P_e$ transitions implies different carrier-phonon coupling rates. Specifically, the origin of this

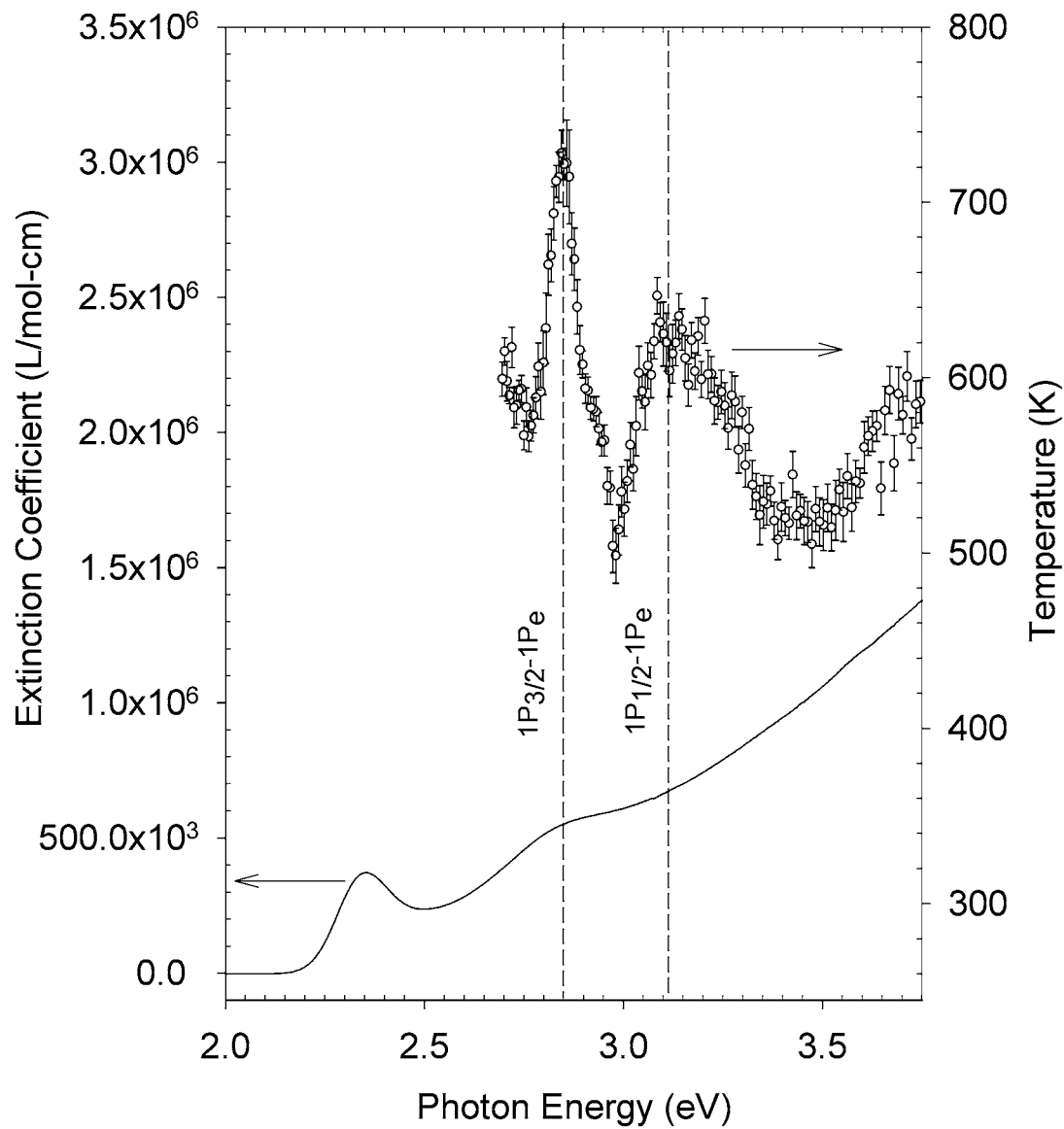


Figure 7.3: CdSe(3.5nm)-HDA dissolved in toluene at room temperature extinction spectrum, and excited state temperatures extracted at different excitation energies using the detailed balance method. Vertical dashed lines indicate expected positions of $1P_{3/2} - 1P_e$ and $1P_{1/2} - 1P_e$

effect can be traced back to hole-phonon coupling, since the two transitions differ only in the hole spin-orbit coupling ($J_h=1/2$, $J_h=3/2$) and more concisely in the hole orbital angular momentum ($L_h=0$, $L_h=1$). This angular momentum dependence suggests multi-phonon processes are involved in efficient carrier relaxation through angular momentum conservation.

7.8 The Photoluminescence Lineshape

The observed structure in the frequency-dependent Bolton-Archer experiment arises from changes in the lineshape of the photoluminescence spectrum. In fact, if temperature is the primary factor in the change in the lineshapes, then we would expect strong distortions in the blue edge of the photoluminescence profile, reminiscent of “hot bands[59]”. Careful examination of the photoluminescence lineshapes as a function of excitation energies as shown in Figure 7.4 shows that this is in fact true. We observe that only the higher energy edge of the photoluminescence spectrum shows an excitation energy-dependent distortion. This can be traced back to a changes in the Boltzmann distribution width, which must be linked to the excited state temperature. In fact, the detailed balance fitting is biased toward the blue edge of the photoluminescence spectrum, where “hot bands” are expected to arise.

7.8.1 Hot Carriers

The high excited state temperature measured for CdSe by the detailed balance method is reminiscent of temperatures of confined systems obtained by molecular-beam epitaxy, wherein the phonon-bottleneck was found to be the primary culprit in inhibiting efficient thermal equilibration[4]. However, since the phonon-bottleneck process can be surpassed in colloidal systems through Auger electron-hole energy transfer, another explanation must be found that sets apart these chemically prepared materials from their MBE cousins. Since the core crystal structures between the colloidal and MBE versions are identical, then the difference must primarily arise from passivation and surface state processes. The presence of the organic shell in the colloidal version may be the primary cause for poor heat transfer as it is effectively uncoupled to the excited state as measured by Resonance Raman. This would result in poor relaxation pathways for the excited state via bath coupling. In effect, the passivating layer acts as an insulating jacket that contains the excess thermal energy within

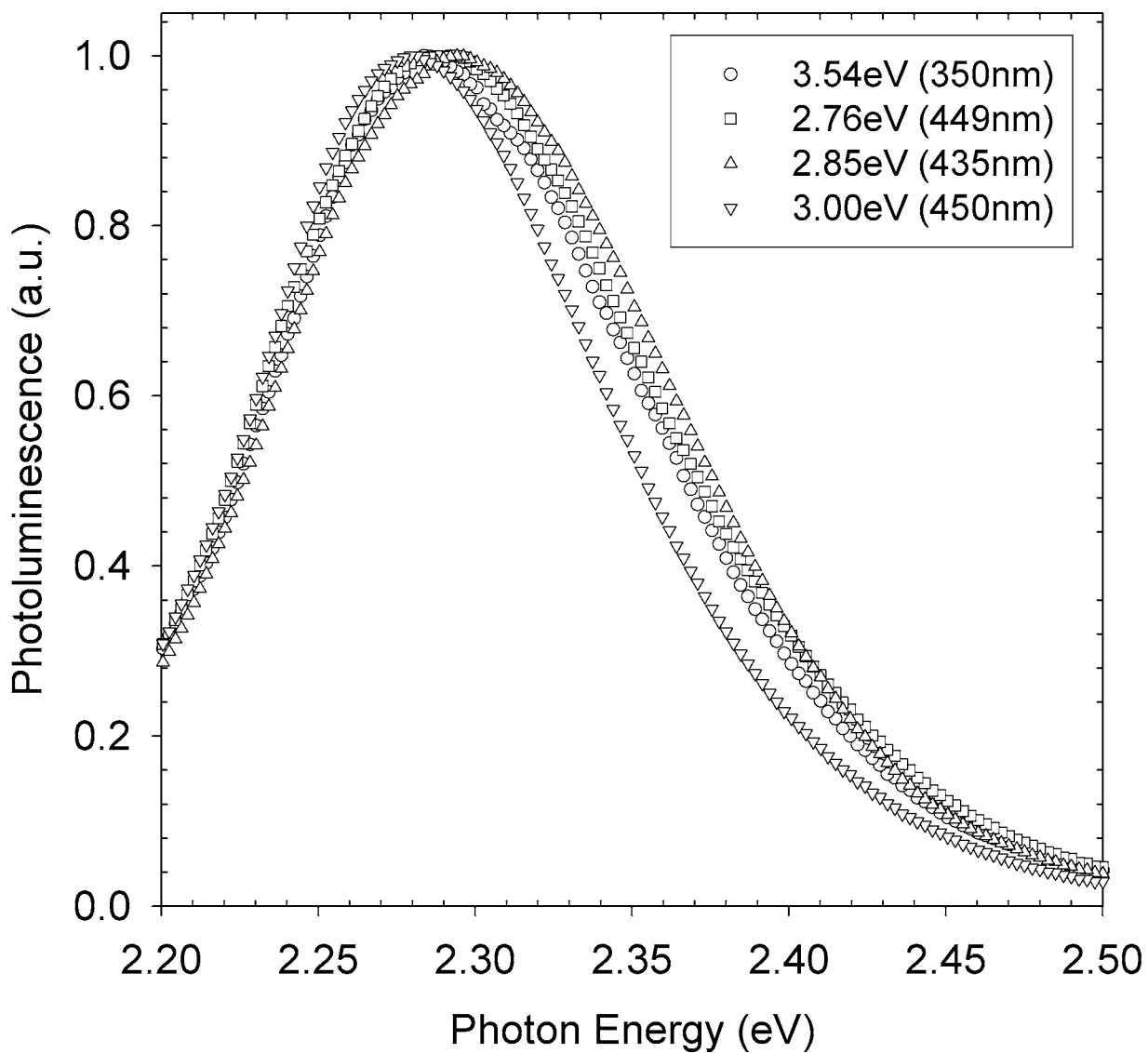


Figure 7.4: The intensity-normalized photoluminescence lineshape obtained for CdSe(3.5nm) at different excitation energies.

the dot resulting in “hot photoluminescence”, reminiscent of gas-phase “hot bands[60]” since only phonon modes (LO, TA, IF, etc.) [61, 56] are available for relaxing the excited state.

7.9 Integrated Photoluminescence

An important question raised by the data is whether nonradiative decay pathways linked to higher energy exciton states play a role in the excitation energy dependent carrier relaxation. Spectral integration of the entire photoluminescence manifold as a function of excitation energy is overlaid onto the absorption spectrum in Figure 7.5. The close agreement between the excitation energy-dependent spectrally integrated photoluminescence and the absorption spectrum shows that high energy exciton coupling to nonradiative paths are not a major component in the carrier relaxation. Therefore, since the total quantum yield does not change as a function of excitation energy, but the spectral shape of the photoluminescence changes, we conclude that given different excited states in CdSe QDs, the photon energy delivered to them ($\beta(\nu)$) is eventually released as band-edge emission ($f_i(\nu)$) subject to the conservation relationship, $(\int_0^\infty \beta(\nu)d\nu = \int_0^\infty f_i(\nu)d\nu - G)$ where G is the number of photons that were lost due to nonradiative band-edge relaxation. In essence, all of the energy absorbed comes out as a proportional amount of emission, though some of that emission may arise from higher temperature states resulting in a distorted photoluminescence profile.

7.10 Explaining Thermal Relaxation

The strong dependence of the band-edge carrier temperature on the initially formed excited state suggests that some form of relaxation must occur in the initially formed excited state, prior to relaxation to the band-edge state. In fact, for this change to be detectable, this rate of relaxation must be comparable to the rate of Auger electron-hole energy transfer. Femtosecond transient absorption studies reveal that phonon relaxation occurs on timescales comparable to the Auger process and may account for this competitive relaxation process [53, 4].

In Figure 7.6 we illustrate this process, beginning with formation of high energy excitons and carrier-carrier thermalization (not shown). If phonon-bath coupling is strong then the carrier states are relaxed (right pathway), causing a narrowing of the Boltzmann distribution. Conversely, if phonon-bath coupling is poor, the Boltzmann distribution will

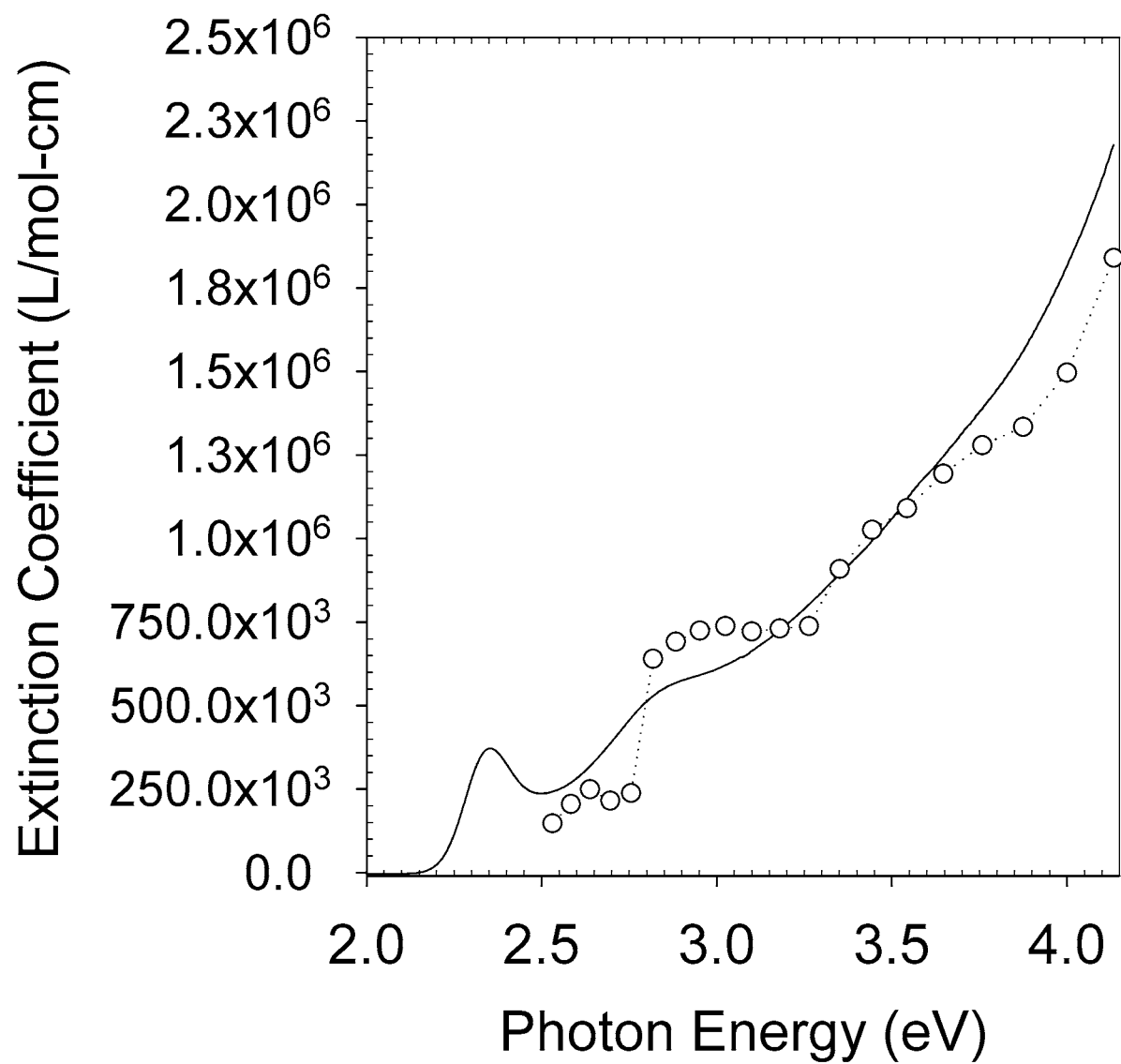


Figure 7.5: CdSe(3.5nm)-HDA dissolved in toluene at room temperature, extinction spectrum, and spectrally integrated band-edge photoluminescence(arb.u.) at different excitation energies

remain relatively unaffected (left pathway). Auger electron-hole energy transfer relaxes the carriers to the band-edge where more phonon-bath coupling may take place, followed by electron-hole recombination. However, since the two pathways arrive at the band-edge state with different Boltzmann distributions, one can expect that their band-edge photoluminescence profiles will reflect this, especially if phonon-bath coupling in the band-edge state is very poor.

The result will be distortions in the blue edge of the spectra for higher temperatures, which is exactly what we observe (Figure 7.6). This distortion arises as a result of the additive contribution to the spectrum from high energy hot band-like transitions, which is measurable by comparison to the thermal distribution found in the absorption through the Bolton-Archer method. Close examination of Figure 7.6 reveals that, in fact, as more blue bands appear at the edge of the photoluminescence spectrum, the higher the measured Bolton-Archer temperature. The spectrum with the least amount of hot bands (probed at 3.0eV) produces a 500K temperature while the spectrum with the largest contribution of hot bands (probed at 2.85eV) shows a correspondingly higher temperature (750K).

7.11 Chapter Summary

Carrier temperatures of CdSe quantum dots are measured using the detailed balance method which is based solely on steady state absorption and photoluminescence spectra. We obtain very high carrier temperatures (500K-700K) that can be correlated to poor phonon-bath coupling. In addition, features are found in the carrier temperatures that correspond to the $1P_{\frac{3}{2}}-1P_e$ and $1P_{\frac{1}{2}}-1P_e$ transitions. The dependence on the band-edge exciton temperature on the initially formed exciton states suggests phonon-bath coupling is competitive with carrier relaxation and imply carrier-phonon interactions may play a role as well.

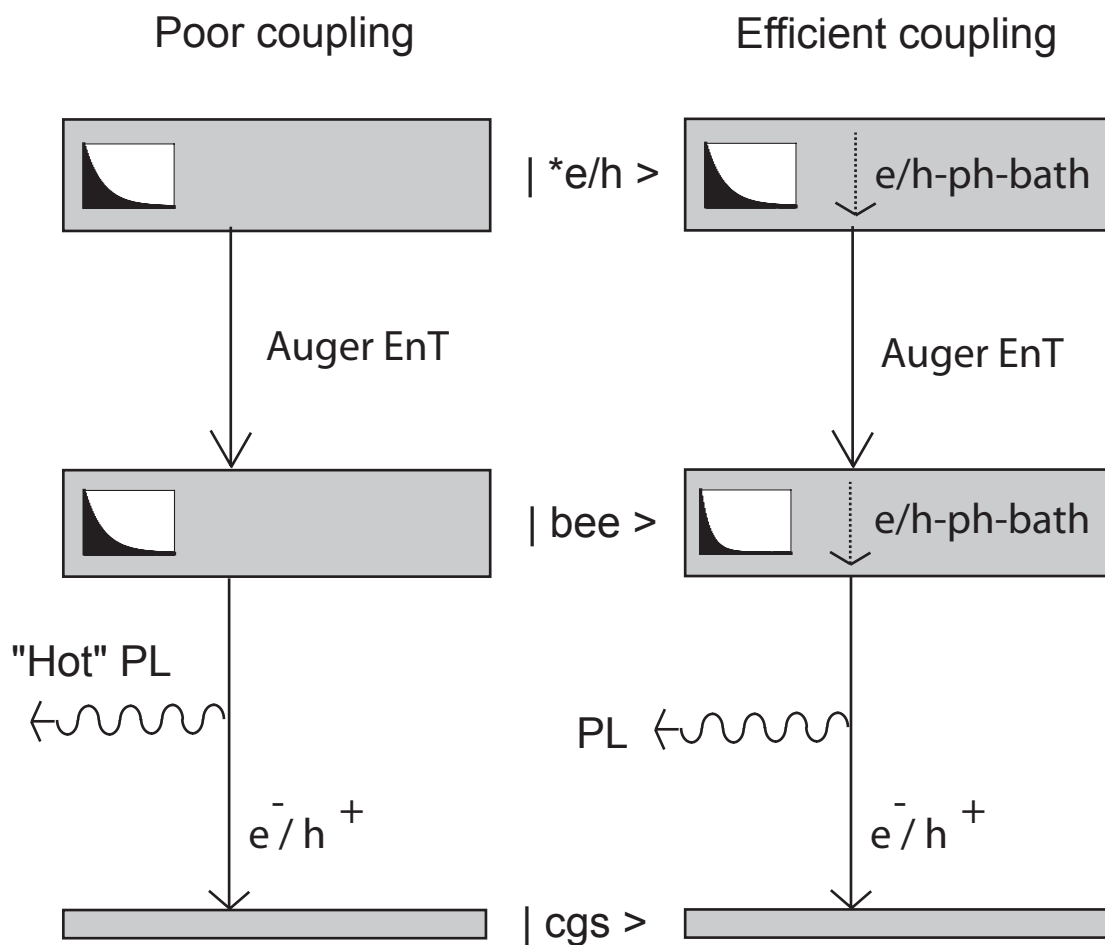


Figure 7.6: Illustration of the effect of the efficiency of carrier-phonon-bath coupling on the photoluminescence lineshape, showing “poor coupling” (left) and “strong coupling” (right). The states shown are: bee=band-edge exciton, cgs=crystal ground state and e/h=higher-lying excited state.

APPENDIX A

DERIVATION OF THE STERN VOLMER EQUATION

A.1 Equation

Consider a molecule that can be excited into a singlet electronic state, which will be called A. If we look at the excited donor molecule, A^* , in solution, it will decay back to its ground state, A, determined by k_1 through the process of radiative and nonradiative relaxation, primarily fluorescence and thermal relaxation:



The lifetime of A, τ_o , can be defined as:

$$\tau_o \equiv \frac{1}{k_1} \quad (\text{A.2})$$

If a quenching molecule is introduced in solution, another possibility of deactivation must be considered:



The mechanism through which the quencher deactivates the excited donor can consist of several processes, including energy transfer and electron transfer. In this case, the lifetime of A can be written as:

$$\frac{1}{\tau} = k_1 + k_q[Q] \quad (\text{A.4})$$

The inverse lifetime is the sum of the rates with no quencher present plus the rate of quenching which is dependent on the quencher concentration.

$$\frac{\tau_o}{\tau} = \frac{\frac{1}{k_1}}{\frac{1}{k_1 + k_q[Q]}} \quad (\text{A.5})$$

Eqn. A.5 can then be simplified to

$$\frac{\tau_o}{\tau} = 1 + k_q\tau_o[Q] \quad (\text{A.6})$$

Need to relate lifetime to fluorescence intensity then...that leads us to the general first order Stern Volmer equation:

$$\frac{I_o}{I} = 1 + k_q\tau_o[Q] = 1 + K_{SV}[Q] \quad (\text{A.7})$$

In Eqn. A.7, I_o is the intensity of the donor with no quencher present, I the intensity with increasing aliquots of quencher added, k_q is the rate of quenching, τ_o is the lifetime of the donor without quencher present, and $[Q]$ is the concentration of the quencher in solution. In the Stern Volmer mechanism, k_q cannot exceed the diffusional rate constant k_d for a given solution at a given temperature. The slope of a plot of $\frac{I_o}{I}$ vs concentration of quencher molecules provides a measure of k_q . It is important to note that in this model, the lifetime and steady state PL for the donor and molecule will decrease inversely with increasing quencher concentration[24].

APPENDIX B

STERN VOLMER DILUTION CORRECTIONS

This appendix details the mathematical corrections needed for Stern-Volmer style experiments using serial addition of aliquots of quencher. Briefly, this corrects the fluorescence intensity for progressively more dilute solutions.

B.1 Experimental Description

Two stock solutions were prepared: the sensitizer and the quencher. The sensitizer is the fluorescent species being monitored. The quencher is the species whose exact concentration is known that acts to reduce the photoluminescence of the sensitizer.

In a clean cuvette, a small volume of sensitizer is added, V_0 . The exact sensitizer concentration is not explicitly used in the calculations, though in general the concentration should be in the optically dilute limit. The fluorescence spectrum is recorded and as the integrated fluorescence of the sensitizer with no quencher present (I_0).

As quencher is added, the subscript i will be used to track the number of aliquots of quencher. Quencher of known concentration $[Q]_{stock}$ is then added in aliquots with a known volume (V_i). The total volume (V_{TOT}) is the sum of the initial volume (V_0) and the volumes of all the aliquots added (V_i).

$$V_{TOT} = V_0 + V_1 + V_2 + \dots V_i = \sum_{n=0}^i V_n \tag{B.1}$$

The integrated fluorescence signal for this aliquot addition is (I_i).

B.2 Volume Correction for Quencher Concentration

As more quencher is added to the sensitizer, the concentration of the quencher will be offset by the volume of the sensitizer initially in the cuvette. A correction to the quencher concentration based on the volume is therefore necessary.

In general, the concentration of the quencher can be determined with the law of the conservation of mass in mind. Since no chemical change occurs as a result of the interaction between sensitizer and quencher, the moles of quencher with($n_{Q(S=i)}$) and without the sensitizer($n_{Q(S=0)}$) are the same.

$$n_{Q(S=0)} = n_{Q(S=i)} \quad (\text{B.2})$$

This is a simple dilution correction, using the relationship which describes the i th concentration of quencher $[Q]_i$, given a stock solution having quencher concentration $[Q]_{stock}$ after i th aliquots.

In general, $[Q]_i = n_{Q(S=i)}/V_{TOT}$ and $[Q]_i = n_{Q(S=0)}/V_i$, which substituting into Eqn. B.2, produces

$$[Q]_i V_{TOT} = [Q]_{stock} V_0 \quad (\text{B.3})$$

Substitution of Eqn. B.1 into Eqn. B.3 produces

$$[Q]_i = [Q]_{stock} \left(\frac{V_i}{\sum_{n=0}^i V_n} \right) \quad (\text{B.4})$$

after rearrangement.

As more aliquots of quencher are added, V_i increases and $[Q]_i$ approaches $[Q]_{stock}$. In other words, as the amount of quencher increases, the effect of the sensitizer volume on the stock quencher concentration approaches zero.

B.3 Intensity Correction for Dilution of Sensitizer

As the concentration of quencher increases, the effective concentration of the sensitizer decreases due to the increase in volume from the addition of aliquots of quencher. Therefore, the intensity of the fluorescence must be corrected for this effective dilution. In general,

the integrated fluorescence intensity (I_i) is directly proportional to the concentration($[S]_i$), typically related through an instrumental factor(k),

$$I_i = k[S]_i \quad (\text{B.5})$$

Similar to Eqn. B.2, the sensitizer undergoes no chemical change with increasing aliquot additions, such that

$$n_{S(Q=0)} = n_{S(Q=i)} \quad (\text{B.6})$$

In general, the sensitizer concentration will be related to the total volume, $[S]_i = n_i/V_{TOT}$. Substituting this relationship into Eqn. B.5, solving for n then substituting into Eqn. B.6 and rearranging produces,

$$I_i = I_0 \left(\frac{V_0}{\sum_{n=0}^i V_n} \right) \quad (\text{B.7})$$

In order to correct for this effect, we multiply the empirically obtained integrated intensity by a factor that returns the intensity to its value prior to any dilution. This factor(k_{corr}) happens to be the inverse of the right hand term in the parentheses of Eqn. B.7,

$$k_{corr} = \frac{\sum_{n=0}^i V_n}{V_0} \quad (\text{B.8})$$

The corrected intensity($I_{i,corr}$) can be obtained by multiplying the integrated intensity value by k_{corr} ,

$$I_{i,corr} = k_{corr} I_i \quad (\text{B.9})$$

B.4 An MSEExcel Algorithm

In general, it is more accurate to perform Stern-Volmer using an analytical balance rather than volumetric techniques. In this way, a tared cuvette that is weighed after every aliquot addition produces a mass that is related to the total volume through the density of the solvent. In this way, raw x-y data consisting of intensity vs. mass are converted to intensity v. volume. Using the volume corrections discussed above, this can be further converted to the meaningful intensity v. quencher molarity.

In general, two corrections are applied: one for each axis.

The appropriate quencher concentration is found by using the formula,

$$= K @ 1 @ * A @ 1 @ / A @ 1 \quad (\text{B.10})$$

where the cell $(K, 1)$ contains the stock concentration of the quencher and column A is the total volume of the solution. The fluorescence intensity can be corrected by the formula,

$$= B @ 1 * A @ 1 / A @ 1 @ \quad (\text{B.11})$$

where column B is the integrated fluorescence intensity.

APPENDIX C

MATHEMATICA[®] ALGORITHM: SAMPLE STERN VOLMER CALCULATIONS

The following is the annotated algorithm for a Mathematica[®] v4.1 program that was written for automatic calculations, fitting and graphical analysis of solution-phase kinetics.

General Settings

Turns off Spelling Error Messages, and changes plot-style appearances

```
Off[General::spell, General::spell1];
```

```
$TextStyle = {FontFamily → "Arial", FontSize → 12};
```

Loads the standard graphics and nonlinear fitting packages

```
<< Graphics`
```

```
<< Graphics`Legend`
```

```
<< Statistics`NonlinearFit`
```

```
<< Graphics`MultipleListPlot`
```

```
<< Statistics`LinearRegression`
```

Data Input

File Location

Specify the directory and the name of the file. Note that the file should be a tab-delimited text file. In addition, none of the directories should be named only with numbers

```
SetDirectory["C:\\WINDOWS\\Desktop\\Anth 5nm DDA"];
```

```
Data[1] = Import["0.txt", "Table"];
```

```
Data[2] = Import["1.txt", "Table"];
Data[3] = Import["2.txt", "Table"];
Data[4] = Import["3.txt", "Table"];
Data[5] = Import["4.txt", "Table"];
```

Enter the name of the file with the masses of the corresponding solutions above. The data must be given in the following order, separated each by a carriage return:

```
-Concentration of Acceptor (in mol/L)
-Mass of the cuvette
-Mass of cuvette + donor solution
-Mass of cuvette + donor solution+acceptor aliquot[1]
-Mass of cuvette + donor solution+acceptor aliquot[2]
-Mass of cuvette + donor solution+acceptor aliquot[3]
. . .
. .
.
```

Note that the file should be a tab-delimited text file

```
Masses = Import["Mass.txt", "Table"];
```

Enter the solvent density in g/mL. Enter the solvent viscosity in Poise's (which will then be converted to Pa-s)

```
SolventDensity = 0.88;
SolventViscosity = .0052610-1;
```

Enter the row number limits of the inputted data file that actually contains spectral data

```
Starts = 1;
Ends = 231;
```

Enter the total number of points in the S/V, including the zero point

```
nmax = 5;
```

Enter the range (in nanometers) where integration should take place

```
λmin = 375;
λmax = 500;
```

Enter the Donor and Acceptor RADIUS in meters

$$\text{RadiusDonor} = 4.6410^{-10};$$

$$\text{RadiusAcceptor} = 2.410^{-9};$$

Enter the lifetime of the donor (in seconds)

$$\tau = 410^{-9};$$

Enter the Temperature in units of Kelvin

$$\text{Temp} = 298;$$

Boltmann Constant in Joules Kelvin⁻¹

$$\text{kB} = 1.3806532410^{-23};$$

Avogadro's Number 1/mol

$$\text{NA} = 6.02310^{23};$$

Enter the errors associated with the balance (in grams) and the fluorimeter (in percentage error)

$$\text{BalanceError} = 0.001;$$

$$\text{InstrumentError} = 0.01;$$

Stokes-Einstein Relationship (Second⁻¹ Meter²)

$$\text{DiffCoeff}[\text{Radius}]:= \frac{\text{kBTemp}}{6\pi\text{SolventViscosityRadius}};$$

Smoluchowski Equation [Theoretically predicted diffusion rate] (Units of Molar⁻¹ Second⁻¹)

$$\text{kDiff}[\text{DonorRad.}, \text{AcceptorRad.}] := 10004\pi\text{NA}(\text{DonorRad} + \text{AcceptorRad}) \\ (\text{DiffCoeff}[\text{DonorRad}] + \text{DiffCoeff}[\text{AcceptorRad}])$$

Predicted Diffusion Coefficient

$$\text{kDiff}[\text{RadiusDonor}, \text{RadiusAcceptor}]$$

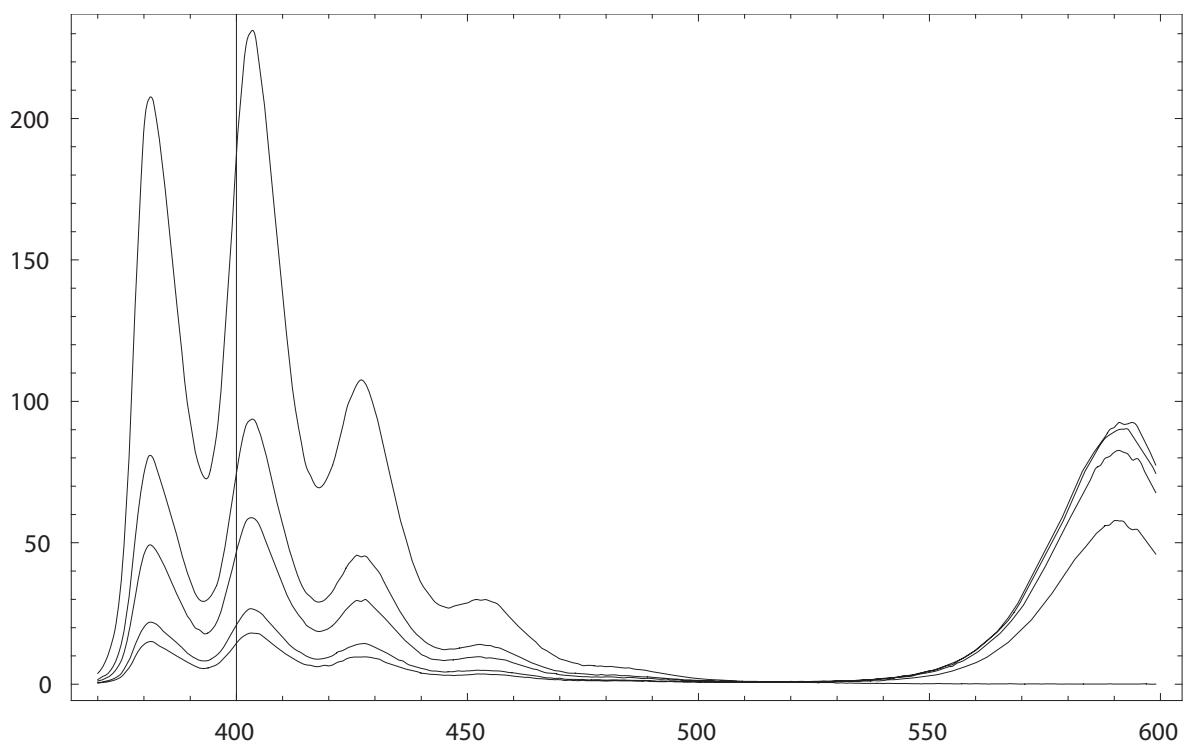
$$2.31341 \times 10^{10}$$

$KD = kDiff[RadiusDonor, RadiusAcceptor]\tau$

92.5366

Computation

```
InitialAccConc = Masses[[1]];
Weight[i_]:=Masses[[i]] - Masses[[2]]
Volume[i_]:=Weight[i + 2]/SolventDensity
Concentration[i_]:=  $\frac{Volume[i] - Volume[1]}{Volume[i]}$  InitialAccConc
SVX = Flatten[Table[Concentration[i], {i, 1, nmax}]]
PL[1] = Interpolation[Drop[Data[1], -1]][λ];
PL[2] = Interpolation[Drop[Data[2], -1]][λ];
PL[3] = Interpolation[Drop[Data[3], -1]][λ];
PL[4] = Interpolation[Drop[Data[4], -1]][λ];
PL[5] = Interpolation[Drop[Data[5], -1]][λ];
Plot[{PL[1], PL[2], PL[3], PL[4], PL[5]}
, {λ, Data[1][[1, 1]], Data[1][[-2, 1]]},
PlotRange → All, Frame → True];
```



```

Int[i_]:=NIntegrate[PL[i] - Min[Data[i][[All, 2]]],
{λ, λmin, λmax}, Method → Trapezoidal, MaxRecursion → 10000]
Int[2]
3431.19
CorrectedInt[i_]:=Volume[i]/Volume[1] Int[i]
SVY = Flatten [Table [Int[1]/CorrectedInt[i], {i, 1, nmax}]]
{1., 1.89847, 2.48007, 3.89591, 4.53931}
ErrorPropY[i_]:=SVY[[i]]

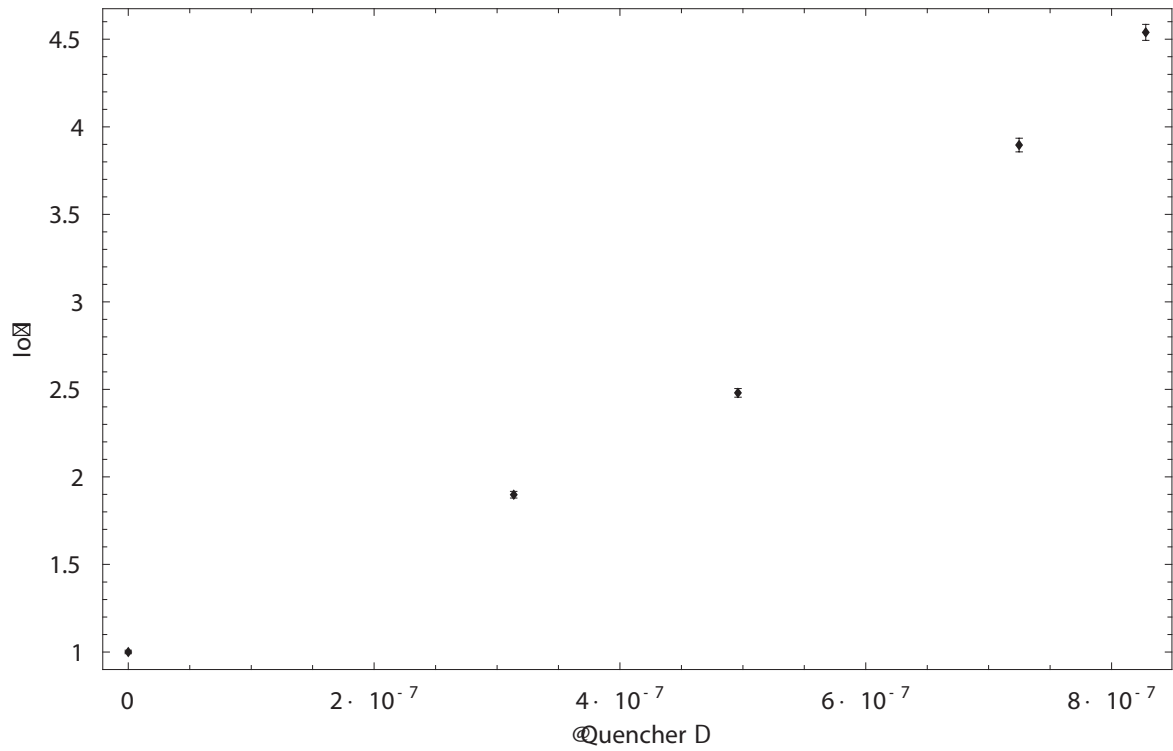
```

$$\sqrt{\left(\frac{\text{BalanceError}}{\text{Volume}[1]\text{SolventDensity}}\right)^2 + \left(\frac{\text{BalanceError}}{\text{Volume}[i]\text{SolventDensity}}\right)^2 + \text{InstrumentError}^2}$$

```

ErrorPropX[i_]:=SVX[[i]]
SV = Transpose[{SVX,SVY}]
SVwithError = Table[{SVX[[i]], SVY[[i]], ErrorPropX[i][[1]],
ErrorPropY[i][[1]]}, {i, 1, nmax}]
SVPlot = MultipleListPlot[
Table[
{SV[[i]], ErrorBar[ErrorPropX[i][[1]], ErrorPropY[i][[1]]]}
, {i, 1, nmax}]
, Frame → True, Axes → None, PlotRange → All,
FrameLabel → {"[Quencher]", "Io/I"}];

```

```
Export["SVData_With_Errors.dat", SVwithError];
Export["SV_Plot.jpg", SVPlot, ImageSize -> 480, ImageResolution -> 100];
```

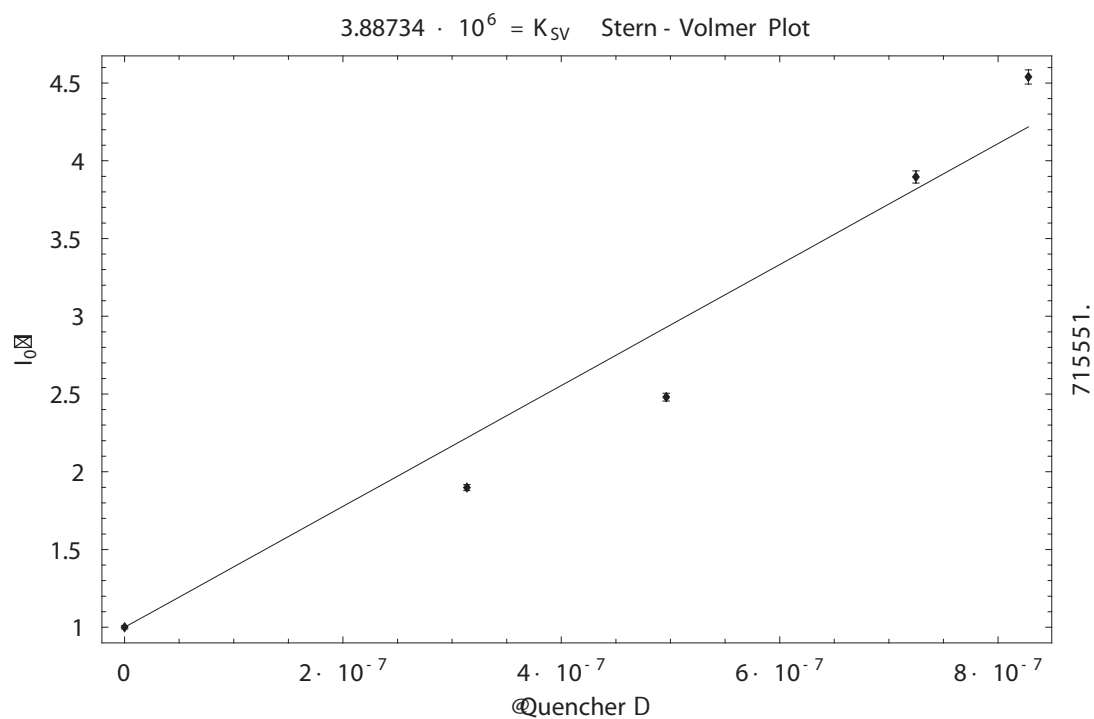
$$K_{SV} = K_D = k_q \tau$$

```
SVEqn = 1 + KSVQ;
SVFit = NonlinearFit[SV, SVEqn, Q, {KSV, 1}]
1 + 3.88734 x 106Q
SVRegress = NonlinearRegress[SV, SVEqn, Q, {KSV, 1},
```

```

RegressionReport->ParameterCITable]
SVError = Abs  $\left[ \frac{\text{SVRegress}[[1,2,1,1,3,1]] - \text{SVRegress}[[1,2,1,1,3,2]]}{2} \right]$ 
715551.
KSVFit = SVRegress[[1, 2, 1, 1, 1]]
 $3.88734 \times 10^6$ 
kq = KSVFit/ $\tau$ 
 $9.71834 \times 10^{14}$ 
SVPlot = Show[{
MultipleListPlot[
Table[
{SV[[i]], ErrorBar[ErrorPropX[i][[1]], ErrorPropY[i][[1]]]}
, {i, 1, nmax}]
, DisplayFunction -> Identity],
Plot[SVFit, {Q, 0, SV[[-1, 1]]}, DisplayFunction -> Identity]
}, DisplayFunction -> $DisplayFunction,
Frame -> True, Axes -> None, PlotRange -> All,
FrameLabel -> {"[Quencher]", " $I_0/I$ ", "
Stern-Volmer Plot"KSVFit" =  $K_{SV}$ ", SVError}];

```



```
Export["SV_Plot.jpg", SVPlot, ImageSize -> 480, ImageResolution -> 100];
```

$$K_S, K_D$$

```
SVModEqn = 1 + (KS + KD)Q + (KSKD)Q^2;
```

```
SVFit = NonlinearFit[SV, SVModEqn, Q, {KS, 1}]
```

$$1 + 3.88709 \times 10^6 Q + 3.5969 \times 10^8 Q^2$$

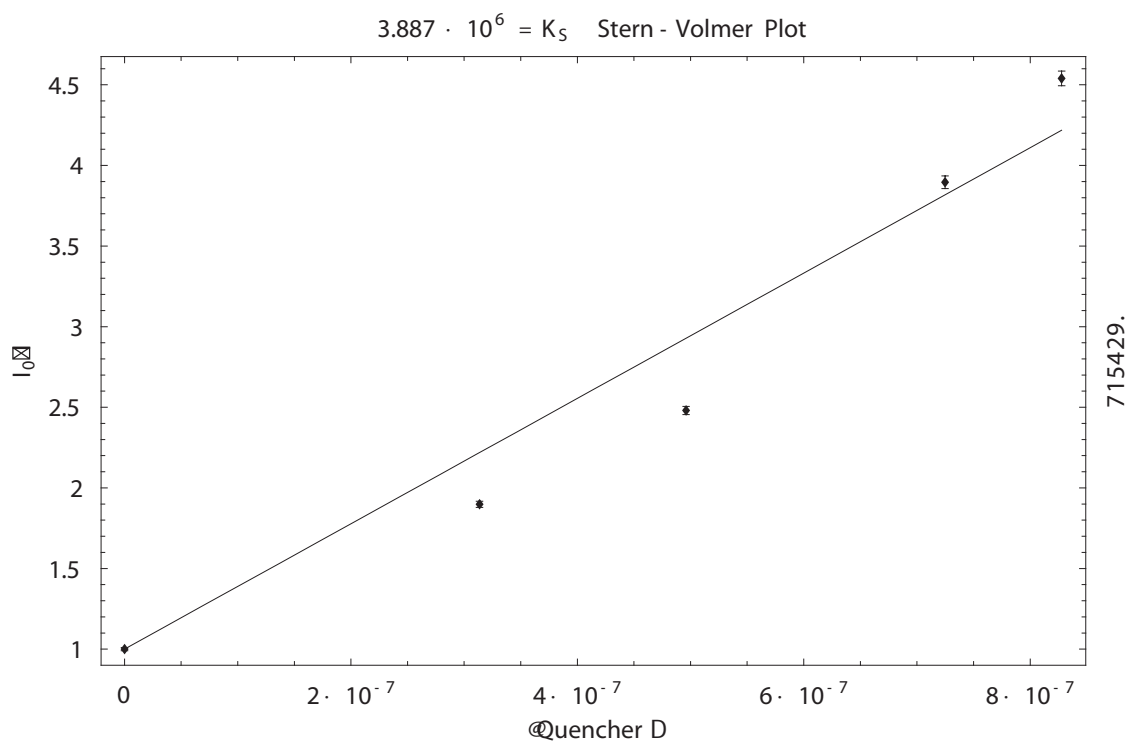
```
SVRegress = NonlinearRegress[SV, SVModEqn, Q, {KS, 1},
```

```
RegressionReport->ParameterCITable]
```

```

KSFit = SVRegress[[1, 2, 1, 1, 1]]
3.887 × 106
SVError = Abs  $\left[ \frac{\text{SVRegress}[[1,2,1,1,3,1]] - \text{SVRegress}[[1,2,1,1,3,2]]}{2} \right]$ 
715429.
SVPlot = Show[{
MultipleListPlot[
Table[
{SV[[i]], ErrorBar[ErrorPropX[i][[1]], ErrorPropY[i][[1]]]}
, {i, 1, nmax}]
, DisplayFunction → Identity],
Plot[SVFit, {Q, 0, SV[[-1, 1]]}, DisplayFunction → Identity]
}, DisplayFunction → $DisplayFunction,
Frame → True, Axes → None, PlotRange → All,
FrameLabel → {"[Quencher]", "I0/I", "
Stern-Volmer Plot"KSFit" = KS", SVError}];

```



```
Export["KS_Plot.jpg", SVPlot, ImageSize → 480, ImageResolution → 100];
```

APPENDIX D

DERIVATION: THE BOLTON-ARCHER EQUATION USING A DETAILED BALANCE APPROACH

This method was pioneered by Bolton and Archer and a full, detailed derivation appears elsewhere[57]. This appendix summarizes key assumptions and provides a shortened, but mathematically complete derivation of the equation utilized for determination of excited state temperatures.

D.1 Thermal Equilibrium

Measuring the carrier temperature of the excited state by the detailed balance method requires the primary assumption that an optically accessible thermal equilibrium exists between an electronic excited state and its ground state. The rate of the absorption transitions (dg_0) will be balanced with the rate of the spontaneous emission transitions (du_0) at thermal equilibrium,

$$dg_0 = du_0 \tag{D.1}$$

D.2 The Absorption Rate

The rate of absorption (dg_0) is proportional to the incident spectral flux, ($j(\nu)$), mediated by the molecular absorption coefficient, ($\alpha(\nu)$), such that $dg_0 = \alpha(\nu)j(\nu)d\nu$. Rewriting the spectral flux density as a product of the spectral density and photon travel time component, $j(\nu) = \rho(\nu)c/\eta$, and incorporating Planck's black body spectral density formula, $\rho(\nu) = \frac{8\pi\eta^3\nu^2}{c^3} \frac{1}{\exp(h\nu/k_BT)-1}$, the absorption rate can be determined,

$$dg_0 = \left(\frac{8\ln(10)\pi N_g}{10c^2 N_A} \right) \frac{\eta(\nu)^2 \nu^2 \epsilon(\nu)}{\exp(h\nu/k_B T) - 1} d\nu \quad (\text{D.2})$$

where $\alpha(\nu) = \frac{\ln(10)N_g}{10N_A}\epsilon(\nu)$.

D.3 The Emission Rate

The rate of spontaneous emission(du_0) is the product of the radiative decay rate and the equilibrium population of the upper state, $du_0 = k_r(\nu)N_u d\nu$. The radiative decay rate is therefore proportional to the normalized fluorescence spectral distribution divided by the radiative lifetime, such that we can rewrite the spontaneous emission rate as,

$$du_0 = \frac{1}{\tau_r} \frac{f(\nu)}{\int_0^\infty f(\nu) d\nu} N_u d\nu \quad (\text{D.3})$$

D.4 The Boltzmann distribution

Utilizing the Boltzmann distribution, ($N_u/N_g = (q_u/q_g)\exp(-E_g/k_B T)$), substituting Eqn. D.2 and Eqn. D.3 into Eqn. D.1 and taking logarithms produces

$$\ln \left[\frac{f(\nu)/\int_0^\infty f(\nu) d\nu}{\epsilon(\nu)\eta(\nu)^2 \nu^2} \right] = \left(\frac{-h}{k_B T} \right) \nu + \left[\ln \left(\frac{8\pi\ln(10)\tau_r q_g}{10c^2 N_A q_u} \right) + \frac{E_g}{k_B T} \right] \quad (\text{D.4})$$

D.5 Graphical Analysis

Eqn. D.4 is expressed as a straight line ($y=mx+b$) such that a plot of the logarithm of the emission spectrum divided by the absorption spectrum (and divided by an energy squared factor) will produce a straight line whose slope is the inverse temperature of the thermalized excited state. The refractive index of CdSe[62] has been shown to have no strong frequency dependence in the region of interest (1.9-3.5eV). Therefore, extracting the optical temperature of the excited state is as straightforward as measuring the slope of a line whose equation involves only the continuous-wave photoluminescence and absorption data. The other variables appearing here are: q_g =ground state degeneracy, q_u =excited state degeneracy, N_A =Avogadro's Number, c =speed of light, $f(\nu)$ =fluorescence spectrum, $\epsilon(\nu)$ =extinction spectrum. Eqn. D.4, however to do so accurately requires knowing the energy gap (E_g) to at least 5 significant digits, which is currently not obtainable.

APPENDIX E

MATHEMATICA[®] ALGORITHM: SAMPLE HOT BAND CALCULATIONS

The following is the annotated algorithm for a Mathematica[®] v4.1 program that was written for automatic calculations, fitting and graphical analysis of the Bolton-Archer equation.

General Settings

Turns off Spelling Error Messages, and changes plot-style appearances

```
Off[General::spell, General::spell1];
```

```
$TextStyle = {FontFamily → "Arial", FontSize → 12};
```

Loads the standard graphics and nonlinear fitting packages

```
<< Graphics`Graphics`
```

```
<< Statistics`NonlinearFit`
```

CdSe[3.44nm] - Ex:300nm:4.133eV

Specify the directory

```
SetDirectory["D:\Research\Calculations\Data\CdSe(4.0)-DDA"];
```

Specify the name of the file

```
RawPL = Import["ex 300.txt", "Table"];
```

```
RawExt = Import["Ext CdSe(4.0)-DDA.txt", "Table"];
```


Constants

$$h = 4.1356672710^{-15};$$

$$kB = 8.61734210^{-5};$$

$$NA = 6.02210^{23};$$

$$c = 2.9910^8;$$

Normalizes PL with PL area (Unitless)

$$PLArea = \sum_{i=1}^{\text{Length}[\text{RawPL}[[\text{All}, 1]]] - 1} (\text{RawPL}[[i, 2]] - \text{RawPL}[[1, 2]]) \left(\frac{1240}{\text{RawPL}[[i, 1]]} - \frac{1240}{\text{RawPL}[[i+1, 1]]} \right)$$

$$PL = \text{Interpolation} \left[\text{Table} \left[\left\{ \frac{1240}{\text{RawPL}[[i, 1]]}, \text{RawPL}[[i, 2]] - \text{RawPL}[[1, 2]] \right\}, \{i, 1, \text{Length}[\text{RawPL}[[\text{All}, 1]]]\} \right]; \right]$$

$$NPL = \frac{PL[\text{En}]}{PLArea};$$

$$49.7854$$

Formats Extinction Coefficient into (M^{-1} , m^{-1})

$$\text{Ext} = \text{Interpolation} \left[\text{Table} \left[\left\{ \frac{1240}{\text{RawExt}[[i, 1]]}, 100(\text{RawExt}[[i, 2]] - \text{RawExt}[[1, 2]]) \right\}, \{i, 1, \text{Length}[\text{RawExt}[[\text{All}, 1]]]\} \right][\text{En}]; \right]$$

Parameters

$$Eg = 3.24353;$$

$$\eta = 2.41;$$

Defines y-axis for plotting

$$y = \text{Log} \left[\frac{NPL h^2}{\text{Ext} \text{En}^2 \eta^2} \right];$$

$$\text{ShowMin} = 2.0;$$

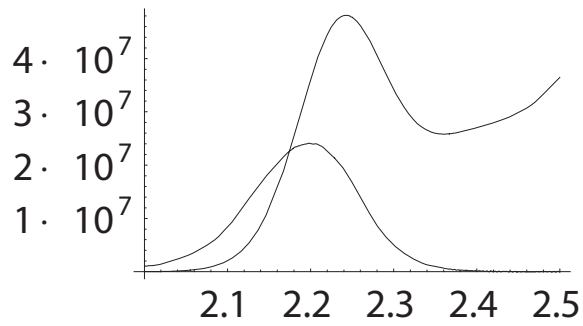
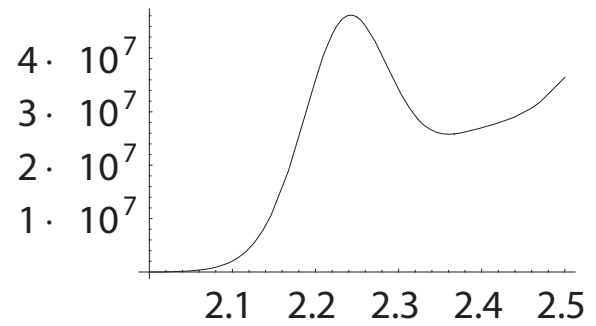
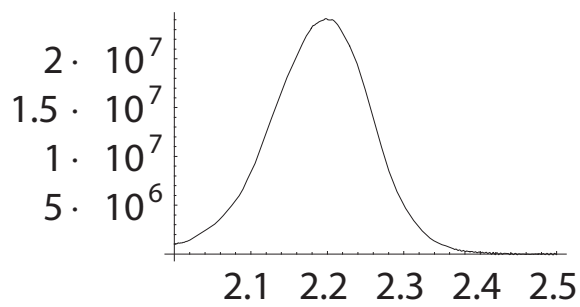
$$\text{ShowMax} = 2.5;$$

$$\text{Scaler} = 4200000;$$

Show[{

Plot[ScalerNPL, {En, ShowMin, ShowMax}, PlotRange \rightarrow All],

```
Plot[Ext, {En, ShowMin, ShowMax}, PlotRange → All]
];
```



```
EnMin = 2.15;
EnMax = 2.3;
EnStep = 0.005;
```

Creates a list to be fit using y

```
yData = Table[{k, y/.En → k}, {k, EnMin, EnMax, EnStep}];
```

Fits Data

```

Analysis = NonlinearRegress [Evaluate[yData],  $\frac{-E_n}{kBT} + b$ , En, {{T, 298}, {b, -50}},
MaxIterations → 1000, RegressionReport → ParameterCITable]
AnalysisFit = NonlinearFit [Evaluate[yData],  $\frac{-E_n}{kBT} + b$ , En, {{T, 298}, {b, -50}},
MaxIterations → 1000, RegressionReport → ParameterCITable]

$$\left\{ \begin{array}{l} \text{ParameterCITable} \rightarrow \begin{array}{cccc} & \text{Estimate} & \text{Asymptotic SE} & \text{CI} \\ T & 733.513 & 7.55782 & \{718.055, 748.97\} \\ b & -50.3771 & 0.362765 & \{-51.119, -49.6352\} \end{array} \end{array} \right\}$$

-50.3771 - 15.8205En

```

Extracts Results from Fitting

```

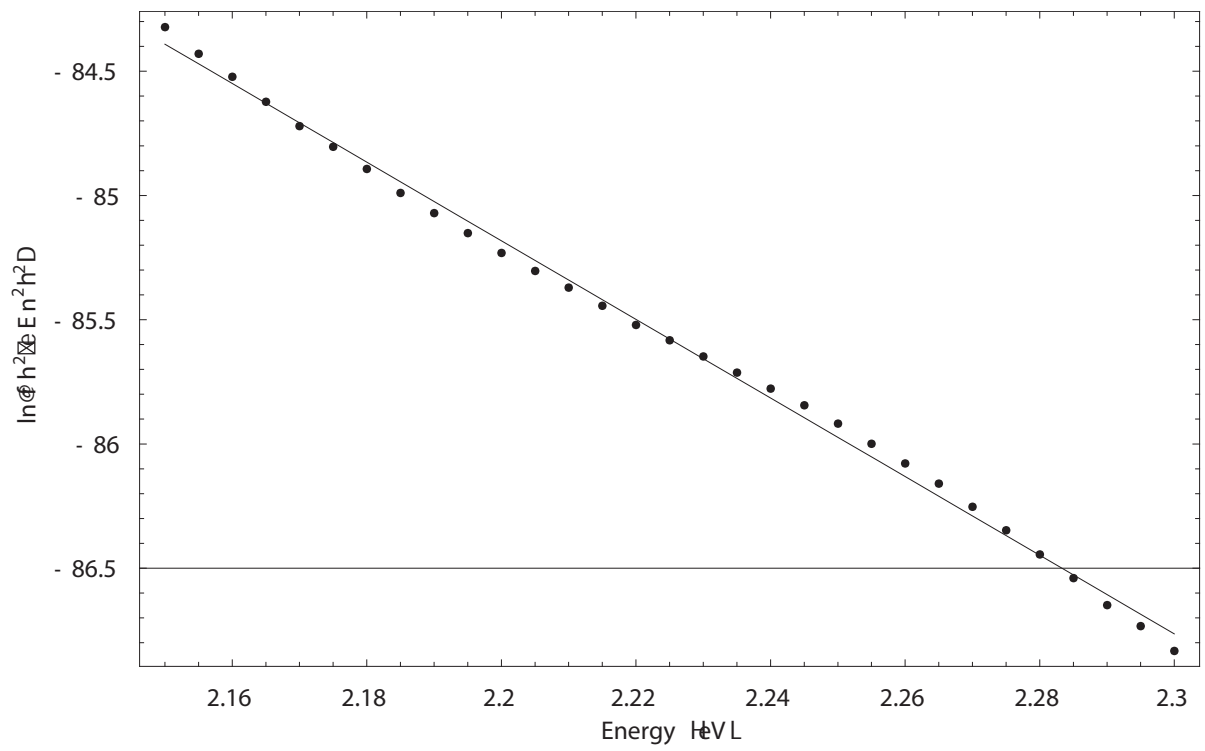
TempFit = Analysis[[1, 2, 1, 1, 1]];
TempFitErr = Analysis[[1, 2, 1, 1, 3, 1]];
bFit = Analysis[[1, 2, 1, 2, 1]];
bFitErr = Analysis[[1, 2, 1, 2, 3, 1]];

$$\tau = \frac{10NAc^2h}{8\pi\text{Log}[10]} \text{Exp} \left[ b\text{Fit} - \frac{E_g}{kB\text{TempFit}} \right]$$


$$\tau\text{Err} = \frac{10NAc^2h}{8\pi\text{Log}[10]} \text{Exp} \left[ b\text{FitErr} - \frac{E_g}{kB\text{TempFitErr}} \right]$$

2.637705889463222*^-19
4.1617036732444444*^-20
Show[
ListPlot[yData, DisplayFunction → Identity],
Plot[AnalysisFit, {En, yData[[1, 1]], yData[[-1, 1]]},
DisplayFunction → Identity], DisplayFunction → $DisplayFunction,
Frame → True, FrameLabel → {"Energy (eV)", "ln[f h^2/ε En^2η^2]"}];

```



```

Temp[1] = TempFit;
TempErr[1] = TempFitErr;
Data[1] = yData;
FitLine[1] = AnalysisFit;

```

REFERENCES

- [1] A.D Yoffe. *Advances in Physics*, 50:1–208, 2001. [1.1](#), [7.1](#)
- [2] Jacques I. Pankove. *Optical Processes in Semiconductors*. Dover Publications, Inc., 1971. [1.2.1](#), [1.3.2](#), [1.4.1](#), [1.4.2](#)
- [3] S.L. Cumberland, A. Javier, G. Khitrov, G. Strouse, S. Woessner, and C.S Yun. *Chemistry of Materials*, 14:1576, 2002. [1.2.1](#), [1.6.1](#), [2.2](#), [3.2.3](#), [4.3.1](#), [6.3.1](#)
- [4] Arthur J. Nozik. *Annu. Rev. Phys. Chem.*, 52:193–231, 2001. [1.3.1](#), [7.3.1](#), [7.8.1](#), [7.10](#)
- [5] N.J. Turro. *Modern Molecular Photochemistry*. University Science Books, 1991. [1.3.2](#), [1.5.2](#)
- [6] V.I. Klimov. *Journal of Physical Chemistry B*, 104:6112, 2000. [1.4.3](#)
- [7] L. Brus. *Journal of Physical Chemistry*, 90:2555, 1971. [1.4.4](#)
- [8] D.J. Norris and M.G. Bawendi. *Phys. Rev. B*, 53(24):16338–53, 1996. [1.5.1](#), [7.7.3](#)
- [9] J.N. Demas. *Excited State Lifetime Measurements*. Academic Press, 1983. [1.5.2](#)
- [10] X. Michalet, F. Pinaud, T.D. Lacoste, M. Dahan, M.P. Alivisatos, and S. Weiss. *Single Molecules*, 2:261, 2001. [2.1.2](#)
- [11] W.J. Parak, D. Gerion, T. Pellegrino, D. Zanchet, C. Micheel, S.C. Williams, R. Boudreau, M. A. Le Gros, C.A. Larabell, and A.P. Alivisatos. *Nanotechnology*, 14:R15, 2003. [2.1.2](#)
- [12] A.V Firth, D.J. Cole-Hamilton, and J.W Allen. *Applied Physics Letters*, 75:3120, 1999. [2.1.2](#)
- [13] H. Sohn, M.J. Sailor, D. Magde, and W.C. Trogler. *Journal of the American Chemical Society*, 125:3821, 2003. [2.1.2](#), [2.1.2](#)
- [14] H. Mattoussi, I.L Medintz, A.R Clapp, E.R. Goldman, J.K Jaiswal, S.M Simon, and J.M Mauro. *Jala*, 9:28, 2004. [2.1.2](#)
- [15] D.J Winzor. *Journal of Chromatography A*, 1037:351, 2004. [2.1.2](#), [2.4](#)
- [16] Y. Kiso, T. Kitao, and K. Nishimura. *Journal of Applied Polymer Science*, 74:1037, 1999. [2.1.2](#)

- [17] B.H. Robinson, N.C White, and C. Mateo. *Advances in Molecular Relaxation Processes*, 7:321, 1975. [2.1.2](#), [2.4](#)
- [18] A.J Visser, K. Vos, A. Van Hoek, and J.S Santema. *Journal of Physical Chemistry*, 92:759, 1988. [2.1.2](#)
- [19] R. Meulenberg and G. Strouse. *Journal of Physical Chemistry B*, 105:7438, 2001. [2.1.2](#), [2.3.5](#), [2.4](#)
- [20] A.R. Clapp, I.L. Medintz, B.R. Fisher, G.P. Anderson, and H. Mattoussi. *Journal of the American Chemical Society*, 127:1242, 2005. [2.1.2](#), [2.4](#)
- [21] C. Fan, S. Wang, J.W. Hong, G.C. Bazan, K.W Plaxco, and A.J. Heeger. *Proceedings of the National Academy of Sciences of the United States of America*, 100:6297, 2003. [2.1.2](#)
- [22] I.L. Medintz, A.R Clapp, H. Mattoussi, E.R Goldman, B. Fisher, and J.M Mauro. *Nature Materials*, 2:630, 2003. [2.1.2](#)
- [23] E.R. Goldman, A.R. Clapp, G.P. Anderson, H.T. Uyeda, J.M. Mauro, I.L Medintz, and H. Mattoussi. *Analytical Chemistry*, 76:684, 2004. [2.1.2](#)
- [24] J.R. Lakowicz. *Principles of Fluorescence Spectroscopy, Second Edition*. Kluwer Academic/Plenum, New York, 1999. [2.1.3](#), [2.1.4](#), [2.5](#), [A.1](#)
- [25] A.R. Clapp, I.L Medintz, J.M. Mauro, B.R Fisher, M.G. Bawendi, and H. Mattoussi. *Journal of the American Chemical Society*, volume =, 2004. [2.3.2](#)
- [26] T. Forster. *Discussions from the Faraday Society*, 27, 1959. [2.3.2](#)
- [27] B.B. Nikoobakht, Clemens, M. Braun, M. Hun, and M. El-Sayed. *Photochemistry and Photobiology*, 75:591, 2002. [2.4](#)
- [28] T. Huang and R.W. Murray. *Langmuir*, 18:7077, 2002. [2.4](#)
- [29] W.R. Glomm, S.J. Moses, M.K. Brennaman, J.M Papanikolas, and S. Franzen. *Journal of Physical Chemistry B*, 109:804, 2005. [2.4](#)
- [30] Pearl Pui Hand Cheng, Debbie Sivester, Gangli Wang, Gregory Kalyuzhny, Alicia Douglas, and Royce W. Murray. *J. Phys. Chem. B*, 110:4637–4644, 2006. [2.4](#)
- [31] Sujit Kumar Ghosh, Anjali Pal, Subrata Kundu, Sudip Nath, and Tarasankar Pal. *Chemical Physics Letters*, 395:366–372, 2004. [2.4](#)
- [32] S. T. Selvan, C. Bullen, M. Ashokkumar, and P. Mulvaney. *Advanced Materials*, 13:985–988, 2001. [3.1](#)
- [33] Indika U. Arachchige and Stephanie L. Brock. *Journal of the American Chemical Society*, 129:1840, 2007. [3.1](#)

- [34] Indika U. Arachchige, Kennedy K. Kalebaila, and Stephanie L. Brock. *Comments on Inorganic Chemistry*, 27:103–106, 2006. [3.1](#)
- [35] Indika U. Arachchige and Stephanie L. Brock. *Journal of the American Chemical Society*, 128:7964–7971, 2006. [3.1](#)
- [36] Indika U. Arachchige, J.L. Mohanan, and Stephanie L. Brock. *Chemistry of Materials*, 17:6644–6650, 2005. [3.1](#)
- [37] D. A. Hummell, I. L. Torriani¹, A. F. Craievich, N. De La Rosa Fox, A. Y. Ramos, and O. Lyon. *Journal of Sol-Gel Science and Technology*, 8:285–291, 2006. [3.1](#)
- [38] E. Lifshitz, I. Daga, I. Litvin, G. Hodes, S. Gorer, R. Reisfeld, M. Zelner, and H. Minti. *Chemical Physics Letters*, 288:188–196, 1998. [3.1](#)
- [39] Larry Hench and Jon West. *Chemical Reviews*, 90:33–72, 1990. [3.2.1](#)
- [40] Bing Tan and Stephen E. Rankin. *Journal of Physical Chemistry B*, 2006. [3.2.2](#)
- [41] Lindsey Sorensen, Geoffrey F. Strouse*, and A. E. Stiegman. *Advanced Materials*, 18:1965–1967, 2006. [3.2.3](#)
- [42] S. R. Cordero, P. J. Carson, R. A. Estabrook, G. F. Strouse, and S. K. Buratto. *Journal of Physical Chemistry, B*, 104(51):12137–12142, 2000. [3.4.1](#), [3.4.2](#), [4.2.3](#), [4.2.3](#), [4.2.4](#), [4.5.2](#)
- [43] S.E. Letant and T.F. Wang. *Applied Physics Letters*, 88:103110, 2006. [5.1.2](#)
- [44] D. Enke, F. Janowski, and W. Schwieger. *Microporous and Mesoporous Materials*, 60:19–30, 2003. [5.2.1](#)
- [45] S.E Letant and T.F. Wang. *Nano Letters*, 6(12):2877–2880, 2006. [5.2.2](#)
- [46] S.E Letant and T.F. Wang. *Applied Physics Letters*, 88:103110, 2006. [5.2.2](#)
- [47] Lourdes Basabe-Desmonts, David N. Reinhoudt, and Mercedes Crego-Calama. *Chemical Society Reviews*, 36:993–1017, 2007. [6.1.1](#)
- [48] Alexander Beveridge. *Forensic Investigation of Explosions*. CRC, 1998. [6.2.3](#)
- [49] Jin Z. Zhang. *Acc. Chem. Res.*, 30:423–9, 1997. [7.1](#), [7.3.1](#)
- [50] Clemens Burda, Stephan Link, Mona B. Mohamed, and Mostafa El-Sayed. *J. Chem. Phys.*, 116:3828–33, 2002. [7.1](#)
- [51] D.M. Mittleman, R.W. Schoenlein, J.J. Shiang, V.L. Colvin, A.P. Alivisatos, and C.V. Shank. *Phys. Rev. B*, 49(20):14435–47, 1994. [7.1](#)
- [52] Mayrose R. Salvador, Margaret A. Hines, and Gregory D. Scholes. *J. Chem. Phys.*, 118(20):9380–8, 2003. [7.1](#)

- [53] Philippe Guyot-Sionnest, Moonsub Shim, Chris Matranga, and Margaret Hines. *Phys. Rev. B*, 60(4):R2181–R2184, 1999. [7.3.1](#), [7.10](#)
- [54] V.I. Klimov, D.W. McBranch, C.A. Leatherdale, and M.G. Bawendi. *Phys. Rev. B*, 60(19):13740–9, 1999. [7.3.1](#)
- [55] U. Woggon, H. Giessen, F. Gindele, O. Wind, B. Fluegel, and N. Peyghambarian. *Phys. Rev. B*, 54(24):17681–90, 1996. [7.3.1](#)
- [56] A.A.P. Silva, A.C.S. Algarte, A.R. Vasconcellos, and R. Luzzi. *J. Appl. Phys.*, 90(8):3973–8, 2001. [7.3.1](#), [7.8.1](#)
- [57] James R. Bolton and Mary D. Archer. *J. Phys. Chem.*, 95:8453–61, 1991. [7.3.3](#), [7.6.1](#), [D](#)
- [58] D.J. Norris and M.G. Bawendi. *J. Chem. Phys.*, 103(13):5260–8, 1995. [7.7.3](#)
- [59] J.M. Lupton and J. Klein. *Chem. Phys. Lett.*, 363:204–210, 2002. [7.8](#)
- [60] Arthur Marki, Wolfgang Quapp, and Stefan Klee. *J. Mol. Spec.*, 171(2):420–34, 1995. [7.8.1](#)
- [61] R.M. de la Cruz. *Superlattices and Microstructures*, 16(4):427–31, 1994. [7.8.1](#)
- [62] Susumu Ninomiya and Sadao Adachi. *J. Appl. Phys.*, 78(7):4681–9, 1995. [D.5](#)

BIOGRAPHICAL SKETCH

Melissa L. Fisher

Education

Ph.D. Inorganic Chemistry (2009, anticipated), Florida State University, Tallahassee, FL 32306-4390 Advisor: Geoffrey F. Strouse Thesis: CdSe Quantum Dot Optical Sensing

Graduate Education (Ph. D. Candidacy) (2001-2003), University of California, Santa Barbara CA 93106-9510 Advisor: Geoffrey F. Strouse

B.S. Chemistry and B.S. Biology (2001), University of La Verne, La Verne CA 91750 Cum Laude, Departmental Honors in Chemistry

Fellowships/ Awards

Graduate Opportunity Fellowship (UCSB, 2001) Graduate Opportunity Fellowship (UCSB, 2003)

Presentations and Posters

Southern California Inorganic Photochemistry Conference (Summer 2002) Stern-Volmer Kinetics of CdSe Nanocrystals

Publications

1. Carrier Temperatures of CdSe Quantum Dots using the Detailed Balance Method A. Javier, M. Fisher, B. Eidelson, G.F. Strouse (manuscript in preparation)
2. Optically Probed Molecular Adsorption on Nanoscale CdSe Surfaces M. Fisher, A. Javier, J. Sorena, G.F. Strouse, (manuscript in preparation)
3. Nanometal Surface Energy Transfer in Optical Rulers, Breaking the FRET Barrier C.S. Yun, A. Javier, T. Jennings, M. Fisher, S. Hira, S. Peterson, B. Hopkins, N.O. Reich, and G.F. Strouse, J Am Chem Soc, 127 (9), 3115-9 (2005)

Primary Proficiencies

Sol Gel Synthesis: Silica Xero gels, Silica Aerogels , CdSe incorporation

Nanoparticle Synthesis: Colloidal Au, CdSe nanoparticles

Spectroscopy: Standard UV/Vis and PLE, solid-state PL, Quantum Yields

Analysis: SigmaPlot, Adobe Illustrator and Photoshop, MS Excel

Word Processing: MS Word, MS PowerPoint, LaTeX

Teaching

Teaching Assistant at FSU General Chemistry, Chemistry for Liberal Arts (2003-2006)

Teaching Assistant at UCSB General Chemistry, Inorganic Chemistry (2001-2003)

Teaching Assistant at ULV General Chemistry, General Biology (1998-2001)